

TRACING OF INTERNAL LAYERS IN RADAR ECHOGRAMS
FROM A GREENLAND STUDY REGION

A Thesis presented to the Faculty of the Graduate School
University of Missouri-Columbia

In Partial Fulfillment
Of the Requirements for the Degree

Master of Science

by
XIN GAO

Dr. Justin Legarsky, Thesis Supervisor

AUGUST 2006

The undersigned, appointed by the Dean of the Graduate School, have examined the thesis entitled

TRACING OF INTERNAL LAYERS IN RADAR ECHOGRAMS
FROM A GREENLAND STUDY REGION

Presented by Xin Gao

A candidate for the degree of Master of Science

And hereby certify that in their opinion it is worthy of acceptance.

Dr. Justin Legarsky

Dr. Dominic Ho

Dr. Kathleen Trauth

ACKNOWLEDGEMENTS

A special thanks to my advisor Dr. Legarsky for his guidance, supervision and valuable suggestions. He was always available to answer my questions, teach me the research skill, and share his invaluable ideas with me. Moreover, I cannot thank him enough for the time and patience he spent on revising my thesis. Without his support, I could not have accomplished this.

I would like to thank Dr. Trauth and Dr. Ho for being on my thesis committee and for their effort in reviewing my thesis. I am deeply grateful to Dr. Trauth for the valuable suggestions on my thesis writing and really appreciate the comments Dr. Ho made on my thesis.

I am greatly thankful to my friends, Yonghong Li and Heng Huang for their help during my study.

Finally, I would like to express my deepest appreciation to my loving parents as well as my husband for their constant support and encouragement.

TABLE OF CONTENTS

ACKNOWLEDGEMENTS	ii
LIST OF TABLES	vi
LIST OF FIGURES	vii
ABSTRACT	ix
Chapter	
1. INTRODUCTION	
1.0 Polar Ice Sheets.....	1
1.1 Ice Sheet Mass Balance.....	3
1.1.1 Greenland Ice Sheet.....	3
1.1.2 PARCA.....	4
1.2 Past Climate Record from Ice Core.....	5
1.2.1 Ice Core and Internal Layers.....	5
1.3 Study Focus.....	7
1.4 References.....	8
2. RADAR AND ICE CORE DATA	
2.0 Introduction.....	11
2.1 Coherent Ice Sounding Radar.....	11
2.2 Parameters Associated with PARCA Radar	12
2.2.1 Radar Center Frequency	13
2.2.2 Dielectric Constant for Ice	13
2.2.3 Depth Resolution in Ice.....	14

2.2.4	Range Sample Spacing	15
2.2.5	Radar Data Collection.....	15
2.2.6	Archive Radar Data Format.....	18
2.3	Ice Core Data.....	19
2.3.1	GRIP Ice Core Introduction.....	20
2.3.2	GRIP Ice-core Relationship.....	20
2.4	References.....	21
3. LAYER TRACING METHOD		
3.0	Method Introduction.....	23
3.1	Image Preprocessing.....	24
3.1.1	Average of Columns form Input Image.....	24
3.1.2	Exponential Fit to Average of All Columns.....	25
3.2	Peak-following Methods for Layer Tracing.....	28
3.3	Cross-correlation Method.....	29
3.4	Layer Tracing Implementation.....	31
3.5	Crossover Point Inspection	31
3.6	Flightline Nearest to GRIP Site.....	34
3.7	Internal Layer Continuity.....	36
3.8	References.....	38
4. PROCESSING RESULTS AND DISCUSSION		
4.0	Introduction.....	39
4.1	Traced Layers	39
4.2	Crossover Point Analysis.....	41

4.3	The Age-depth Relationship of Traced Layers.....	42
4.4	Radar Internal Layer Tracing Results.....	44
4.5	References.....	52
5. CONCLUSIONS		
5.0	Summary.....	53
5.1	Future Work.....	53
APPENDIX		
	OVERVIEW.....	54
A	THE LIST OF FILENAMES IN OUR STUDY AREA.....	54
B	THE RESULTS OF TRACED INTERNAL LAYERS.....	56
C	LAYER TRACING FILE FORMATS.....	101

LIST OF TABLES

Table	Page
1. Estimated potential maximum sea-level rise from the total melting of the current Antarctic and Greenland ice sheet	2
2. A summary of the KU ISR system parameters.....	13
3. Summary of archive file parameters for ISR data.....	18
4. Typical Parameters Used in Study	24
5. Crossover Results.....	43
6. Age-Depth Relationship.....	44

LIST OF FIGURES

Page		
1.	Dielectric constant of ice frequency dependence at -10°C	14
2.	PARCA Flight lines with KU ISR data are illustrated on the Greenland map.....	16
3.	Greenland map illustrating the flight lines from the ice divide towards Jakobshavn, Greenland. The location of the Greenland Ice Core Project (GRIP) site is denoted as an asterisk on the map.....	17
4.	A radio echogram example from the vicinity of the GRIP deep drilling site.....	18
5.	An archive A-scope example. The ice thickness is the difference between the ice bottom return value and the ice top return value on the scale shown.....	19
6.	An age-depth relation plot for the GRIP ice core is shown. Years BP is years before 1950.....	21
7.	A diagram is shown of the layer tracing and layer age identification approach...	23
8.	An example of an exponential fit superimposed on a single column.....	27
9.	An example column with the exponential function applied to visually enhance the deeper layers.....	28
10.	A radio diagram with a traced layer. The blue line and the red line illustrate the result using peak-following and cross-correlation methods, respectively.....	30
11.	Flow chart of layer tracing process.....	31
13.	Five internal ice layers of radio echogram from the vicinity of the GRIP deep drilling site are superimposed on a radar echogram along with the ice surface and bedrock	33
14.	Five layers superimposed on radar echogram are shown at crossover point #1....	34

15.	The mapping from spherical coordinates to three-dimensional Cartesian coordinates is shown	35
16.	Long flight lines of study area.....	37
17.	Layer continuity of Line 3.....	38
18.	A part of Greenland map illustrating the flight line of the study area. The location of GRIP ice core is denoted as a yellow circle mark. The diamond dotted line illustrates a portion of ice divide. The crossover points are shown as red asterisks on the map.....	40
19.	Five internal layers are shown on a radar echogram from nearby GRIP.....	41
20.	Thickness of Layer 1.....	46
21.	Thickness of Layer 2.....	47
22.	Thickness of Layer 3.....	48
23.	Thickness of Layer 4.....	49
24.	Thickness of Layer 5.....	50
25.	Thickness to the Bedrock.....	51

TRACING OF INTERNAL LAYERS IN RADAR ECHOGRAMS FROM A GREENLAND STUDY REGION

Xin Gao

Dr. Justin Legarsky, Thesis Supervisor

ABSTRACT

Signs of long-term glaciological processes and past ice sheet structure are preserved in the internal layer signatures of the Greenland ice sheet. Internal layer data have been collected over a considerable portion of the Greenland ice sheet using ice-sounding radar. We traced these layers along thousands of kilometers of flight lines from the ice divide toward Jakobshavn, which is the most active glacier in Greenland. We determined the traced-radar layers age at the GRIP site using the GRIP core age-depth relationship. Since the depth varies spatially for a layer of a specific dated age, an age-depth relationship for each position along the flight lines of this study can be found using the traced layers. We analyzed 31 points where flight lines crossover one another. From the flight line crossover analysis, we found a 9 m maximum difference, which is less than a 1% difference.

Chapter 1 Introduction

1.0 Polar Ice Sheets

Ice sheets were mainly formed from layers of snow that were compressed together for many thousands of years. They cover about 10 percent of the Earth's land area, and interact with the Earth's atmosphere and oceans to influence the global climate system. Therefore, National Aeronautics and Space Administration (NASA) started a polar research project in support of a global climate study in 1991. About 70 percent of the earth's surface is covered with water and the remaining parts are covered by the continental landmasses. Water exists in the natural environment in many forms, such as snow and ice. At high elevations and/or high latitudes, snow that falls to the ground can gradually condense to form thick consolidated ice masses called glaciers. Glaciers, large, thickened masses of ice, accumulate from snowfall over long periods of time. Rising temperatures can shrink polar glaciers and lead to sea level rise. Worldwide measurements from tidal gauges indicate that global mean sea level has risen between 10 and 25 cm (18 cm average) during the last 100 years [Dahl-Jensen, 2000]. The estimated rate of sea level rise over the last century has been on the order of 1-2 mm/yr [Church, 2001]. The contribution of all mountain glaciers to rising sea levels during the last century is estimated to be 0.2 to 0.4 mm/year [Meier, 1984; Zuo *et al.*, 1997; Dyurgerov *et al.*, 1997].

Even small amounts of sea-level rise would have substantial societal and economic impacts through coastal flooding, increased susceptibility to storm surges, groundwater contamination by salt intrusion, and other effects. A 50-cm sea-level rise could inundate up to 50% of North American coastal wetlands [Shriner and Street, 1998]. The costs of responding to it are estimated at between \$20 and \$200 billion in the United States alone [Shriner and Street, 1998]. Therefore, finding the changing information of current ice sheets is important for the overall picture of their role in sea level rise.

The Antarctic and Greenland ice sheets are the largest ice sheets on the earth. The Greenland and Antarctica ice sheets cover 10% of the Earth's land area and contain 77% of the world's freshwater [Khazenie and Price, 1994]. The ice sheets comprise 99% of all the glacier ice on earth [Glacier, 2006]. A significant portion of recent sea-level rise is attributed to thermal expansion of the oceans and the melt of the earth's ice. Both ice sheets contain enough ice to raise sea levels approximately 80 m [Williams and Hall, 1993] (see Table 1-1).

Table 1-1. Estimated potential maximum sea-level rise from the total melting of the current Antarctic and Greenland ice sheets

Ice sheet	Volume (km ³)	Percent of world ice (%)	Maximum surface elevations (m)	Potential maximum sea level rise (m)
Antarctica	30,109,800	91.5	>4200	73.4
Greenland	2,600,000	7.9	>3000	6.5

1.1 Ice Sheet Mass Balance

An ice sheet gains mass through snow and ice accumulation, and loses mass from glacier discharge and melting of surface ice and floating ice shelves. The difference between the ice gain and loss is called the mass balance. A negative balance contributes to global sea-level rise and vice versa. Mass balance may vary seasonally and annually due to different loss and gain. It is determined by the annual precipitation, ablation, drainage at the edges, and iceberg calving. Each year about 8 mm (0.3 inches) of water from the entire surface of the oceans goes into the Antarctica and Greenland ice sheets as snowfall [Legates, 2006]. The changing mass of the great ice sheets of Greenland and Antarctica represents the largest unknown in predictions of global sea-level rise over the coming decades.

1.1.1 Greenland Ice Sheet

The Greenland ice sheet would raise global sea level by about 7 m if it melted completely [Gregory *et al.*, 2004]. It gains mass through snowfall and loses it by surface melting and runoff to the sea, together with the production of icebergs and melting at the base of its floating ice shelves. In recent years, some important changes of the Greenland glaciers have been observed. First, the floating ice shelves of several outlet glaciers have broken up [Joughin *et al.*, 2004]. Second, the flow rates of a number of glaciers have approximately doubled over the past 5 years or so [Joughin *et al.*, 2004]. These effects cause more ice discharge, which increases the mass deficit of the ice sheet from a little

more than 50 km³/year to in excess of 150 km³/year [Rignot, 2006]. The behavior of these outlet glaciers influences the mass balance of the ice sheet.

Jakobshavn (pronounced “yah-cub-SAH-ven”) glacier is a fast moving glacier, draining 6.5 percent of Greenland's ice sheet area [Allen *et al.*, 1997]. Its discharge of ice has nearly doubled since late 2000. The ice stream's speed-up and near-doubling of ice flow from land into the ocean has increased the rate of sea level rise by about 0.06 millimeters (about .002 inches) per year, or roughly 4 percent of the 20th century rate of sea level increase [Joughin *et al.*, 2004]. Therefore, the ice sheets can respond rather dramatically and quickly to climate changes.

1.1.2 PARCA

To determine whether the Greenland ice sheet mass is increasing or decreasing and how this will affect the global sea level, Program for Arctic Regional Climate Assessment (PARCA) was started in 1991 and formally initiated by NASA to measure the elevation and thickness of the Greenland ice sheet [Gogineni *et al.*, 2001].

PARCA conducts a variety of tasks including [Thomas *et al.*, 2001]:

1. Ice thickness and ice surface motion measurements along the same flight lines using Airborne Radar Measurements;
2. Periodic airborne laser-altimetry surveys along precise repeat tracks across all major ice drainage basins;

3. Deducing recent climate history, atmospheric chemistry, and inter annual variability of snow-accumulation rates by detecting shallow ice cores (10 - 200 meters) at many locations;
4. Investigating individual glaciers and ice streams responsible for much of the outflow from the ice sheet; and,
5. Continuously monitoring of crustal motion using Global Positioning System (GPS) receivers at coastal sites.

1.2 Past Climate Record from Ice Cores

The Greenland ice sheet provides a record of the climate covering the previous tens of thousands of years, both chemically (e.g., isotope and particle data) and physically (e.g., in the layering structure of the ice) [Fahnestock *et al.*, 2001]. Layers of snow different in chemistry and texture, fall over the ice sheets throughout each year. Inasmuch the ice forms from the incremental buildup of annual layers of snow, lower layers are older than upper layers. Each layer gives scientists a great amount of useful information about the climate each year. The properties of the ice can then be used to reconstruct a climatic record [Fahnestock *et al.*, 2001].

1.2.1 Ice Core and Internal Layers

The ice cores can provide an annual record of temperature, precipitation, atmospheric composition, volcanic activity, and wind patterns. The thickness of each annual layer is

an indicator of how much snow accumulated at that location during the year. More importantly, the make-up of the snow itself can tell scientists about past temperatures [Fahnestock *et al.*, 2001].

The climate history may be recovered by drilling deep cores in the ice [Fahnestock *et al.*, 2001]. An ice core is a core sample of ice removed from an ice sheet, most commonly from the polar ice caps of Antarctica, Greenland or from high mountain glaciers elsewhere. As a deep ice core may contain ice formed hundreds of thousands of years ago, it provides a vertical timeline of past climates stored in ice sheets and mountain glaciers. Ice cores have been drilled in many locations around the world. Deep cores from Greenland and Antarctica and shorter cores from minor ice caps and glaciers have recorded annual and decadal climate change back to the last interglacial. The Greenland Ice Core Project (GRIP) and Greenland Ice Sheet Project (GISP) cores, each about 3000 m long, were drilled by European and US teams, respectively on the summit of Greenland. Ice cores provide chemical and isotopic records that can be used to determine the age-depth relationship. Many different approaches may be used such as chemical analysis, physical analysis and ice flow modeling [Dansgaard and Johnsen, 1969; Johnsen *et al.*, 1997]. The isochronous nature of internal ice-sheet layers in radar data can be used to correlate age-depth relationships between ice-core sites [Siegert *et al.*, 1998].

A modern ice-sounding radar (ISR) system has been widely accepted and used as an effective technique to determine ice thickness and the depth distribution of internal ice

layers [Fahnestock *et al.*, 2001]. ISR has been flown over Greenland to collect ice-sounding data for the NASA PARCA Program [Tee *et al.*, 1998]. A large amount of flight tracks (more than 100,000 km) were collected by the University of Kansas (KU) ISR from 1993 to 2002 [Fahnestock *et al.*, 2001]. The internal layers in the ice sheet detected from ISR have been observed to be isochronous and relatively coherent along hundreds of kilometers [Jacobel and Hodge, 1995]. A recent method including cross-correlation and peak-following techniques [Fahnestock *et al.*, 2001] has been developed to trace internal ice layers starting from the flight line through the GRIP site and across the ice sheet. Knowledge of the age-depth relationship over large spatial area can be established using GRIP ice core age-depth relationship.

1.3 Study Focus

This study analyzed the internal ice layers measured by ISR from the ice divide toward the Jakobshavn region. The Fahnestock *et al.* [2001] method is used to trace the internal layers from about 4000 km worth of flight lines. The ages of these layers are determined according to information from the GRIP ice core site. These ages are extended along the flight lines in the study area.

1.4 References

- Allen, C., S. Gogineni, B. Wohletz, K. Jezek, and T. Chuah, (1997). "Airborne Radio Echo Sounding of Outlet Glaciers in Greenland," *International Journal of Remote Sensing*, Vol. 18, No. 14, pp. 3103-3107.
- Church, J. A., (2001). "Climate Change: How Fast Are Sea Levels Rising?" *Science*, Vol. 294, No. 5543, pp. 802-803.
- Dahl-Jensen, D., (2000). "The Greenland Ice Sheet Reacts," *Science*, Vol. 289, No. 5478, pp. 404-405.
- Dansgaard, W., and S. J. Johnsen, (1969). "A flow model and a time scale for the ice core from Camp Century, Greenland," *Journal of Glaciology*, Vol. 8, No. 53, pp. 215-223.
- Dowdeswell, J. A., (2006). "The Greenland Ice Sheet and Global Sea-Level Rise," *Science*, Vol. 311, No. 5763, pp. 963-964.
- Dyurgerov, M. and M. Meier, (1997). "Mass balance of mountain and sub-polar glaciers: a new global assessment for 1961-1990," *Arctic Alpine Research*, Vol. 29, pp. 392-401.
- Fahnestock, F., W. Abdalati, S. Luo, and S. Gogineni, (2001). "Internal layer tracing and age-depth-accumulation relationship for the northern Greenland ice sheet," *Journal of Geophysical Research*, Vol. 106, No. D24, pp. 33789-33797.
- Fujita, S., H. Maeno, S. Uratsuka, T. Furukawa, S. Mae, Y. Fujii, and O. Watanabe, (1999). "Nature of radio-echo layering in the Antarctic ice sheet detected by a two-frequency experiment," *Journal of Geophysical Research*, Vol. 104, No. B6, pp. 13013-13124.
- Glacier, (2006). *Britannica Student Encyclopedia*. Retrieved June 16, 2006, from Encyclopædia Britannica: <http://www.britannica.com/ebi/article-65675>
- Gogineni, S., D. Tammana, D. Braaten, C. Leuschen, T. Akins, J. Legarsky, P. Kanagaratnam, J. Stiles, C. Allen and K. Jezek, (2001). "Coherent radar ice thickness measurements over the Greenland ice sheet," *Journal of Geophysical Research (Atmosphere)*, Vol. 106, No. D24, pp. 33,761-33,772.
- Gregory, J. M., P. Huybrechts, and S. C. B. Raper, (2004). "Threatened loss of the Greenland ice-sheet," *Nature*, Vol. 428, No. 6983, p. 616.

- Jacobel, R. W., and S. M. Hodge, (1995). "Radar internal layers from the Greenland summit," *Geophysical Research Letters*, Vol. 22, No. 5, pp. 587-590.
- Johnsen, S. J., H. B. Clausen, W. Dansgaard, N. S. Gundestrup, C. U. Hammer, U. Andersen, K. K. Andersen, C. S. Hvidberg, D. Dahl-Jensen, J. P. Steffensen, H. Shoji, A. E. Sveinbjornsdottir, J. White, J. Jouzel, and D. Fisher, (1997). "The $d^{18}O$ record along the Greenland Ice Core Project deep ice core and the problem of possible Eemian climatic instability," *Journal of Geophysical Research*, Vol. 102, No. C12, pp. 26,397-26,410.
- Joughin, I., W. Abdalati, and M. Fahnestock, (2004). "Large fluctuations in speed on Greenland's Jakobshavn Isbræ glacier," *Nature*, Vol. 432, No. 7017, pp. 535-655.
- Khazenie, N., and R. Price, (1994). "Surface and Atmospheric Remote Sensing: Technologies, Data Analysis and Interpretation," *IEEE Geoscience and Remote Sensing Symposium*, IGARSS '94, 8-12 August, Vol.4, pp. 2252-2256.
- Krabill, W., R. Thomas, K. Jezek, K. Kuivinen, and S. Manizade, (1995). "Greenland ice sheet thickness changes measured by laser altimetry," *Geophysical Research Letters*, Vol. 22, No. 17, pp. 2341-2344.
- Krabill, W., W. Abdalati, E. Frederick, S. Manizade, C. Martin, J. Sonntag, R. Swift, R. Thomas, W. Wright, and J. Yungel, (2000). "Greenland ice sheet: high-elevation balance and peripheral thinning," *Science*, Vol. 289, No. 5478, pp. 428-430.
- Legates, D. R., (2006). *Climate Science: Climate Change and Its Impacts*, National Center for Policy Analysis, Dallas, Texas, NCPA Policy Report No. 285, ISBN 156808157X.
- Meier, M., (1984). "Contribution of small glaciers to global sea level," *Science*, Vol. 226, No. 4681, pp. 1418-1421.
- Rignot, E., and P. Kanagaratnam, (2005). "Changes in the velocity structure of the Greenland Ice Sheet," *Science*, Vol. 311, No. 5763, pp. 986-990.
- Shriner, D. S., and R. B. Street, (1998). "North America," in *The Regional Impacts of Climate Change: An Assessment of Vulnerability*, (R. T. Watson, M. C. Zinyowera, R. H. Moss and D. J. Dokken, Editors), Cambridge University Press, Cambridge.
- Siegert, M. J., R. Hodgkins, and J. A. Dowdeswell, (1998). "A chronology for the Dome C

deep ice-core site through radio-echo layer correlation with the Vostok ice core, Antarctica,” *Geophysical Research Letters*, Vol. 25, No. 7, pp. 1019-1022.

Tee, K. L., W. K. Chong, H. Coulter, T. Akins, S. P. Gogineni, C. Allen, and J. Stiles, (1999). “Radar thickness measurements over the southern part of the Greenland ice sheet: 1998 results,” University of Kansas, Lawrence, Kansas, USA, RSL Technical Report 13720-10.

Available: <http://tornado.rsl.ku.edu/1998.htm>

Thomas, R. H., and PARCA Investigators, (2001). “Program for Arctic Regional Climate Assessment (PARCA): Goals, Key Findings, and Future Directions,” *Journal of Geophysical Research (Atmosphere)*, Vol. 106, No. D24, pp. 33,691-33,706.

Williams, R. S., and D. K. Hall, (1993). *Glaciers: Atlas of Earth observations related to global change*, Cambridge University Press, Cambridge, pp.401-422.

Wigley, T. M. L., (1999). *The Science of Climate Change: Global and U.S. Perspectives*, Pew Center on Global Climate Change, Arlington, Virginia, 48 p.

Zuo, Z., and J. Oerlemans, (1997). “Contribution of glacier melt to sea-level rise since AD 1865: a regionally differentiated calculation,” *Climate Dynamics*, Vol. 13, No. 12, pp. 835-845.

Chapter 2 Radar and Ice Core Data

2.0 Introduction

In our study, internal ice sheet layers were traced and dated using radar sounding data and ice core data from Greenland. The radar data were collected by the University of Kansas using the coherent radar depth sounder [Fahnestock *et al.*, 2001]. The ice core data were collected and analyzed by the GRIP participants [Johnsen *et al.*, 1997].

2.1 Coherent Ice Sounding Radar

Since 1991, the NASA PARCA has sought to accurately estimate the mass balance of the Greenland ice sheet using ground, airborne, and spaceborne measurements. The initial airborne program consisted of a laser altimeter for measuring surface elevation of the ice sheet along selected flight lines. In 1993, the airborne instrumentation suite was expanded to include a radar depth sounder to collect the ice thickness data [Gogineni *et al.*, 2001]. The radar uses pulse compression techniques and coherent integration to obtain the high sensitivity required to measure the thickness of more than 4 km of cold ice [Gogineni *et al.*, 2001]. These systems have been used to collect radar data over the interior and margins of the ice sheet and several outlet glaciers. Advanced signal processing techniques are applied to the radar data. Synthetic-aperture radar (SAR) processing for depth sounding radars [Legarsky *et al.*, 2001] improves the along-track resolution and allows the measurement of ice thickness (> 4 km in cold ice).

The radar system operates at a center frequency of 150 MHz. The radar characteristics and coherent processing system result in a depth resolution of about 4.5 m,

assuming a value of 1.78 for the ice index of refraction [Gogineni *et al.*, 2001; Tee *et al.*, 1999; Fletcher, 1970]. Separate transmit and receive antennas are mounted beneath the left and right wings of the P-3 aircraft platform, with each antenna being a four-element, half-dipole array. The transmitter generates a frequency modulated (chirped) pulse over a bandwidth of 17 MHz with duration of 1.6 μ s, using a surface acoustic wave (SAW) expander. It has a peak power of 200 W. The receiver, protected by a blanking switch during transmits events, compresses the received signal using a SAW filter to a pulse about 60 ns wide. The radar transmitter and receiver are mounted in a rack inside the aircraft and connected to their respective antennas with 20 m-long RF cables and a feed network with a combined loss of about 3 dB. The effective transmit power at the antenna is about 100 W [Gogineni *et al.*, 2001].

The received signal is filtered, amplified, compressed and detected by a low-noise receiver with an overall gain of about 100 dB. The coherent system converts the received signal to baseband in-phase (I) and quadrature (Q) analog outputs. I and Q components of the return signal from the coherent detector are digitized and integrated by two 12-bit A/D converters sampling at a rate of 18.75 MHz. The hardware digital signal processor (DSP) allows for averaging of complex amplitudes ($I + j Q$) and/or averaging of power ($I^2 + Q^2$) before storing on a computer hard disk. Also, the on-board GPS receiver collects aircraft positional data [Gogineni *et al.*, 1998; Gogineni *et al.*, 2001].

2.2 Parameters Associated with PARCA Radar

Table 2-1 lists a summary of the KU ISR system parameters.

Table 2-1. A summary of the KU ISR system parameters.

System Parameter	Value	Units
Radar center frequency	150	MHz
Transmitted bandwidth	17	MHz
Nominal aircraft altitude	500	m
Radar type	Pulse Compression	- -
Transmitted pulse duration	1.6	μ s
Compressed pulse duration, t_{pw}	60	ns
A/D sampling rate, f_{AD}	18.75	MHz
Peak transmit power	200	W
Pulse repetition frequency (PRF)	Selectable	Hz
A/D dynamic range	72	dB
Index of refraction for ice, η_{ice}	1.78	- -
Antenna type	4-element dipoles array	- -
Range sample spacing (per pixel in ice)	4.5	m

2.2.1 Radar Center Frequency

The radar system is designed to operate at a center frequency of 150 MHz. The choice of an appropriate frequency is constrained by the absorption of the electromagnetic waves in ice. VHF frequencies are preferred since the absorption is smaller at these frequencies than microwaves, whereas antennas are smaller and resolution can be better than for lower frequencies [Raju *et al.*, 1990].

2.2.2 Dielectric Constant for Ice

The dielectric constant is the ratio of the electrical conductivity of a dielectric material to free space. The dielectric constant for ice depends on the composition and

structure of the ice. Figure 2-1 schematically shows the dielectric constant of pure ice as a function of frequency. The dielectric constant ϵ_{ice} is approximately 3.17 over a large frequency range from 10 MHz to 1000 GHz [Lamb and Turney, 1949; Fletcher, 1970]. The index of refraction, n_{ice} , is related to the dielectric constant over the microwave region as $\epsilon_{ice} = n_{ice}^2$. Thus, the index of refraction for ice would be about 1.78 [Fletcher, 1970] with an ϵ_{ice} value of 3.17.

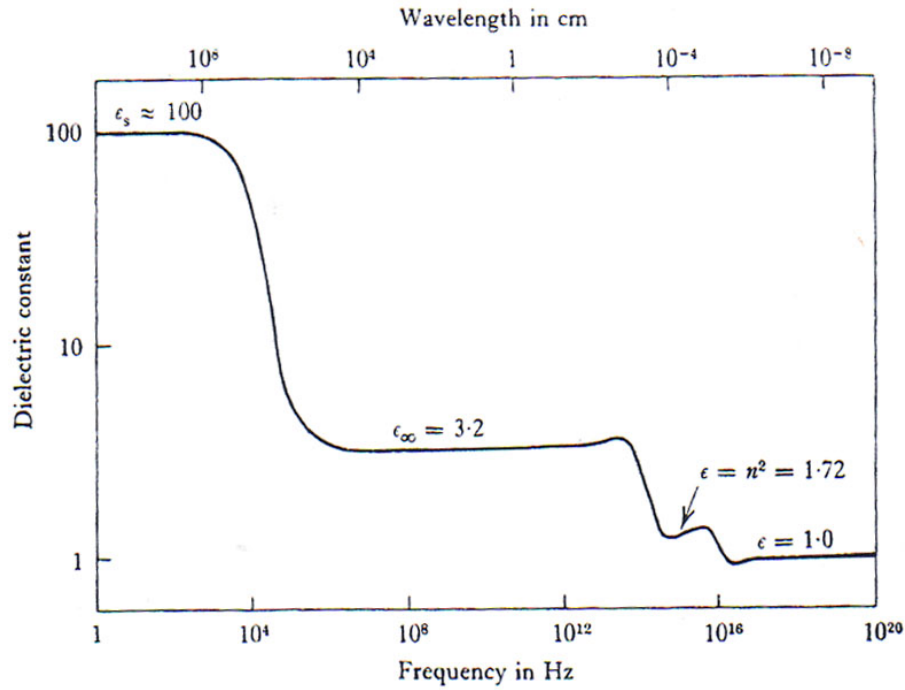


Figure 2-1. Dielectric constant of ice frequency dependence at -10°C [Fletcher, 1970].

2.2.3 Depth Resolution in Ice

The depth resolution in ice is given by [Raju *et al.*, 1990]

$$R_{r,ice} = \frac{ct_{pw}}{2n_{ice}} \quad (2-1)$$

where c is the speed of light in a vacuum ($\sim 3 \times 10^8$ m/s), t_{pw} is the compressed pulse width, and n_{ice} is the ice index of refraction. Thus, the depth resolution is about 5 m.

2.2.4 Range Sample Spacing

The range sample spacing corresponds to the distance traveled in ice depth from one pixel to the next pixel. It is given by

$$R_s = \frac{c}{2n_{ice}f_{AD}} \quad (2-2)$$

where c is the speed of light in a vacuum ($\sim 3 \times 10^8$ m/s), and f_{AD} is the A/D sampling frequency. Thus, the range sample spacing is about 4.5 m.

2.2.5 Radar Data Collection

The PARCA radar system is typically mounted on a NASA P-3 aircraft, which is equipped with a laser altimeter and GPS receiver. As part of PARCA, the NASA P-3 aircraft has flown over the Greenland ice sheet to collect the ice-sounding radar data [Gogineni *et al.*, 2001; Joughin *et al.*, 1996]. The aircraft is usually flown at a 500 m altitude at a speed of about 130 m/s.

Data have been collected over 100,000 km worth of flight lines (see Figure 2-2) [Fahnestock *et al.*, 2001], which covered all major drainage basins and the interior regions in Greenland (e.g., along Greenland's 2000-m elevation contour and the ice sheet summits around 3200 m thick ice). An extensive data set was also obtained for the Jakobshavn outlet glacier, which is considered to have the highest iceberg production of all Greenland glaciers and is a major drainage outlet for a large portion of the western side of the ice sheet [Joughin *et al.*, 2004]. For this study, we analyzed ISR data from the

ice divide toward Jakobshavn, Greenland. Figure 2-3 illustrates on a Greenland map the flight lines used in this study. The GRIP site is denoted as an asterisk on the map.

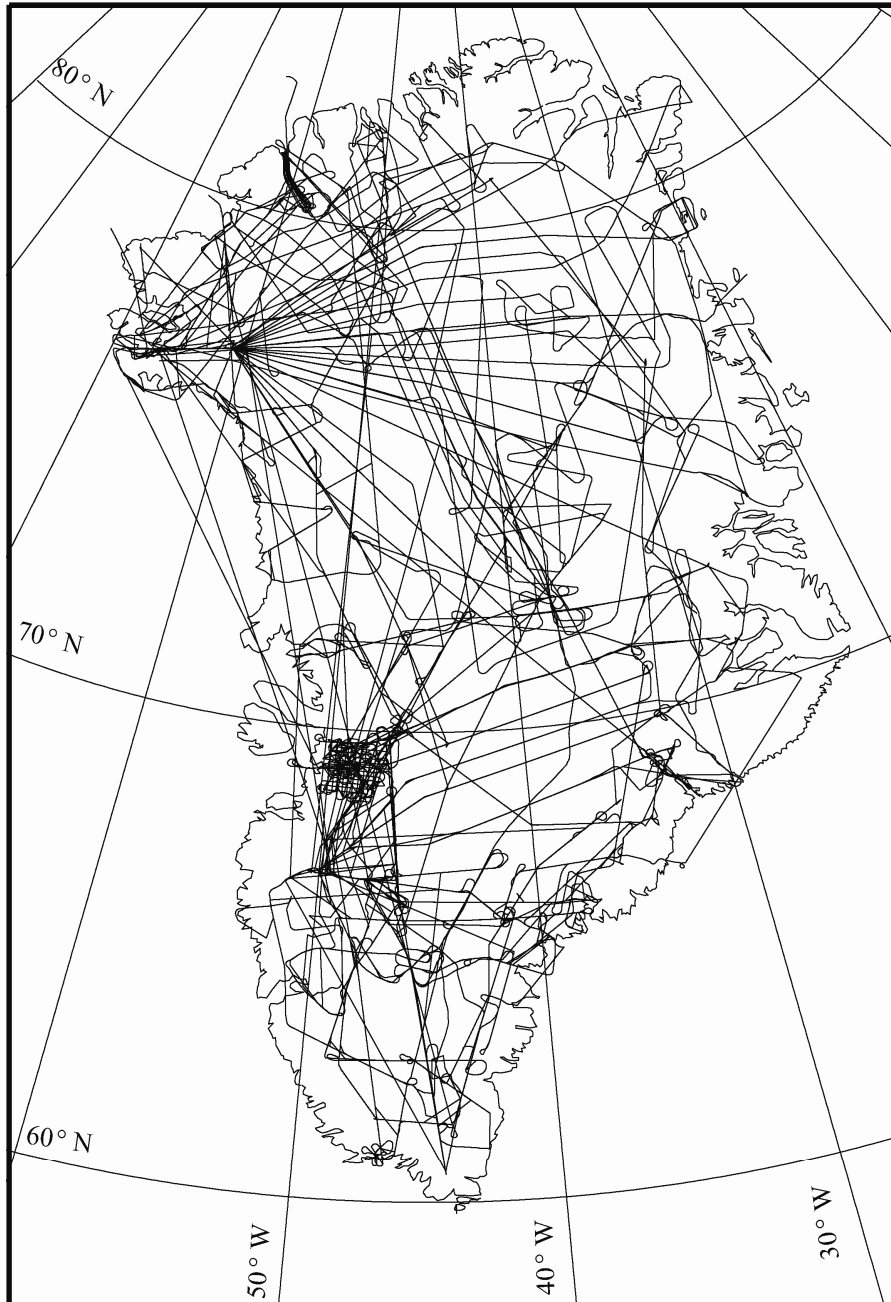


Figure 2-2. PARCA flight lines with KU ISR data are illustrated on the Greenland map.

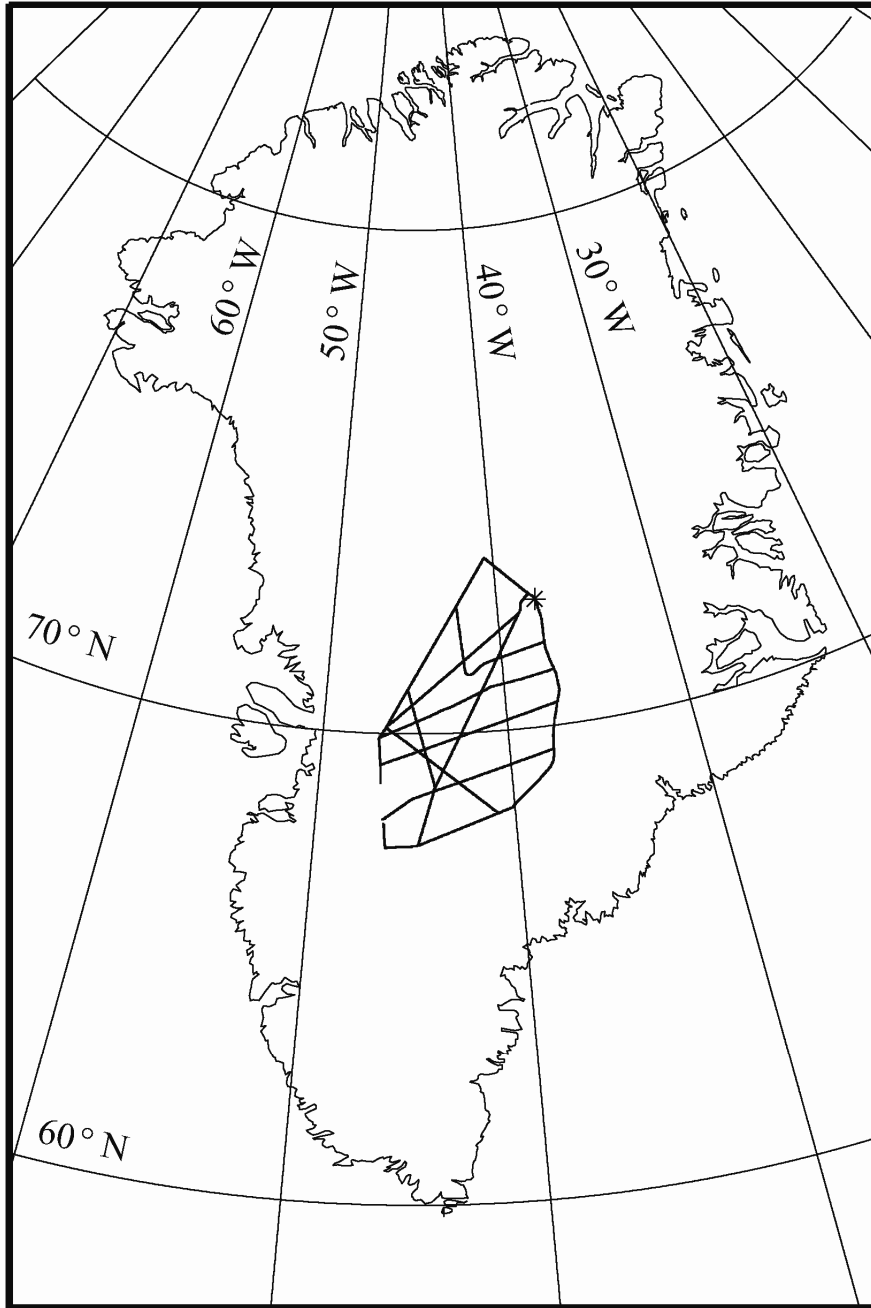


Figure 2-3. Greenland map illustrating the flight lines from the ice divide towards Jakobshavn, Greenland. The location of the Greenland Ice Core Project (GRIP) site is denoted as an asterisk on the map.

2.2.6 Archive Radar Data Format

From the Greenland PARCA missions, radar echograms and ice thickness information are archived on the KU server [Tee *et al.*, 1999]. Figure 2-4 illustrates an example radio echogram. Table 2-2 summarizes the available parameters stored in the archived files.

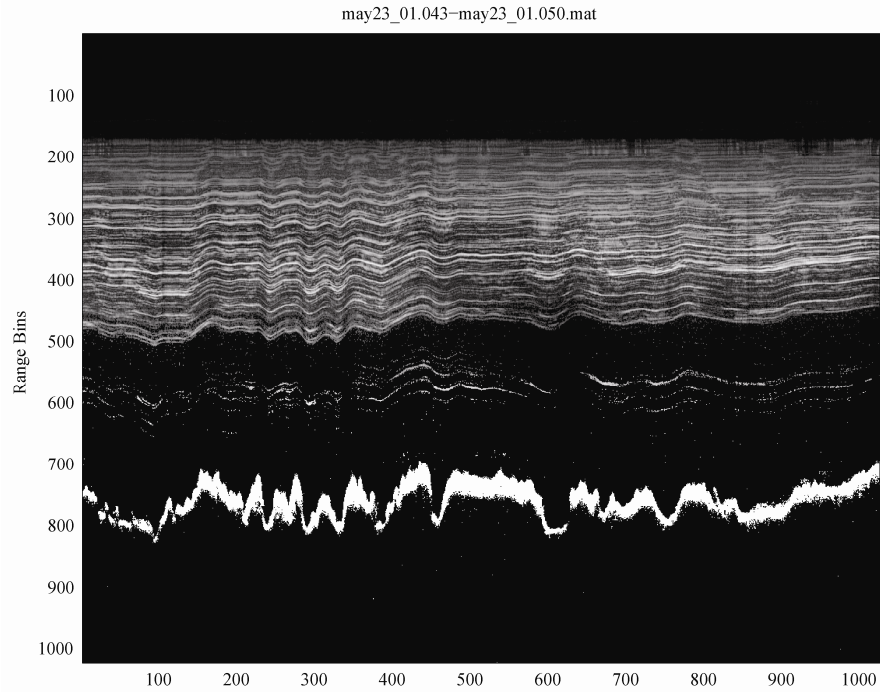


Figure 2-4. A radio echogram example from the vicinity of the GRIP deep drilling site.

Table 2-2. Summary of archive file parameters for ISR data.

File Variable	Name	Unit
A	Radar Echogram	α Volts
lon	Longitude Coordinate for each radar sample	$^{\circ}$ W
lat	Latitude Coordinate for each radar sample	$^{\circ}$ N
top	Ice surface location for each radar sample	Pixels
bot	Bedrock location for each radar sample	Pixels

Each archive file typically consists of 1000 records (or 1000 stacked A-scopes). The location (i.e., latitude and longitude from GPS) at the time of collection is given for each record. Figure 2-5 shows an example of an A-scope signal. The ice thickness is calculated by multiplying the difference in pixels (between the bottom pixel and top pixel locations) by the range sample spacing (i.e., 4.5 m).

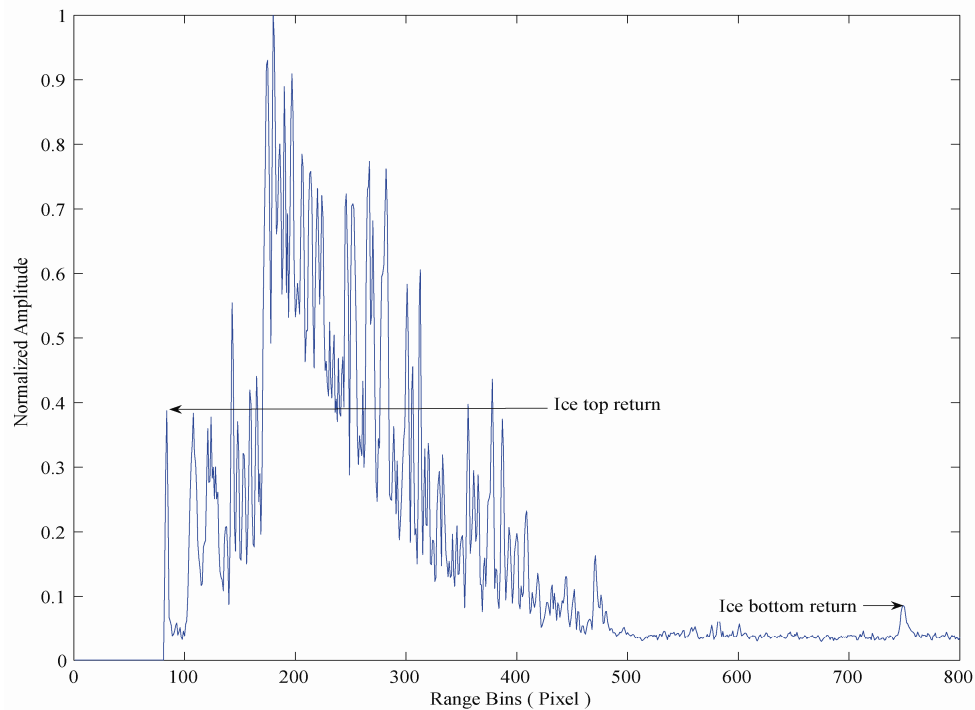


Figure 2-5. An archive A-scope example. The ice thickness is the difference between the ice bottom return value and the ice top return value on the scale shown.

2.3 Ice Core Data

Polar ice cores contain a record of the past atmosphere (e.g., temperature, precipitation, gas content, chemical composition, and other properties). Deep cores from the Greenland ice sheet provide information about the past climate conditions and past environmental conditions. Annual layers from snow deposition can be counted along the

length of the ice core. As snow is compressed to ice near the surface, samples of atmospheric air are trapped as tiny bubbles in the ice. Ancient atmospheres may therefore be studied by analyzing the air in the bubbles. Other characteristics from the past (e.g. temperature, precipitation and storminess) can be estimated by studying the ice and its impurities [Dahl-Jensen *et al.*, 1997; Andersen *et al.*, 2006].

2.3.1 GRIP Ice Core Introduction

The GRIP drilled a 3029 m long ice core from Central Greenland Summit from 1989 to 1992 at the coordinates $72^{\circ} 35' N$, $37^{\circ} 38' W$ [Dahl-Jensen *et al.*, 1997]. The GRIP site is denoted as an asterisk in Fig. 2-3. The age of the ice is estimated to be greater than 200,000 years.

2.3.2 GRIP Ice-core Relationship

The GRIP researchers published the age-depth relationship of the GRIP ice core [Johnsen *et al.*, 1997]. Parameters used to date the core include electrical conductivity measurements (ECM), dust, nitrate and ammonium, which all give excellent annual layers. The age-depth relationship data for the ice core are also archived at the National Snow and Ice Data Center in Boulder, Colorado. Figure 2-6 illustrates the age-depth relationship for the GRIP ice core. The timescale is in years before present (yr BP) where year 0 BP refers to the northern hemisphere summer of the year 1950 A.D. Using the ice-layer tracing techniques discussed in the next chapter, we can trace internal layers in the radar data along flight lines in Greenland. Inasmuch as the internal layers are isochronal nature, each internal layer in the radar data at GRIP can be dated using the GRIP ice core age-depth relationship.

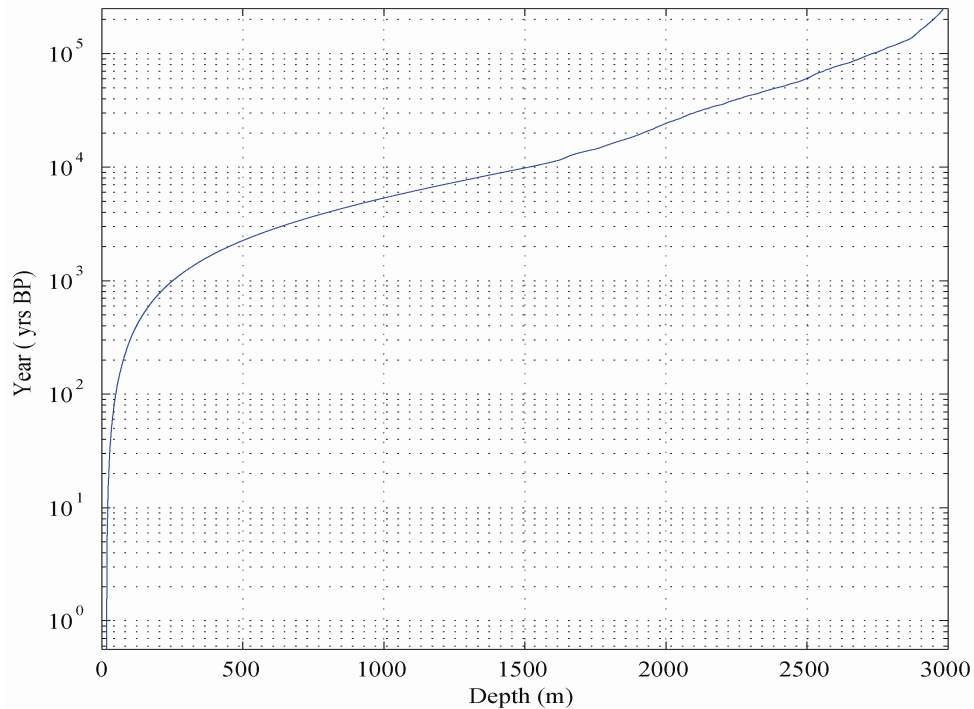


Figure 2-6. An age-depth relation plot for the GRIP ice core. Years BP is years before 1950.

2.4 References

- Andersen, K. A., and GRIP participants, (2006). "North Greenland Ice Core Project," Department of Geophysics, Niels Bohr Institute of the University of Copenhagen, available: www.gfy.ku.dk/~www-glac/ngrip/index_eng.htm.
- Dahl-Jensen, D., N. S. Gundestrup, K. Keller, S. J. Johnsen, S. P. Gogineni, C. T. Allen, T. S. Chuah, H. Miller, S. Kipfstuhl, and E. D. Waddington, (1997). "A search in North Greenland for a new ice-core drill site," *Journal of Glaciology*, Vol. 43, No. 144, pp. 300-306.
- Fahnestock, M., W. Abdalati, S. Luo, and S. Gogineni, (2001). "Internal layer tracing and age-depth-accumulation relationship for the northern Greenland ice sheet," *Journal of Geophysical Research*, Vol. 106, No. D24, pp. 33789-33797.
- Fletcher, N.H., (1970). *The chemical physics of ice*, Cambridge, Cambridge University Press.
- Gogineni, S., T. Chuah, C. Allen, K. Jezek, and R.K. Moore, (1998). "An improved coherent radar depth sounder," *Journal of Glaciology*, Vol. 44, No. 148, pp. 659-669.

- Gogineni, S., D. Tammana, D. Braaten, C. Leuschen, T. Akins, J. Legarsky, P. Kanagaratnam, J. Stiles, C. Allen, and K. Jezek, (2001). "Coherent radar ice thickness measurements over the Greenland ice sheet," *Journal of Geophysical Research*, Vol. 106, No. D24, pp. 33761-33772.
- Hodge, S. M., D. L. Wright, J. A. Bradley, R. W. Jacobel, N. Skou, and B. Vaughn, (1990). "Determination of the surface and bed topography in Central Greenland," *Journal of Glaciology*, Vol. 36, No. 122, pp. 17-30.
- Johnsen, S. J., H. B. Clausen, W. Dansgaard, N. S. Gundestrup, C. U. Hammer, U. Andersen, K. K. Andersen, C. S. Hvidberg, D. Dahl-Jensen, J. P. Steffensen, H. Shoji, A. E. Sveinbjornsdottir, J. White, J. Jouzel, and D. Fisher, (1997). "The $d^{18}O$ record along the Greenland Ice Core Project deep ice core and the problem of possible Eemian climatic instability," *Journal of Geophysical Research*, Vol. 102, No. C12, pp. 26,397-26,410.
- Joughin, I., R. Kwok, and M. Fahnestock, (1996). "Estimation of ice-sheet motion using satellite radar interferometry: method and error analysis with application to Humboldt Glacier, Greenland," *Journal of Glaciology*, Vol. 42, No. 142, pp. 564-575.
- Joughin, I., W. Abdalati, and M. Fahnestock, (2004). "Large fluctuations in speed on Greenland's Jakobshavn Isbræ glacier," *Nature*, Vol. 432, No. 7017, pp. 535-655.
- Lamb, J., and A. Turney, (1949). "Electrical properties of ice at 1.25 cm wavelength," *Proceedings of Physics Society, London*, Vol. B, No. 62, pp. 272-273.
- Legarsky, J. J., P. Gogineni and T. L. Akins, (2001). "Focused synthetic-aperture radar processing of ice-sounder data collected over the Greenland ice sheet," *IEEE Transactions on Geoscience and Remote Sensing*, Vol. 39, No. 10, pp. 2109-2117.
- Matzler, C., and U. Wegmuller, (1987). "Dielectric properties of freshwater ice at microwave frequencies," *Journal of Physics D: Applied Physics*, Vol. 20, No. 12, pp. 1623-1630.
- Raju, G., W. Xin, and R. K. Moore, (1990). "Design, development, field observations, results of the Coherent Antarctic Radar Depth Sounder (CARDS) of the University Kansas, U.S.A.," *Journal of Glaciology*, Vol. 36, No. 123, pp. 247-254.
- Tee, K. L., W. K. Chong, H. Coulter, T. Akins, S. P. Gogineni, C. Allen and J. Stiles, (1999). "Radar thickness measurements over the southern part of the Greenland ice sheet: 1998 results," University of Kansas, Lawrence, Kansas, USA, RSL Technical Report 13720-10, Aug. 1999. Available: tornado.rsl.ku.edu/1998.htm

Chapter 3 Layer Tracing Methods

3.0 Method Introduction

The internal layering in the ice sheet has been shown to be mainly isochronous and relatively coherent along hundreds of kilometers [Jacobel and Hodge, 1995]. By tracing the layers away from the GRIP site with its reported age-depth relationship, the ages of the layers can be determined far from the GRIP site. The layer tracing process is semi-automatic [Fahnestock *et al.*, 2001]. We traced the internal layers along thousands of kilometers of flight lines from the ice divide towards Jakobshavn. The first step of the processing is the enhancement of each echogram to visually optimize the radio image display. Then, cross-correlation and peak-following techniques are used to trace the internal layers. A diagram of the overall approach (i.e., layer tracing and age identification) is illustrated in Figure 3-1. In this chapter, we mainly discuss the layer tracing methods, which include image preprocessing, layer tracing by peak following, and cross-correlation layer tracing. The typical parameters used in the study is shown in Table 3-1. This chapter also includes a discussion of the analysis of flightline crossover points. The ages of the layers are discussed in Chapter 4.

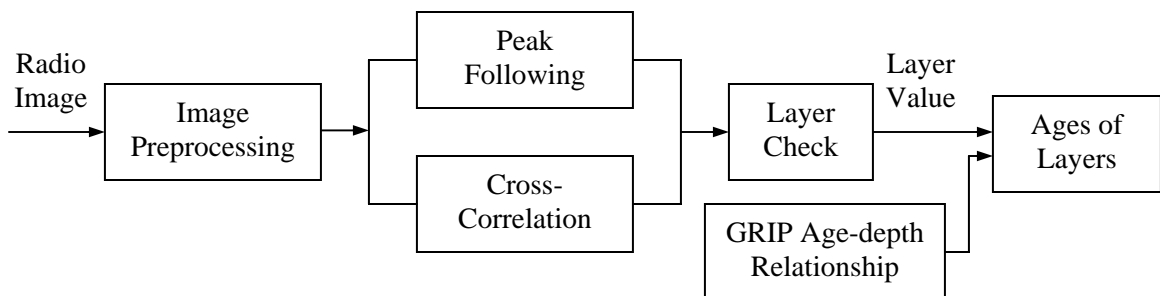


Figure 3-1. A diagram of the layer tracing and layer age identification approach.

Table 3-1. Typical Parameters Used in Study.

Description	Value	Units
Ice index of refraction	1.78	-
Maximum no. of bits used in the A/D converter	12	bits
Sampling rate of A/D converter	18.75	MHz
Lower pixel in threshold computation window, x_{nl}	825	pixels
Upper pixel in threshold computation window, x_{nh}	1024	pixels
Peak parameter search pixels about center	+/-2	pixels
Correlation parameter search pixels about center	+/-9	pixels
Correlation parameter reference pattern	3	pixels

3.1 Image Preprocessing

The purpose of image preprocessing in this study is to optimize the radio image display by applying an exponential normalization [Fahnestock *et al.*, 2001]. Since the strength of the radar return signal diminishes near exponentially with depth due to beam divergence and energy losses in the medium, the return signals from the deeper ice are often weaker than those from the shallower regions. To visually enhance the deeper layers, the image preprocessing consists of three main steps: 1) find an average of the columns of the input image; 2) apply an exponential fit over the desired depth range in ice to the average of all columns; and, 3) normalize the radar echogram using the exponential fit to values above a threshold.

3.1.1 Average of Columns from Input Image

To help identify the layers, which may not be clearly seen, normalized average values of columns from the input image are calculated at the beginning of preprocessing. A radar echogram, A , can be described by an m rows by n columns matrix (typically m is 1024 and n is 1024), which is the amplitude of the complex signal (i.e., A equal $\sqrt{I^2+Q^2}$) where I is the in-phase component and Q is the quadrature component).

$$A = \begin{bmatrix} a_{11} & a_{12} & \cdots & \cdots & a_{1n} \\ a_{21} & a_{22} & \cdots & \cdots & a_{2n} \\ \vdots & \vdots & \vdots & \vdots & \vdots \\ \vdots & \vdots & \vdots & \vdots & \vdots \\ a_{m1} & a_{m2} & \cdots & \cdots & a_{mn} \end{bmatrix}. \quad (3-1)$$

A_i is the i th column of A , that is

$$A = [A_1 \quad A_2 \quad A_3 \quad \cdots \quad A_n]. \quad (3-2)$$

First, A_i is normalized by the max possible value (e.g., 2^{12} based on 12-bit analog to digital converter for each channel, I and Q) [Gogineni *et al.*, 1998] based on the number of A/D converter bits per channel, $numbits$. Thus, each column of the normalized radar echogram is given by

$$A_{i_{nor}} = \frac{A_i}{\sqrt{(2^{numbits})^2 + (2^{numbits})^2}}. \quad (3-3)$$

The normalized average values, $A_{i_{na}}$, of A_i are calculated as

$$A_{i_{na}} = \frac{1}{n} \sum_{i=1}^n A_{i_{nor}}, \quad (3-4)$$

3.1.2 Exponential Fit to Average of All Columns

An exponential function is applied to each column of the normalized radar echogram, $A_{i_{nor}}$, to visually enhance the deeper layers. An exponential function is fit to the normalized average values, $A_{i_{na}}$, over a window of depths (i.e. lowest depth value, d_1 , to the highest depth value, d_2). For our study, the depth values of d_1 and d_2 are 400 m (89 pixels) and 2000 m (445 pixels), respectively [Fahnestock *et al.*, 2001]. Since the ice surface is not normally at a row 1 or a constant row, the ice surface reference is determined by calculating the average value of the top pixel locations ($x_{top\ avg}$) in the

image. Thus, the exponential fit is determined from the windowed values between the lowest pixel number, x_{lf} , and highest pixel number, x_{hf} , in relationship to the surface as

$$x_{lf} = x_{top\ avg} + \frac{d_1}{4.5}, \quad (3-5)$$

$$x_{hf} = x_{top\ avg} + \frac{d_2}{4.5}. \quad (3-6)$$

Thus, the exponential fit will be applied to windowed values over the pixel range,

$$x_f = x_{lf}, x_{lf} + 1, \dots, x_{hf} - 1, x_{hf}. \quad (3-7)$$

The exponential and natural logarithm forms are given by the following equations:

$$A_{ina}(x_f) = ae^{bx_f}, \quad (3-8)$$

$$\ln(A_{ina}(x_f)) = bx_f + \ln(a). \quad (3-9)$$

where a is the exponential fit amplitude factor and b is the exponential fit exponent factor. Inasmuch as the natural logarithm form (Eq 3-9) can be expressed in the *slope-intercept* form of a line, its slope is b and its *intercept* is $\ln(a)$. Given $A_{ina}(x_f)$ and x_f , the exponential fit variables (i.e. a and b) are calculated from the *slope* (i.e., slope equals b) and *intercept* (i.e., a equals $e^{\text{intercept}}$).

After expressing indices, V_x , for each column as a vector,

$$V_x = \begin{bmatrix} 1 \\ 2 \\ 3 \\ \vdots \\ m \end{bmatrix}, \quad (3-10)$$

the fit for an average column using the exponential function may be written as,

$$V_{\text{exp}} = ae^{bV_x}. \quad (3-11)$$

To remove the average exponential fit from each column, $A_{i\text{ nor}}$, that is above a threshold, $N_{\text{threshold}}$, the column is divided (i.e. element by element manner) by the V_{exp} ; therefore, the normalized and exponential removed radar echogram columns are found as

$$D = A_{i\text{ nor exp}} = \begin{cases} \frac{A_{i\text{ nor}}}{V_{\text{exp}}} & \text{for elements} > N_{\text{threshold}} \\ A_{i\text{ nor}} & \text{for elements} \leq N_{\text{threshold}} \end{cases} \quad (3-12)$$

where the threshold is defined by the average of the values in the threshold computation window multiplied by $\sqrt{2}$ (i.e., $20 * \log_{10}(\sqrt{2})$ is about a 3 dB signal-to-noise ratio (SNR))

$$N_{\text{threshold}} = \frac{\sqrt{2}}{(x_{nh} - x_{nl} + 1)} \sum_{\substack{\text{rows} \\ x_{nl} \text{ to } x_{nh}}} A_{i\text{ na}} . \quad (3-13)$$

Figure 3-2 shows an example of an exponential fit superimposed on a single column.

Figure 3-3 illustrates the column with the exponential function applied as in (Eq 3-12) to visually enhance the deeper layers.

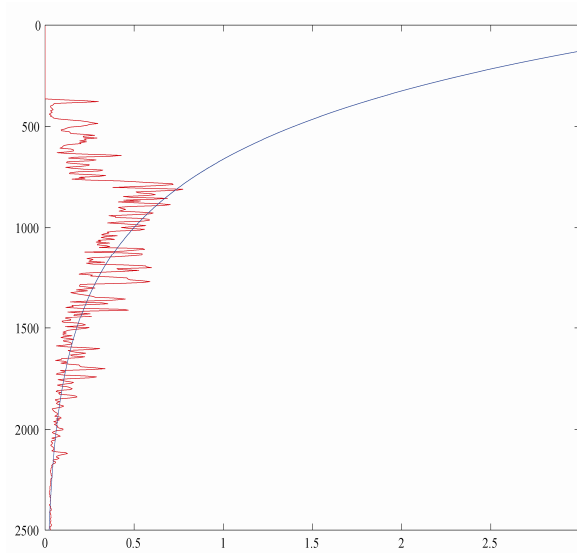


Figure 3-2. An example of an exponential fit superimposed on a single column.

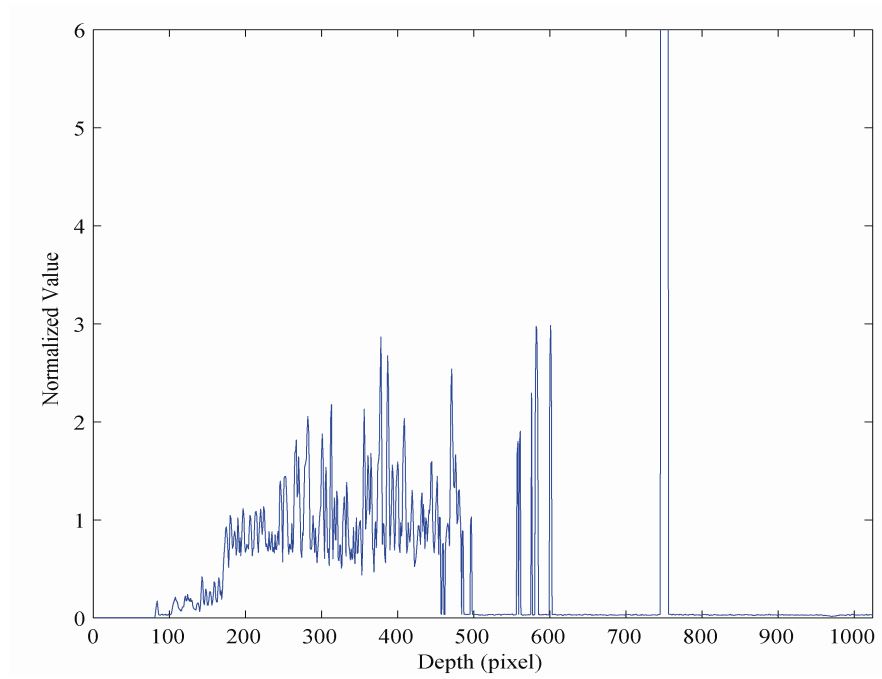


Figure 3-3. An example column with the exponential function applied to visually enhance the deeper layers.

3.2 Peak-following Method for Layer Tracing

A reflecting internal layer often manifests as a peak in the vertical profile (i.e. column) from a radar echogram. A layer in a vertical profile is traced horizontally (i.e. along the flightline) throughout the radar echogram. The preprocessing output radar echogram, D , may be written as

$$D = \begin{bmatrix} d_{11} & d_{12} & \cdots & \cdots & d_{1n} \\ d_{21} & d_{22} & \cdots & \cdots & d_{2n} \\ \vdots & \vdots & \vdots & \vdots & \vdots \\ \vdots & \vdots & \vdots & \vdots & \vdots \\ d_{m1} & d_{m2} & \cdots & \cdots & d_{mn} \end{bmatrix}. \quad (3-14)$$

To begin a layer tracing, we select a point by placing and clicking the cursor on or near a visually observable peak [Fahnestock *et al.*, 2001]. The peaking-following

method is used to search the nearby coordinates in the same column and identify the maximum value (i.e., usually within ± 2 pixels). The coordinates (m, n) of the selected point are recorded in position 1 for a peak layer p (i.e., L_{p1}) in the peak layer p vector, L_p . For the next column, the coordinates (m, n) of the previous selected point are used as the initial guess; moreover, the coordinates for the current column (i.e., L_{p2}) are found by searching the nearby coordinates in the same column and identifying the maximum value (i.e. usually within ± 2 pixels). The same procedure is continued until the coordinates of n th column (i.e., L_{pn}) are found. Thus, the peak layer vector, L_p , may be written as

$$L_p = [L_{p1} \ L_{p2} \ \cdots \ L_{p(n-1)} \ L_{pn}], \quad (3-15)$$

3.3 Cross-correlation Method

To begin a layer tracing, we select a point by placing and clicking the cursor on or near a visually observable peak [Fahnestock *et al.*, 2001]. The cross-correlation method is used to search the nearby coordinates with a window (typically within ± 1 pixel of the peak) in the same column and identify the maximum cross-correlation value (i.e., usually within a Hanning multiplied larger window of ± 9 pixels). The coordinates (m, n) of the selected point are recorded in position 1 for a cross-correlation layer p (i.e., C_{p1}) in the cross-correlation layer p vector, C_p . For the next column, the coordinates (m, n) of the previously selected point are used as the initial guess; moreover, the coordinates for the current column (i.e., C_{p2}) are found by searching the nearby coordinates in the same column and identifying the maximum cross-correlation value (i.e., usually within ± 9

pixels). The same procedure is continued until the coordinates of n th column (i.e. C_{pn}) are found. Thus, the cross-correlation layer vector, C_p , may be written as

$$C_p = [C_{p1} \ C_{p2} \ \dots \ C_{p(n-1)} \ C_{pn}]. \quad (3-16)$$

Figure 3-4 illustrates an example of a traced layer, in which blue and red lines denote the results using the peak-following and cross-correlation methods, respectively. We visually inspect and choose which one appears to better trace the layer [Fahnestock *et al.*, 2001].

For layer tracing, the peak-following technique is straightforward and effective in areas where a peak is distinctly visible. The correlation technique is more appropriate in situations where the peak fades, but the overall layer pattern still remains preserved [Fahnestock *et al.*, 2001].

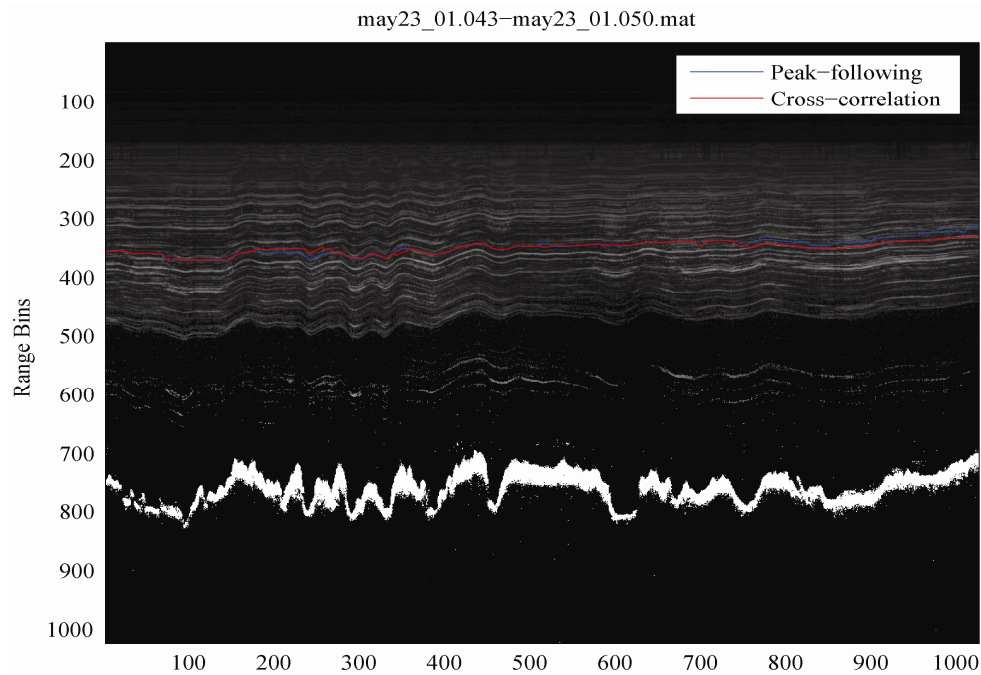


Figure 3-4. A radio diagram with a traced layer. The blue line and the red line illustrate the result using peak-following and cross-correlation methods, respectively.

3.4 Layer Tracing Implementation

The layer tracing methods were implemented in Matlab. A flow chart of the Matlab implementation is shown in Figure 3-5.

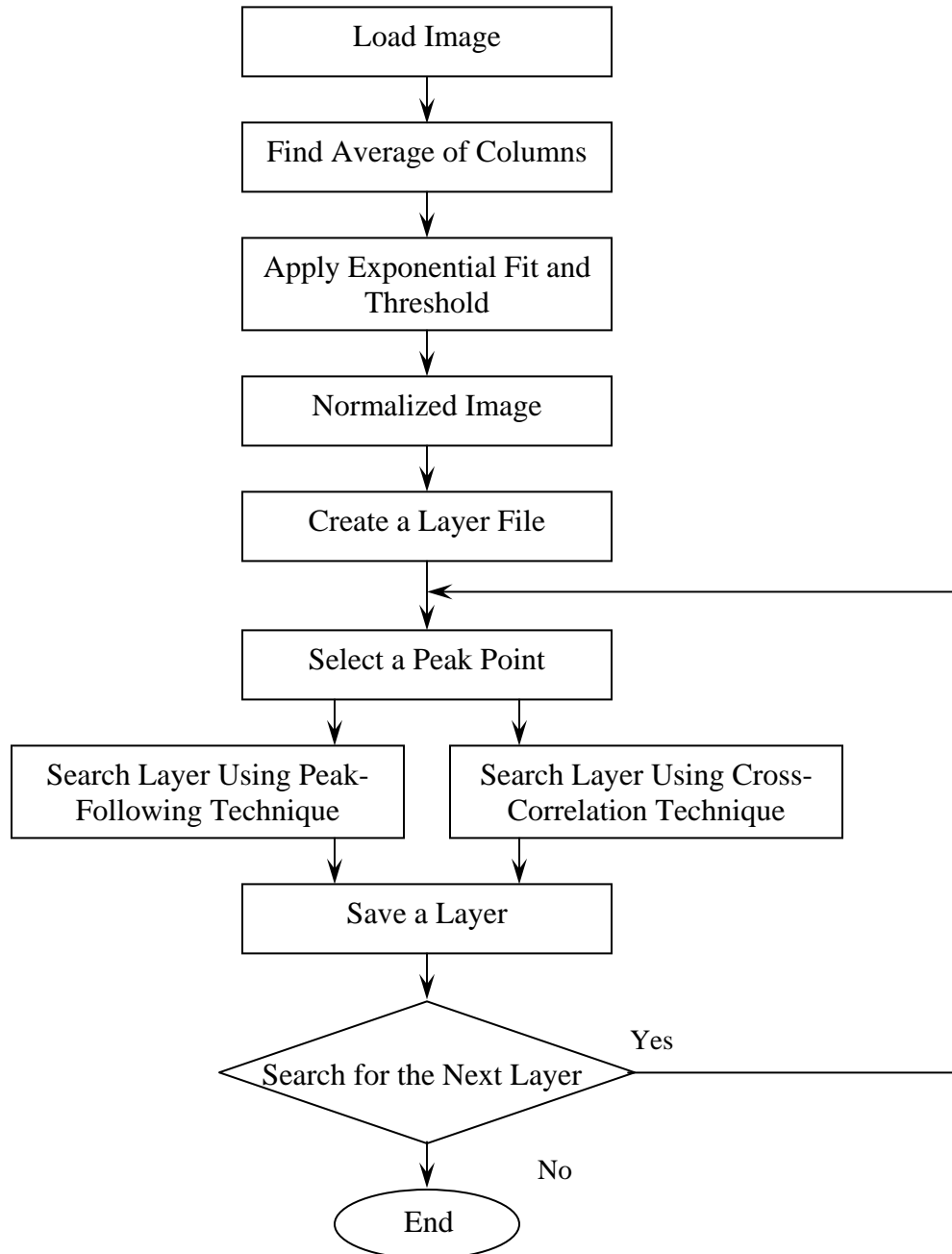


Figure 3-5. Flow chart of layer tracing process

Graphical-interface-driven Matlab routine software is used to implement the layer tracing process. At the beginning of layer tracing, an image file is loaded and preprocessed. The exponential fit is applied to enhance the deeper layer for layer tracing. The normalized average values of columns from the input image are calculated [Fahnestock *et al.*, 2001]. Each layer is processed horizontally throughout the echogram. The software processes the radio echogram of each file along the flight line using peak-following and cross-correlation techniques.

The layer tracing results are visually inspected to insure the layer trace actually lies on a layer in the radar echogram. An incorrect layer trace can occur for a number of reasons [Fahnestock *et al.*, 2001] (e.g., warmer ice [i.e., increased signal absorption in ice] makes it harder to distinguish the layer from its surrounding environment). If the layer can be seen visually and the layer tracing produces incorrect results, then layer locations are picked by hand (i.e., using the mouse input and spline function in Matlab). Once the layer results reasonably match the visible layer line, the results are saved. Additional visual inspections are discussed in the next section. Figure 3-6 shows an image with five layers, the ice surface and the bedrock in the vicinity of the GRIP deep drilling site.

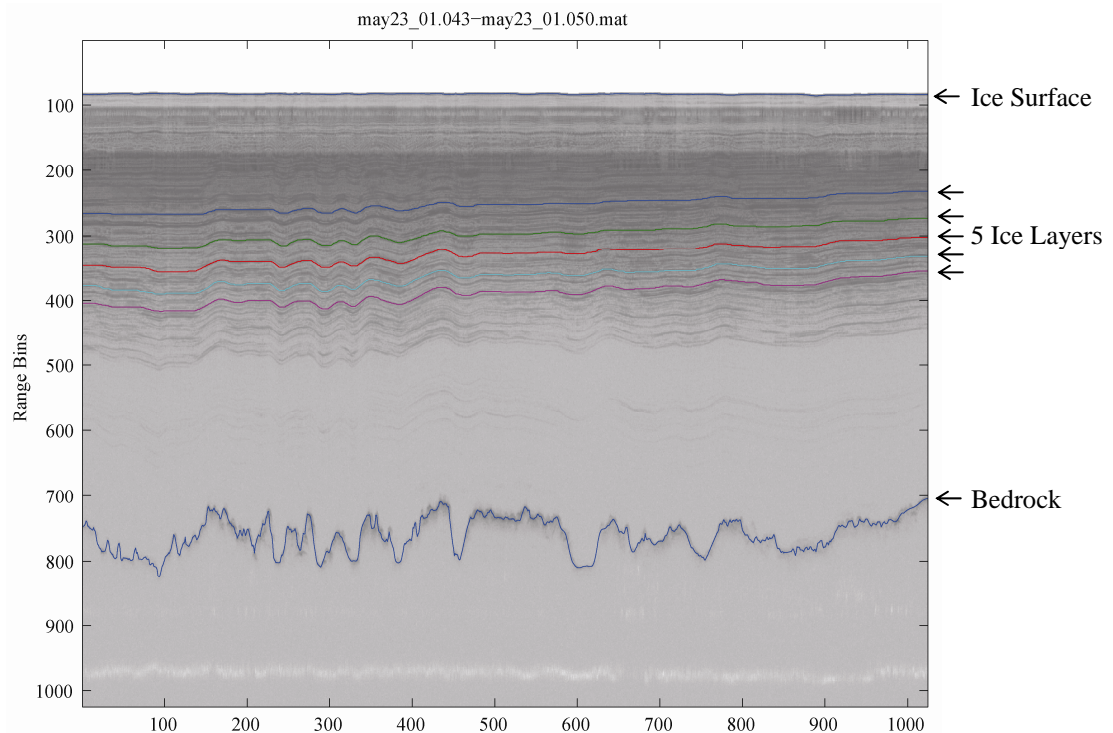


Figure 3-6. Five internal ice layers of radio echogram from the vicinity of the GRIP deep drilling site are superimposed on a radar echogram along with the locations of the ice surface and bedrock

3.5 Crossover Point Inspection

A crossover point occurs when flight lines intersect each other. At a crossover point, the top and bottom pixel values may differ for each flight for various reasons (e.g. the aircraft altitude may slightly differ or the time delay is different before the first A/D sample is collected). To inspect the layer tracing results, the radar images at crossover points are shifted such that the ice surfaces for both images are at the same row. The user visually inspects the shifted images to insure that the layer in one image has been traced to the corresponding layer in the second image. An example inspection of the layers at a

crossover point can be seen in Figure 3-7. The yellow line denotes the location of crossover point #1 (37.406°W, 71.704°N).

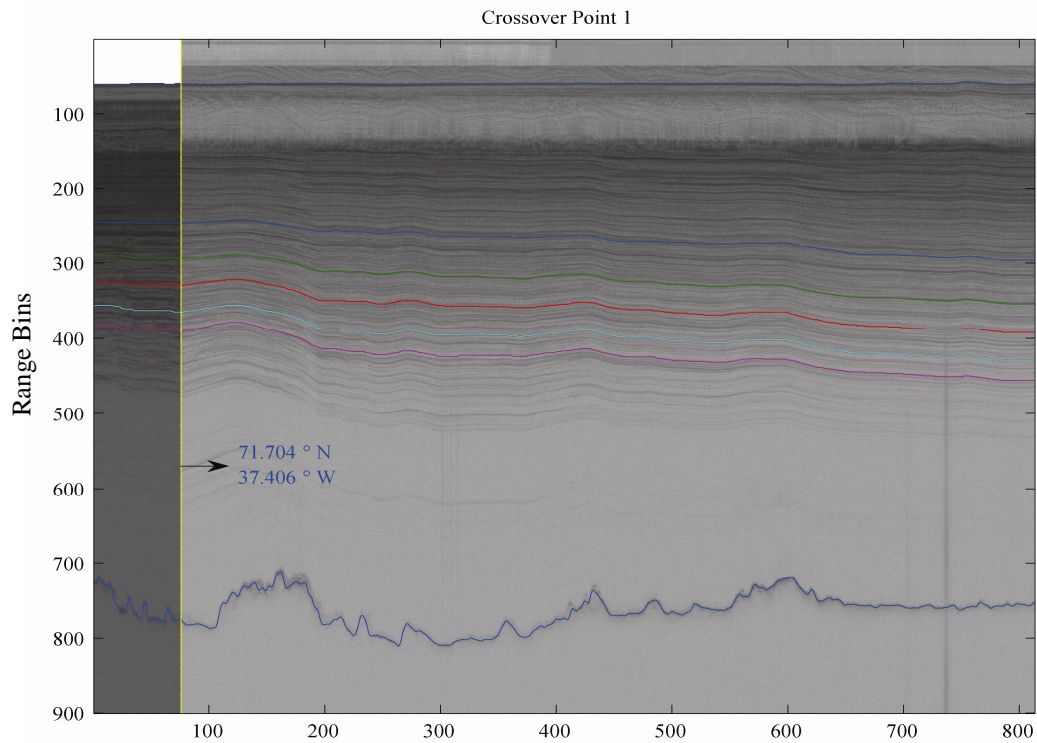


Figure 3-7. Five ice layers superimposed on radar echogram are shown at crossover point #1.

3.6 Flight Line Nearest to GRIP Site

The isochronous nature of the layers and the dating results provided by the GRIP ice core allow us to determine the age-depth relationship in our study area [Fahnestock *et al.*, 2001]. The flight line nearest to the GRIP site is found by calculating the shortest distance between GRIP ice core and each point on the nearby flight lines. To calculate the distance between two points on the earth, the points of spherical coordinate arrays should be transformed to the corresponding points of Cartesian or xyz coordinates. For example, P1 (θ_1, φ_1, R) and P2 (θ_2, φ_2, R) are two points on the earth. θ_1 and θ_2 are longitudes of the corresponding points and φ_1, φ_2 , are the latitudes. The unit of the angles is radians.

The Earth is a rough sphere with the average radius of about 6370 km. Figure 3-8 shows θ_1 , φ_1 and R of P1.

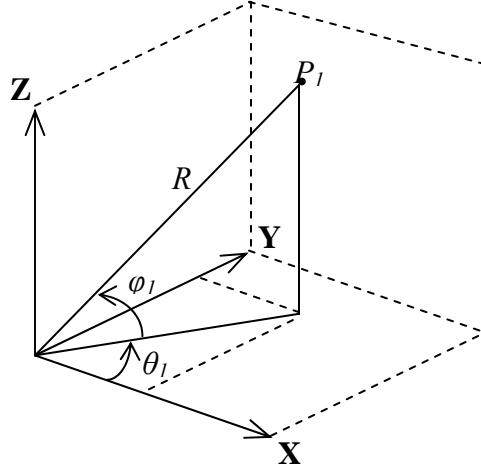


Figure 3-8. The mapping from spherical coordinates to three-dimensional Cartesian coordinates is shown.

The xyz coordinates of P1 are found as follows

$$x_1 = R * \cos(\varphi_1) * \cos(\theta_1), \quad (3-17)$$

$$y_1 = R * \cos(\varphi_1) * \sin(\theta_1), \quad (3-18)$$

$$z_1 = R * \sin(\varphi_1). \quad (3-19)$$

Also, the xyz coordinates of P2 are found as follows

$$x_2 = R * \cos(\varphi_2) * \cos(\theta_2), \quad (3-20)$$

$$y_2 = R * \cos(\varphi_2) * \sin(\theta_2), \quad (3-21)$$

$$z_2 = R * \sin(\varphi_2). \quad (3-22)$$

The distance, d_{12} , between P1 and P2 in the xyz coordinates can be obtained by the following equation.

$$d_{12} = \sqrt{(x_2 - x_1)^2 + (y_2 - y_1)^2 + (z_2 - z_1)^2}. \quad (3-23)$$

The flight line of May 23, 2001 is the closest to the GRIP site. Beginning from this line, the age-depth relationship of all the flight lines in our study area may be found. The total ISR data covers more than 4000 km of flight lines over this region. All these flight lines form an interconnected web over the study area. The flight lines have a total of 31 crossover points. The filenames of the flight lines are listed in Appendix A. The longitudes and latitudes of crossover points can be found in Chapter 4 (see Table 4-1).

3.7 Internal Layer Continuity

To graphically check the internal layer continuity throughout the entire study area, the traced layers are connected with each other based on 11 different long lines. The line numbers are denoted as L1, L2, L3...and L11 as shown in Figure 3-9. The internal layers of L3 are superimposed on the radar echogram given in Figure 3-10. The ice layers are continuously extended from the ice divide to the Jakobshavn region. Based on the continuity of the traced layers and the consistency at the crossover points, the age-depth relationship of these layers can be defined according to the GRIP age-depth relationship discussed in Chapter 2.

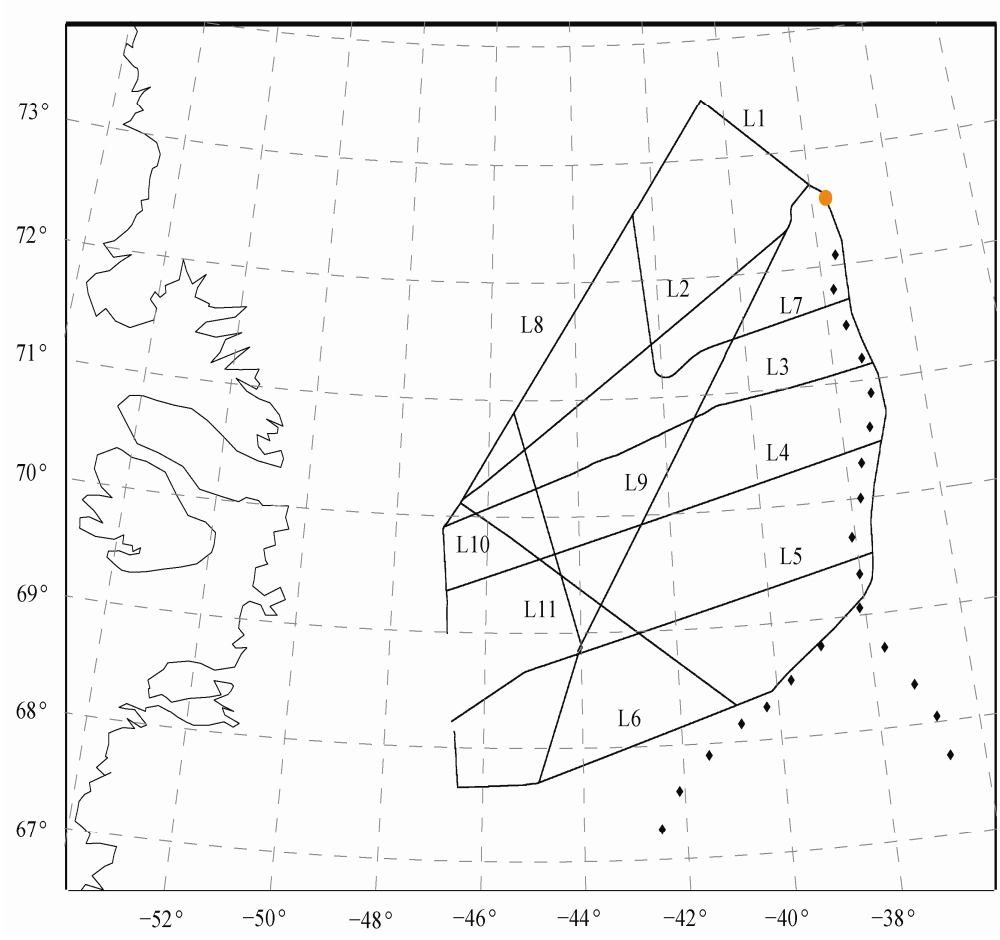


Figure 3-9. Long flight lines of study area.

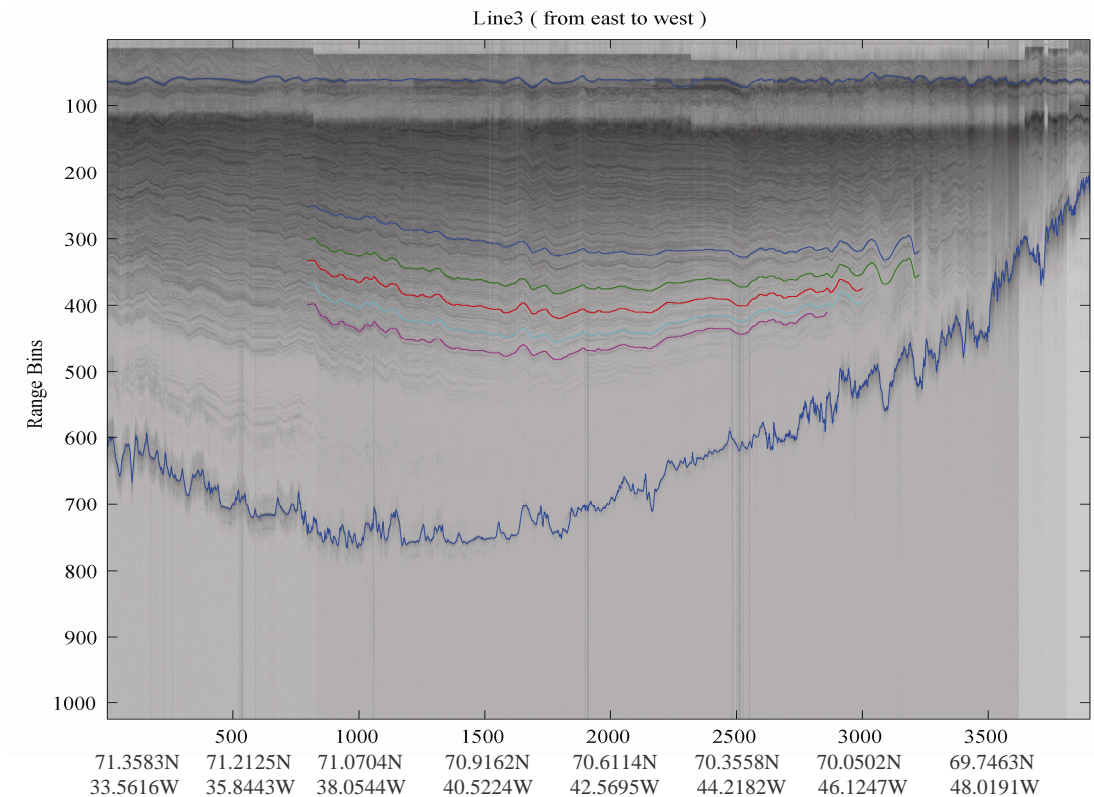


Figure 3-10. Layer continuity of Line 3.

3.8 References

- Fahnestock, M., W. Abdalati, S. Luo, and S. Gogineni, (2001). "Internal layer tracing and age-depth-accumulation relationship for the northern Greenland ice sheet," *Journal of Geophysical Research*, Vol. 106, No. D24, pp. 33789-33797.
- Gaydecki, P., (2004). *Foundations of digital signal processing: theory, algorithms and hardware design*, Institution of Electrical Engineers, London, 166 p.
- Gogineni, S., T. Chuah, C. Allen, K. Jezek, and R.K. Moore, (1998). "An improved coherent radar depth sounder," *Journal of Glaciology*, Vol. 44, No. 148, pp. 659-669.
- Ifeachor, E. C., and B. W. Jervis, (2002). *Digital signal processing: a practical approach*, Prentice Hall, New York, 105 p.
- Jacobel, R. W., and S. M. Hodge, (1995). "Radar internal layers from the Greenland summit," *Geophysical Research Letters*, Vol. 22, No. 5, pp. 587-590.

Chapter 4 Processing Results and Discussion

4.0 Introduction

Our study area spans from the Greenland ice divide line toward the Jakobshavn region in order to provide the layer information needed for ice modeler about the Jakobshavn fast-moving outlet. Using a semi-automated software system including preprocessing, cross-correlation and peak-following techniques, the internal layers of these flight lines are traced along the flight line through the GRIP site located at the summit of Greenland, on the ice divide line. The layer continuity and the consistency at the crossover points are checked. The age-depth relationship of internal layers is found using the GRIP age-depth relationship.

4.1 Traced Layers

Figure 4-1 illustrates the larger view of our study area, in which the dotted line and the circle mark denote the ice divide and the GRIP site respectively. The red asterisks denote the crossover points.

We chose to trace five internal layers that are spaced about 1000 yrs in time over study region. They are traceable over the majority of the study site. Using the method discussed in the last chapter, five layers are traced and illustrated in Figure 4-2. The vertical yellow line denotes the GRIP ice core. The ice surface, bedrock, and the five traced internal

layers, are shown on the radar image. The archived files are traced one by one along the flight lines. After the layers of one whole flight line are found, we begin to trace the layers of next flight line from the corresponding crossover points. The traced layers for each flight line can be seen in Appendix B.

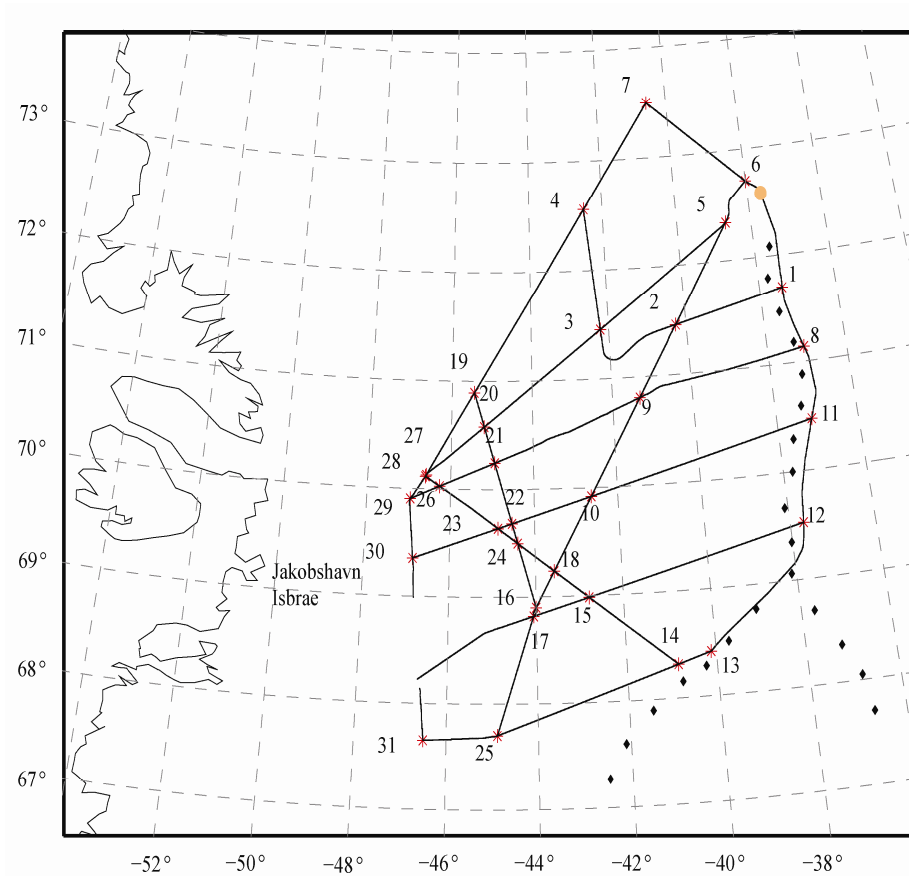


Figure 4-1. A portion of Greenland map illustrating the flight line of the study area. The location of the GRIP ice core is denoted as a yellow circle mark. The diamond dotted line illustrates a portion of ice divide. The crossover points are shown as red asterisks on the map.

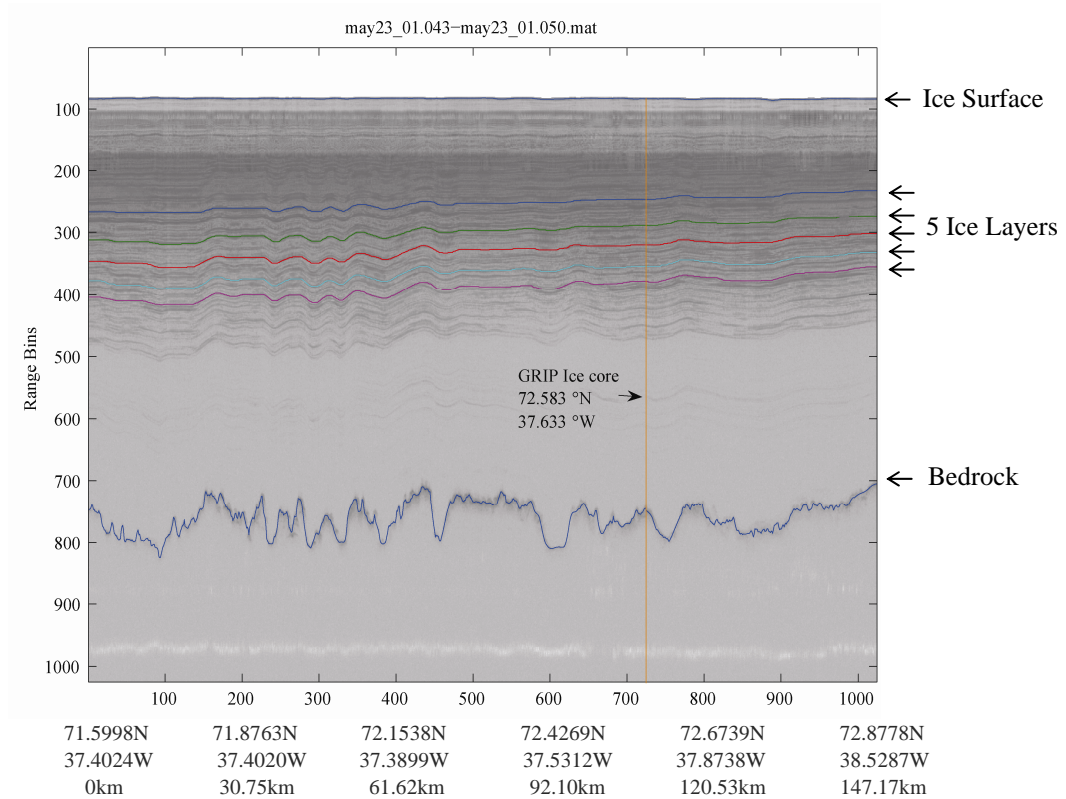


Figure 4-2. Five internal layers are shown on a radar echogram from nearby GRIP.

4.2 Crossover Point Analysis

We analyzed the 31 flight line crossover points that are found within our study region. The difference in each layer thickness for each crossover location is shown in Table 4-1. Closer to the Jakobshavn region, the deeper layers may become not readily discernable mainly by signal absorption loss through relatively warm ice or melt conditions and by clutter from the crevassed surfaces [Braaten *et al.*, 2002]; therefore, the crossover difference for a number of entries is listed in Table 4-1 as ‘-’. As the flight lines crossover at many points, we verified the layers consistency at each crossover point. Since the layers

are known to be isochronal in nature, the consistency at the crossover points is an important check on the tracing process and the temporal variation of the flight lines (e.g. collected between 1993 to 2002). Moreover, analysis of the layer thickness at the crossover points agrees to within 4.5 m (one range bin) for most cases, and 9 m (two range bins) for a few of the worst cases. The high consistency over the crossover points supports the claim, which indicates that once dated, that these layers can define the age-depth relationship throughout much of the study region [Fahnestock *et al.*, 2001]. It is notable that differences were zero for more than 68% of the entries in the crossover Table 4-2.

4.3 The Age-depth Relationship of Traced Layers

Since the GRIP core provides an age estimate for each of the traced layers, the five traced-radar layers ages are determined at the GRIP site using the GRIP core age-depth relationship [Johnsen *et al.*, 1997], which is also described in Chapter 2. No correction was made for the accumulation rate, because the present accumulation rate at GRIP is about 0.22 m ice equivalent/yr [Braaten *et al.*, 2002] or up to 1 radar range bin for the radar data set collected over ten years.

To compare the radar-measured depth to the depth in the ice core, an 8 m correction is added to the radar-measured depth to account for the higher radar velocity in the firn than in ice [Fahnestock *et al.*, 2001]. After correction, the radar-based values correspond to true depth for comparison to the GRIP core. The age-depth relationship of each traced layer at

GRIP is given in Table 4-2. The age range of the traced layers covers a period of 4657 years.

Table 4-1. Crossover Results

<i>Crossover Site</i>	<i>Latitude (°N)</i>	<i>Longitude (°W)</i>	<i>Difference (m)</i>				
			Layer1	Layer2	Layer3	Layer4	Layer5
1	71.704	37.406	0	0	0	0	0
2	71.458	40.269	0	0	0	0	0
3	71.454	42.214	4.5	0	0	0	0
4	72.561	42.508	4.5	0	0	0	4.5
5	72.350	38.683	0	0	0	0	0
6	72.708	38.007	0	0	0	0	0
7	73.498	40.562	0	0	0	0	0
8	71.137	37.074	0	0	0	0	0
9	70.809	41.315	4.5	4.5	4.5	4.5	0
10	69.920	42.635	4.5	4.5	4.5	4.5	-
11	70.469	37.139	0	0	0	0	0
12	69.524	37.682	0	0	0	0	0
13	68.416	40.112	0	0	0	0	-
14	68.317	40.858	0	4.5	0	0	-
15	68.983	42.783	0	0	9	0	-
16	68.90	44.001	0	0	-	-	-
17	68.819	44.057	4.5	9	-	-	-
18	69.237	43.564	4.5	0	-	-	-
19	70.894	45.444	0	0	0	0	0
20	70.577	45.196	4.5	4.5	4.5	4.5	-
21	70.243	44.941	4.5	9	9	4.5	4.5
22	69.682	44.533	4.5	0	-	-	-
23	69.638	44.862	4.5	0	-	-	-
24	69.499	44.405	4.5	0	4.5	0	-
25	67.702	44.889	4.5	4.5	-	-	-
26	70.027	46.265	4.5	4.5	-	-	-
27	70.129	46.592	4.5	0	-	-	-
28	70.115	46.611	0	0	-	-	-
29	69.906	46.959	0	4.5	-	-	-
30	69.356	46.855	0	-	-	-	-
31	67.653	46.498	0	0	-	-	-

Table 4-2. Age-Depth Relationship

<i>Layer #</i>	<i>GRIP Core Depth (m)</i>	<i>Age (yrs BP*)</i>
1	736	3596
2	929	4849
3	1069	5863
4	1221	7102
5	1347	8253

The northeast portion of our study area partially overlaps with the flight line used by Fahnestock *et al.* [Fahnestock *et al.*, 2001]. The overlap covers about 300 km of flight line (i.e. from crossover point 7 to 6 to 1 as shown in Figure 4-1). Our layers 1, 2, and 4 are also shown in the previous study. Over the overlapping line, the corresponding layer thickness values appear to be consistent with each other. At GRIP, these layers are within 1 range bin (4.5 m) for each independent study.

4.4 Radar Internal Layer Tracing Results

To visually describe how the ice thickness changes over our study area, we plotted the each layer thickness (color coded) values (~5 km averages) on a map of the flight lines as shown in Figures 4-3 to 4-7. A portion of the ice divide is illustrated on each map using diamond dotted lines. Each layer is traced over the majority of the study area; however, some layers were not easily traceable, as discussed in the crossover analysis, in the southwest portion of our study area.

Radar-detected thickness values for layers 1 through 5 are shown in Figures 4-3 to 4-7,

respectively. For each layer thickness, the trend is increasing layer thickness from the northeast corner towards the southwest corner of the study area. Since layer thickness and long-term accumulation rate are strongly related [Dahl-Jensen *et al.*, 1997], the layer thickness increases in large part due to increases in the long-term accumulation rate [Fahnestock *et al.*, 2001], which increases towards the Jakobshavn Isbrae in our study area. The increasing layer thickness trend is similar to the increasing long-term accumulation rate trend reported [Bales *et al.*, 2001] over our study area. The thicker layer values are observed in the catchment basin of Jakobshavn Isbrae. In Figures 4-3 to 4-7, this area of thicker layer values corresponds to the higher long-term accumulation rates reported by Bales *et al.* [Bales *et al.*, 2001] in our study area. The thickness to the bedrock is shown in Figure 4-8. The bedrock thickness trend from the ice divide toward Jakobshavn region is decreasing thickness from about 3100 m down to 1500 m.

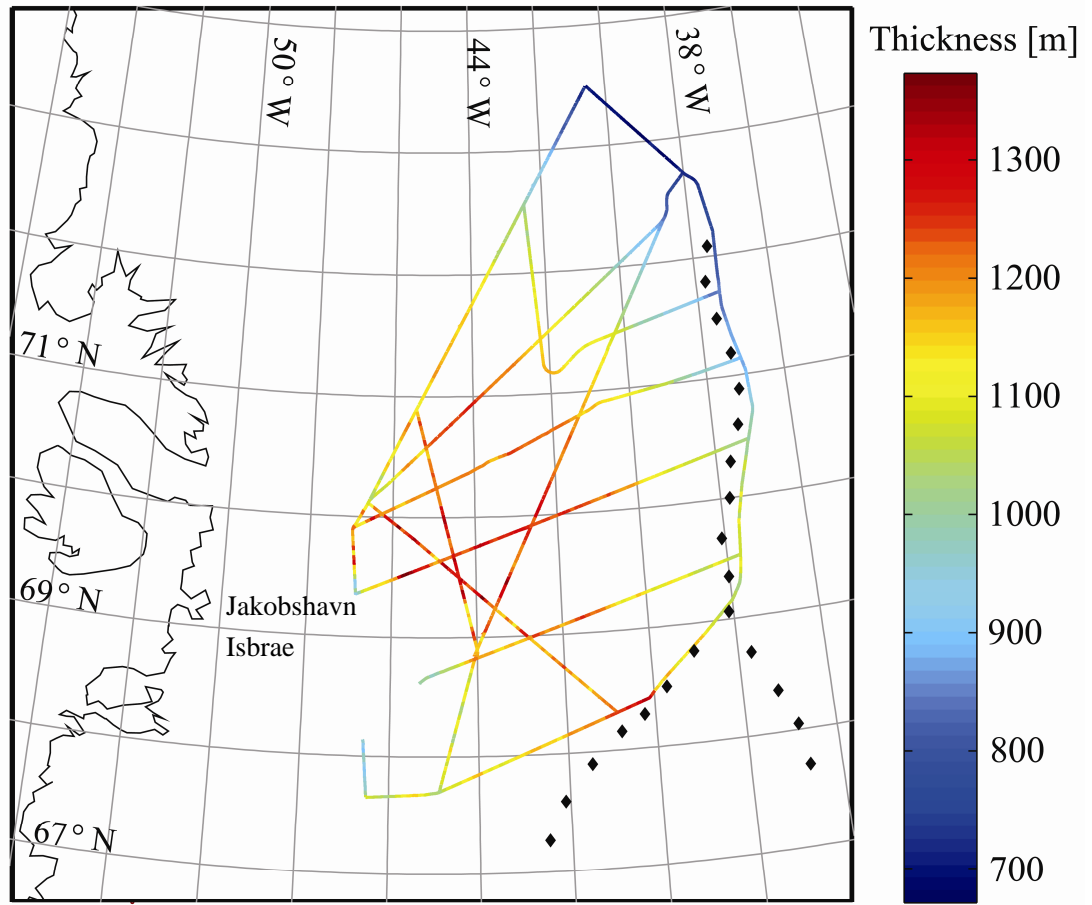


Figure 4-3. Thickness of Layer 1.

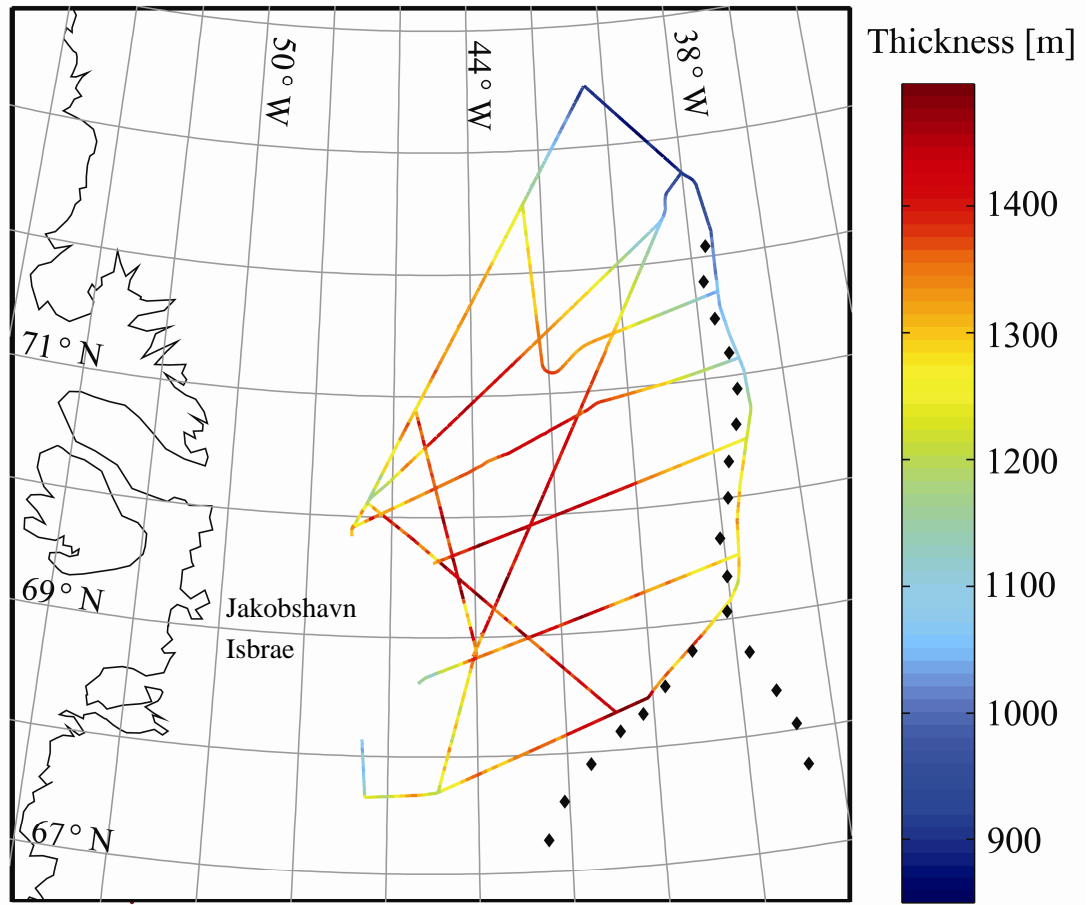


Figure 4-4. Thickness of Layer 2.

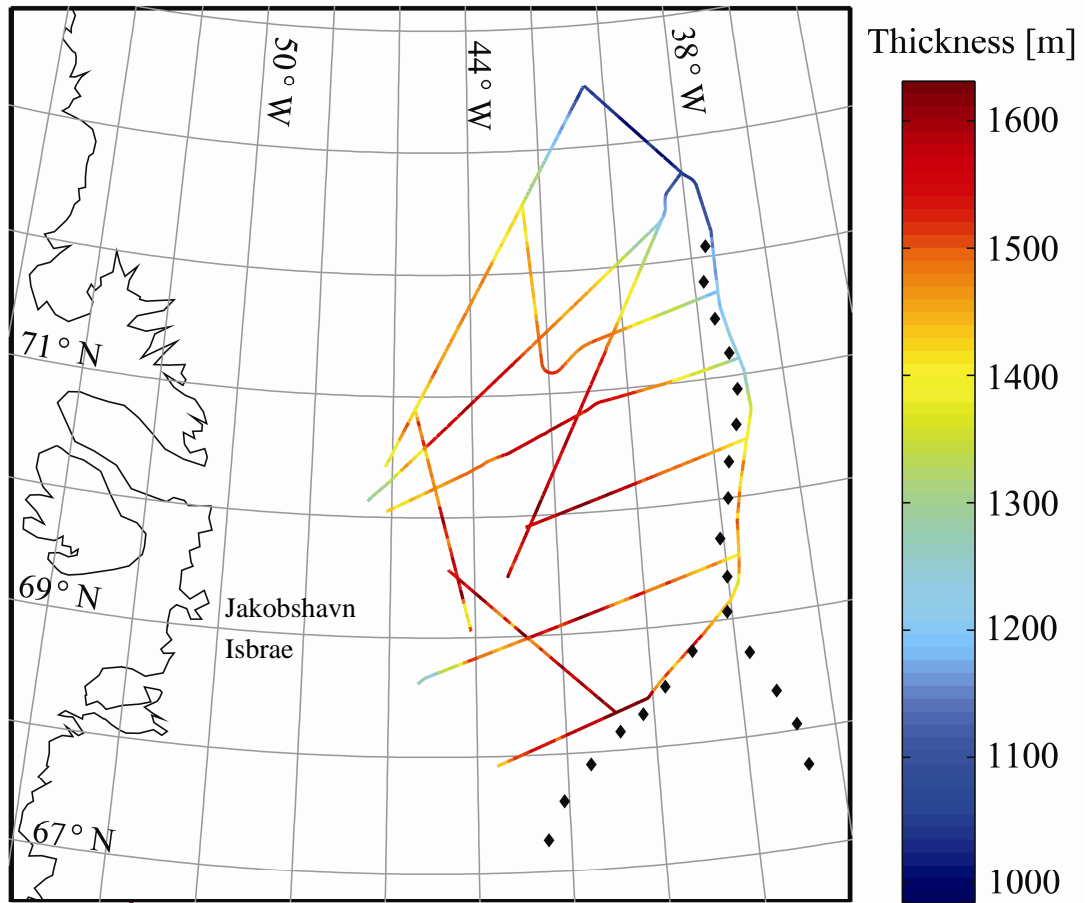


Figure 4-5. Thickness of Layer 3.

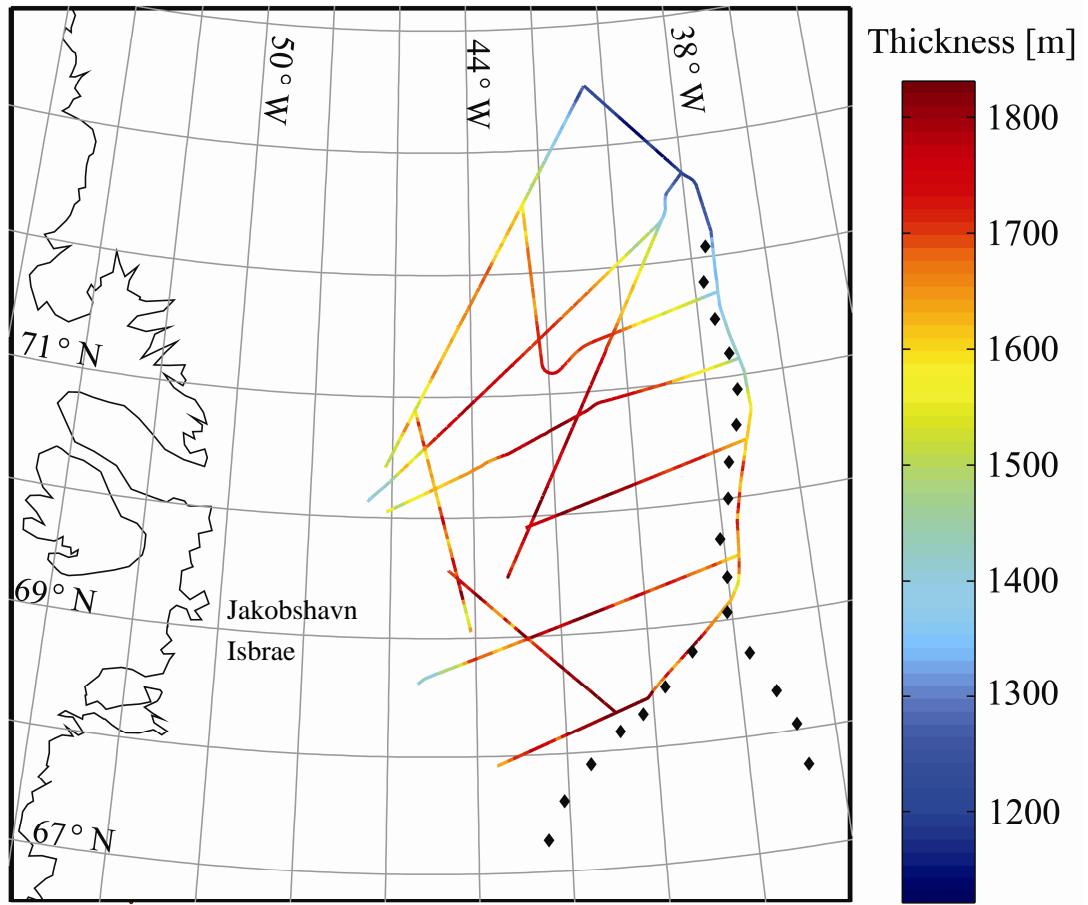


Figure 4-6. Thickness of Layer 4.

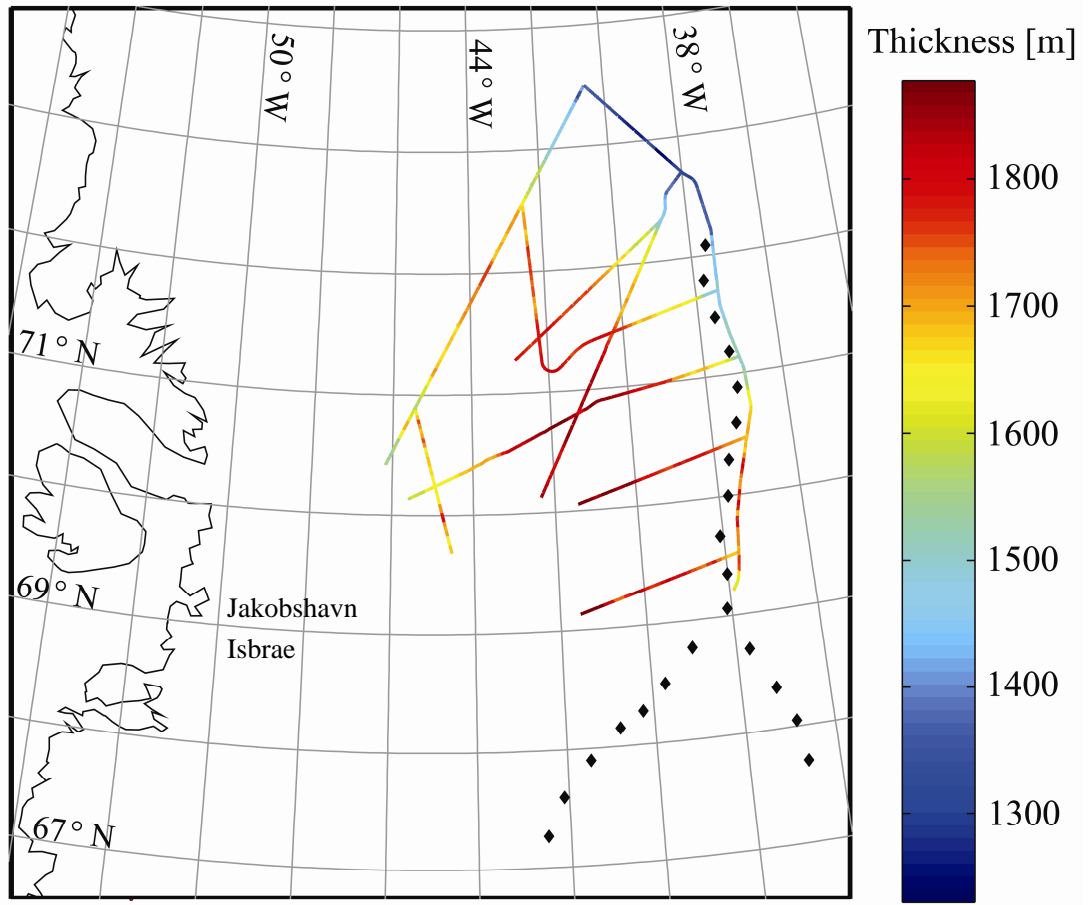


Figure 4-7. Thickness of Layer 5.

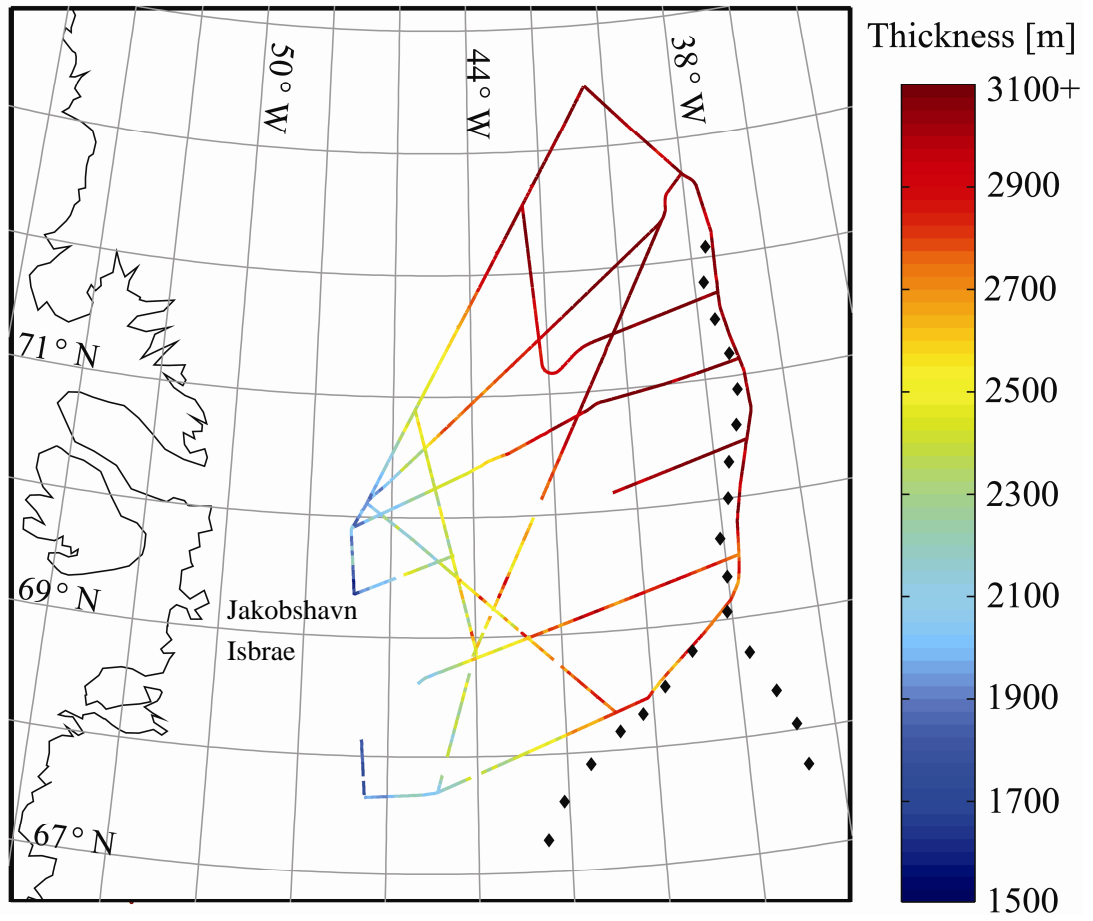


Figure 4-8. Thickness to the Bedrock.

4.5 References

- Bales, R. C., J. R. McConnell, E. Mosley-Thompson, and B. Csatho, (2001). "Accumulation over the Greenland ice sheet from historical and recent records," *Journal of Geophysical Research*, Vol. 106, No. D24, pp. 33813-33825.
- Braaten, D. A., S. P. Gogineni, D. Tammana, S. Namburi, J. Paden, and K. Gurumoorthy, (2002). "Improvement of radar ice-thickness measurements of Greenland outlet glaciers using SAR processing," *Annals of Glaciology*, Vol. 35, pp. 73-78.
- Dahl-Jensen, D., N. S. Gundestrup, K. Keller, S. J. Johnsen, S. P. Gogineni, C. T. Allen, T. S. Chuah, H. Miller, S. Kipfstuhl, and E. D. Waddington, (1997). "A search in North Greenland for a new ice-core drill site," *Journal of Glaciology*, Vol. 43, No. 144, pp. 300-306.
- Fahnestock, M., W. Abdalati, S. Luo, and S. Gogineni, (2001). "Internal layer tracing and age-depth-accumulation relationship for the northern Greenland ice sheet," *Journal of Geophysical Research*, Vol. 106, No. D24, pp. 33789- 33797.
- Gogineni, S. P., and others, (2006). "Greenland Data Site," University of Kansas, Present address: <http://tornado.rsl.ku.edu/Greenlanddata.htm>
- Johnsen, S. J., H. B. Clausen, W. Dansgaard, N. S. Gundestrup, C. U. Hammer, U. Andersen, K. K. Andersen, C. S. Hvidberg, D. Dahl- Jensen, J. P. Steffensen, H. Shoji, A. E. Sveinbjornsdottir, J. White, J. Jouzel, and D. Fisher, (1997). "The $\delta^{18}O$ record along the Greenland Ice Core Project deep ice core and the problem of possible Eemian climatic instability," *Journal of Geophysical Research*, Vol. 102, No. C12, pp. 26,397- 26,410.
- North Greenland Ice Core Project members, (2004). "High-resolution record of Northern Hemisphere climate extending into the last interglacial period," *Nature*, Vol. 431, pp. 147-151.
- Wolff, E.W., J. C. Moore, H. B. Clausen, C. U. Hammer, J. Kipfstuhl, and K. Fuhrer, (1995). "Long-term changes in the acid and salt concentrations of the Greenland Ice Core Project ice core from electrical stratigraphy," *Journal of Geophysical Research*, Vol. 100, pp. 16249-16263.

Chapter 5 Conclusions

5.0 Summary

We demonstrated internal layers could be traced over our study region, which is from the ice divide toward the Jakobshavn outlet glacier region, and areas to the south. We successfully traced layers over multiple flight lines and multiple dates for our study region. These layers are dated using GRIP ice core data. Additionally, the internal layer tracing method has a high degree of consistency based on the crossover point analysis. The traceable internal layers from the ice divide toward Jakobshavn, Greenland maintain their structure over a large area. The age-depth relationships of these known isochronal layers from the ice divide towards the Jakobshavn region can be useful in modeling ice sheet flow far away from the GRIP core site.

5.1 Future Work

This study traced 5 internal layers in radar data from more than 4000 km worth of flight lines, which was a significant accomplishment for this area of high interest. In the future, additional layers beyond 5 could be traced. With additional resources, layers could be traced in the radar data from the entire PARCA Greenland radar data set (> 100,000 km) for archiving in the National Snow and Ice Data Center (NSIDC).

Appendix

Appendix Overview

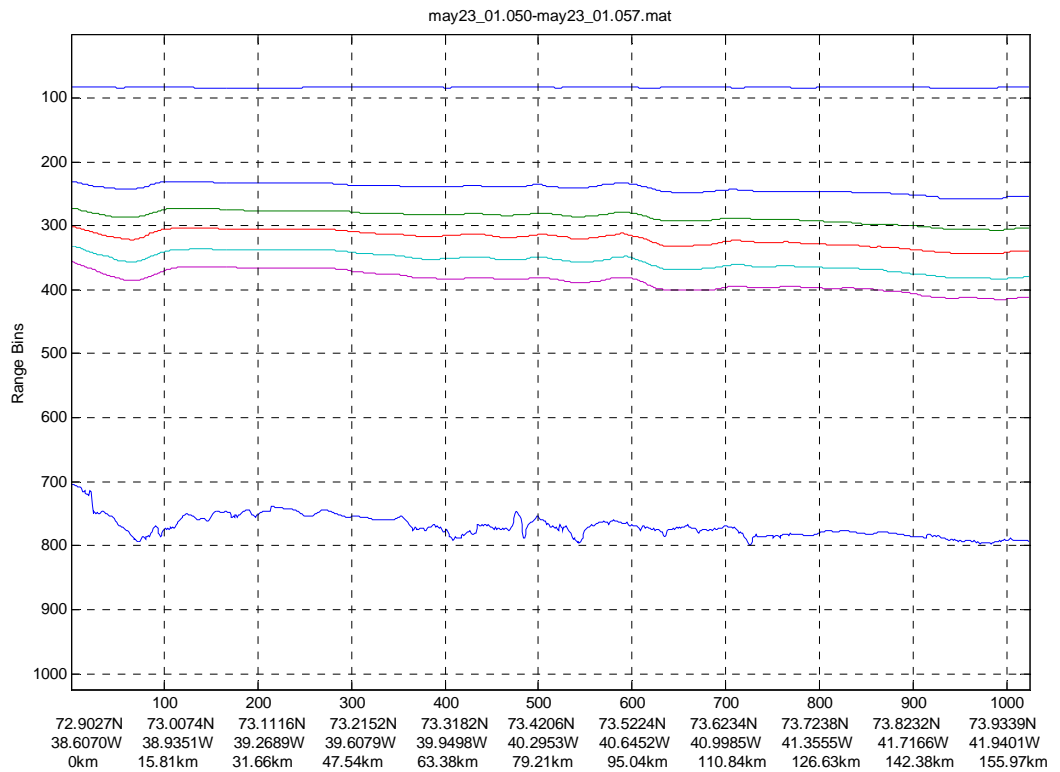
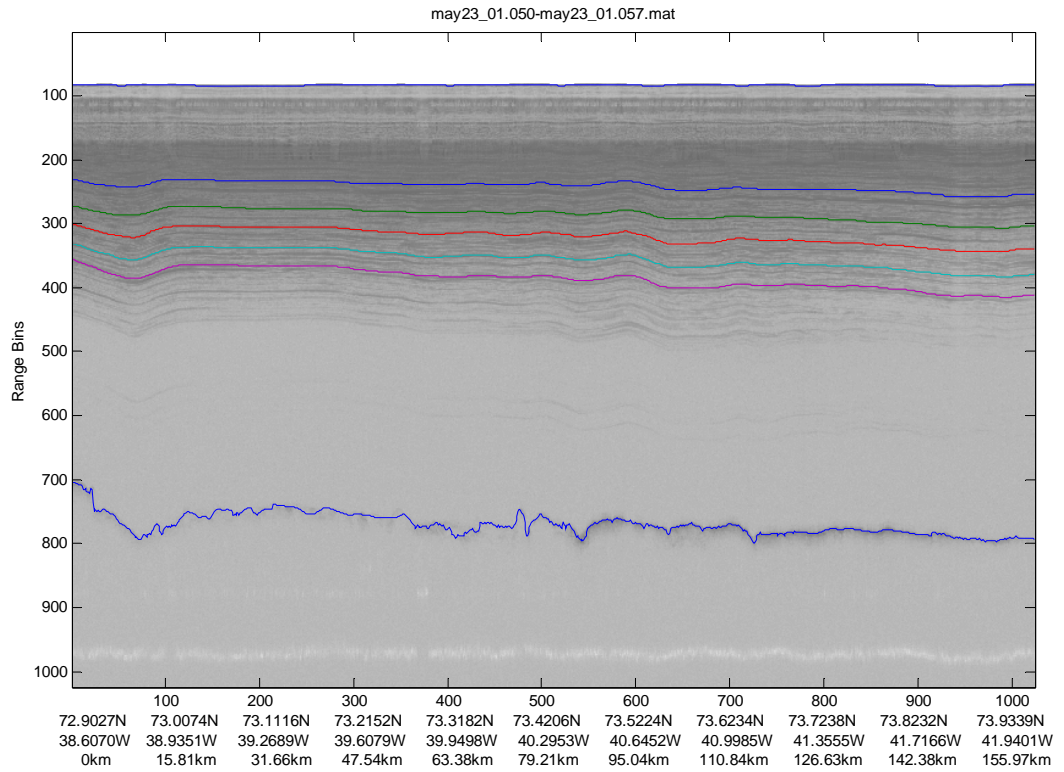
We processed 45 archive files for our study. Appendix A gives the list of these files. The locations of corresponding line numbers can be found in Figure 3-9. Appendix B includes the results of traced internal layers for each archive file. Appendix C lists the file formats for the archive results.

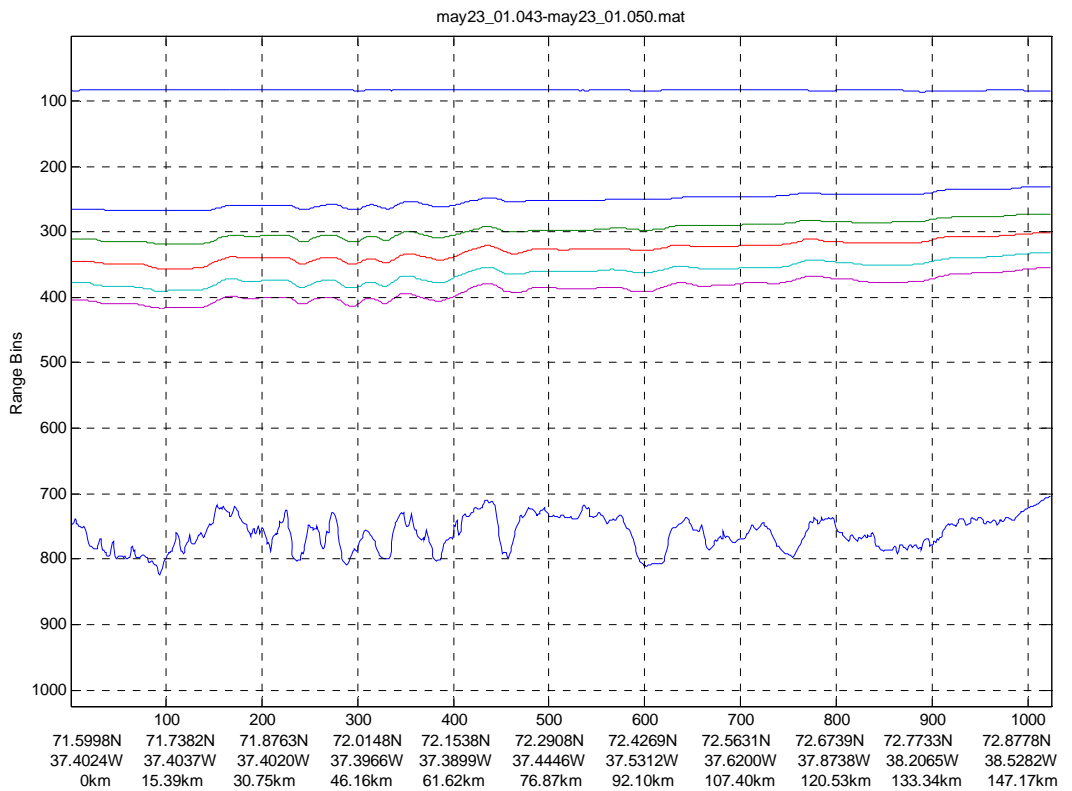
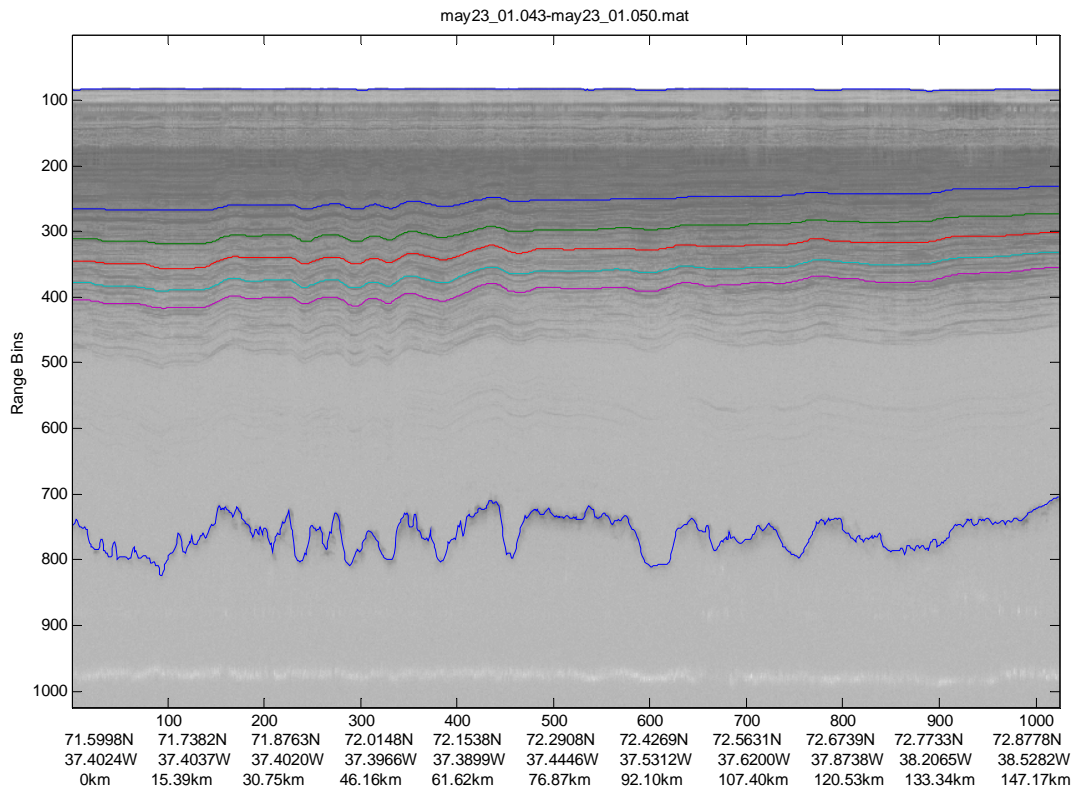
Appendix A The List of Filenames in Our Study Area

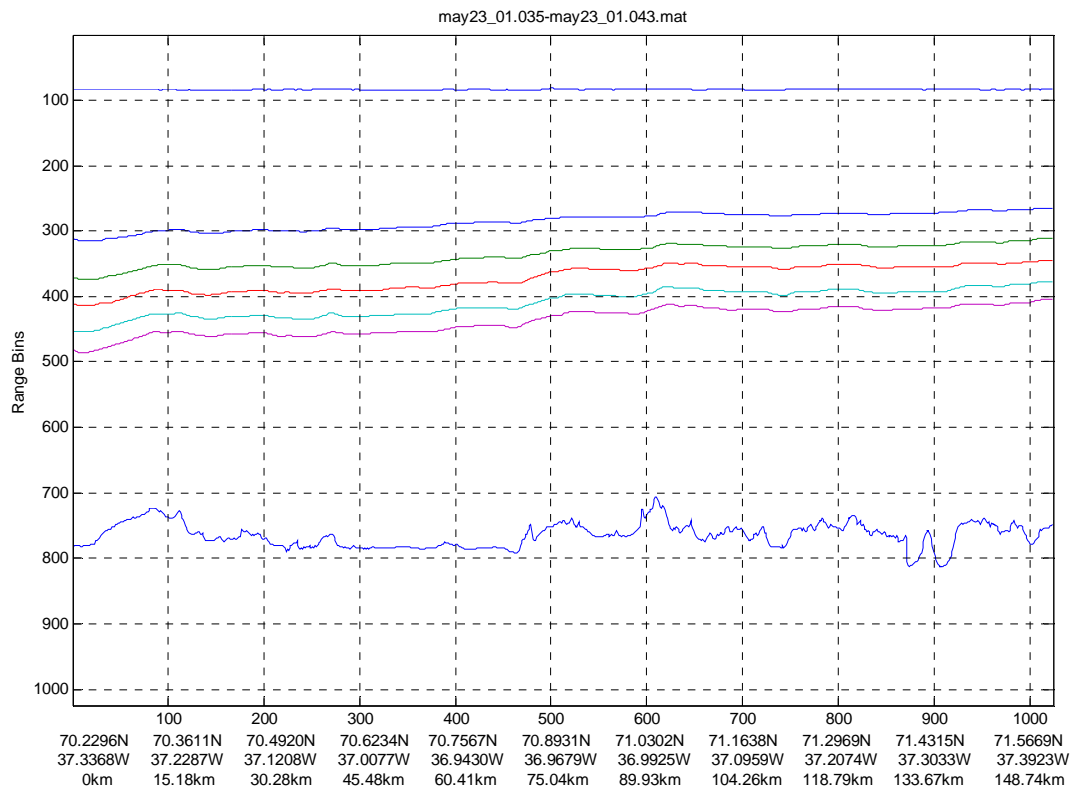
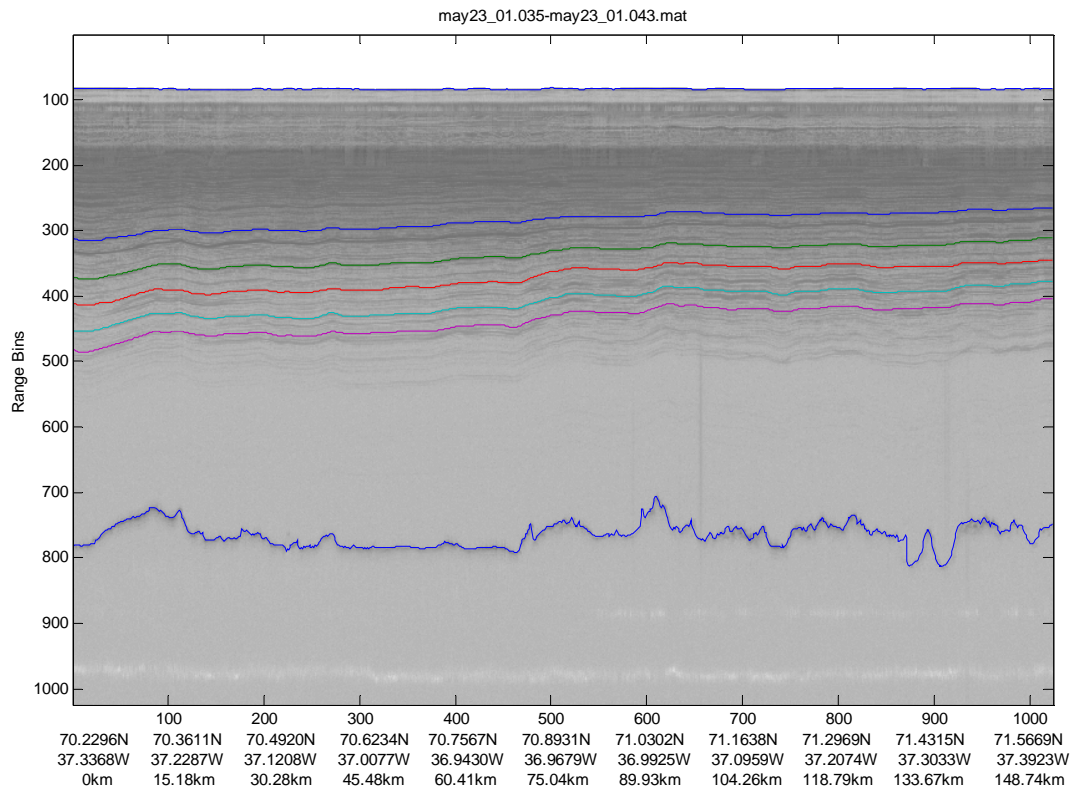
Line number	Filename	Page number
L1	may23_01.050-may23_01.057.mat	56
	may23_01.043-may23_01.050.mat	57
	may23_01.035-may23_01.043.mat	58
	may23_01.028-may23_01.035.mat	59
	may23_01.021-may23_01.028.mat	60
L2	may23_01.079-may23_01.087.mat	61
	may23_01.087-may23_01.094.mat	62
	may23_01.094-may23_01.102.mat	63
L3	jul14_98.059-jul14_98.063.mat	64
	jul14_98.063-jul14_98.066.mat	65
	jul14_98.066-jul14_98.070.mat	66
	jul14_98.070-jul14_98.073.mat	67
L4	jun24_93.003-jun24_93.003.mat	68
	jun24_93.003-jun24_93.004.mat	69
	jun24_93.004-jun24_93.005.mat	70
	jun24_93.005-jun24_93.006.mat	71
L5	jul17_98.003-jul17_98.007.mat	72
	jul17_98.007-jul17_98.010.mat	73
	jul17_98.010-jul17_98.014.mat	74
L6	jul15_98.048-jul15_98.052.mat	75
	jul15_98.052-jul15_98.055.mat	76
	jul15_98.055-jul15_98.059.mat	77
	jun27_98.016-jun27_98.019.mat	78
L7	may18_99.018-may18_99.021.mat	79
	may18_99.021-may18_99.025.mat	80

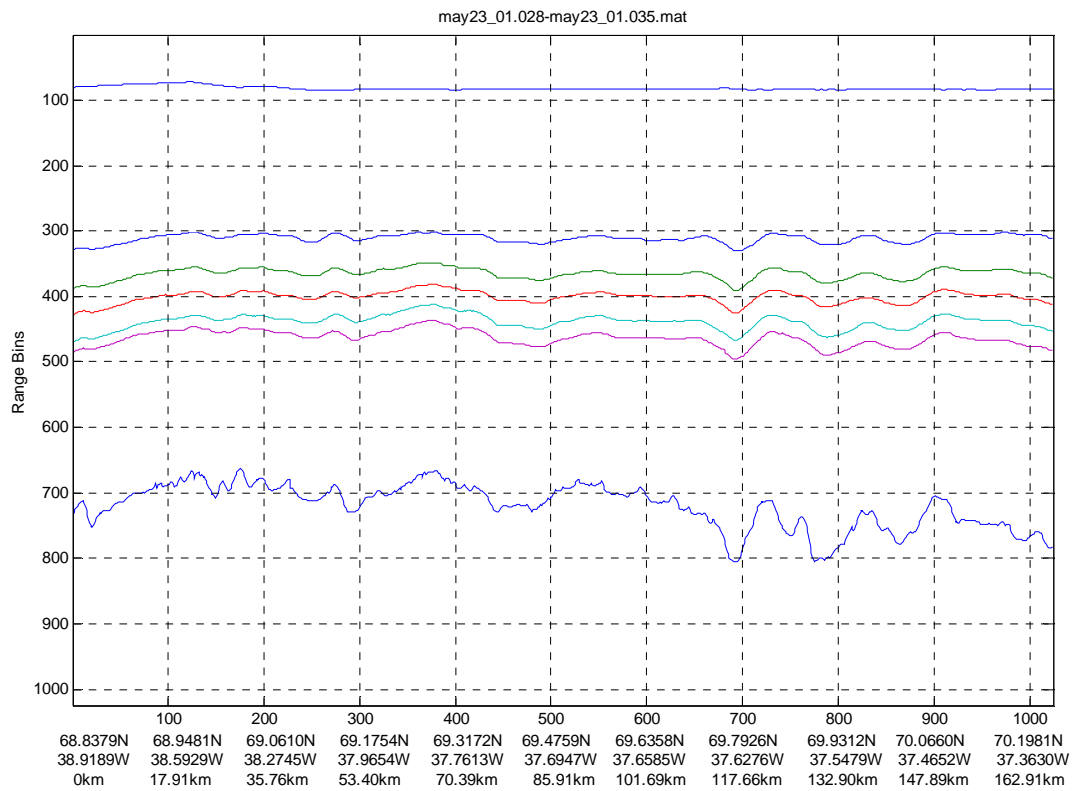
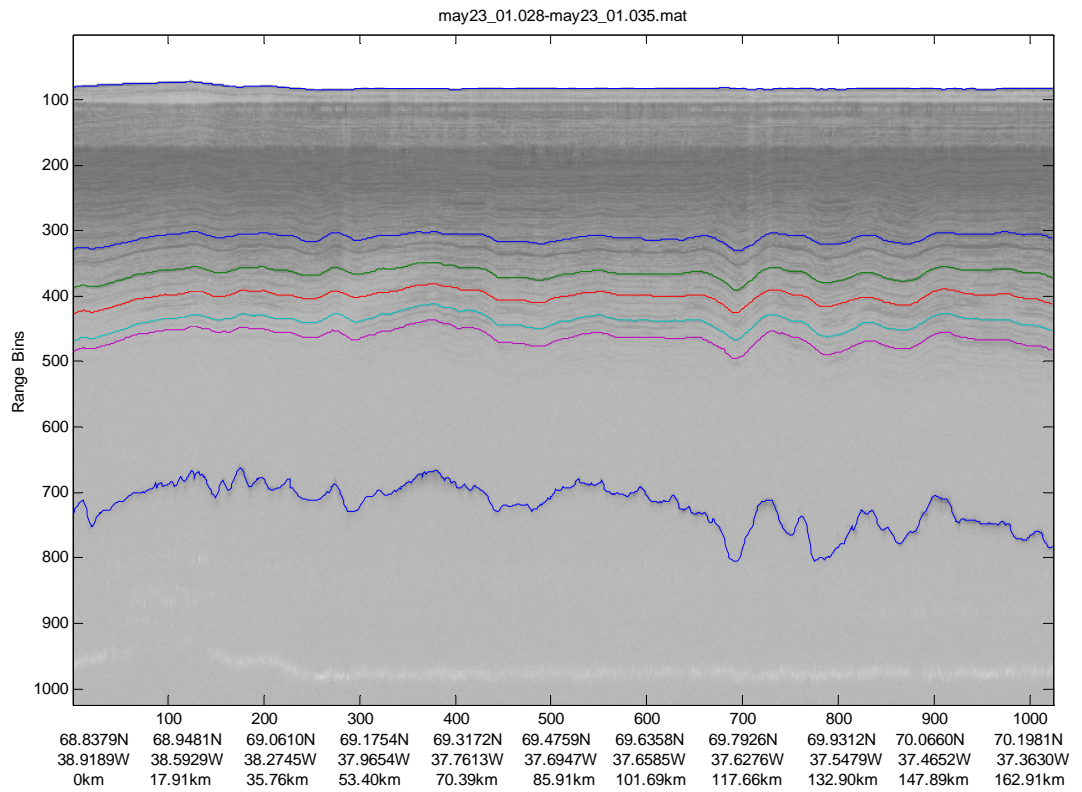
	may18_99.025-may18_99.028.mat	81
L8	may20_96.023-may20_96.025.mat	82
	may20_96.025-may20_96.027.mat	83
	may20_96.027-may20_96.028.mat	84
	may20_96.034-may20_96.035.mat	85
	jun27_98.047-jun27_98.051.mat	86
	jun27_98.051-jun27_98.052.mat	87
	jun27_98.007-jun27_98.010.mat	88
L9	jun04_02.222-jun04_02.229.mat	89
	jun04_02.229-jun04_02.236.mat	90
	jun04_02.236-jun04_02.244.mat	91
	jun04_02.244-jun04_02.251.mat	92
L10	jun01_02.088-jun01_02.095.mat	93
	jun01_02.095-jun01_02.102.mat	94
	jun01_02.102-jun01_02.110.mat	95
	jun01_02.110-jun01_02.117.mat	96
L11	jun30_98.008-jun30_98.011.mat	97
	jun30_98.011-jun30_98.011.mat	98
	jun30_98.012-jun30_98.019.mat	99
	jun30_98.019-jun30_98.026.mat	100

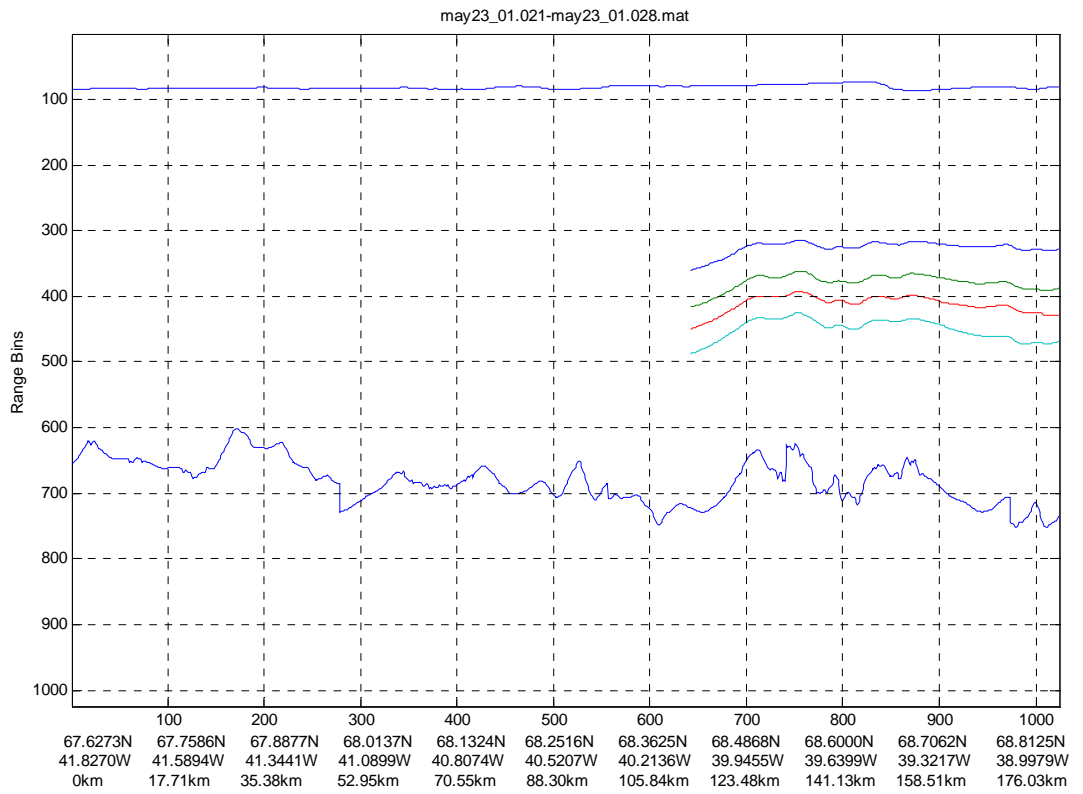
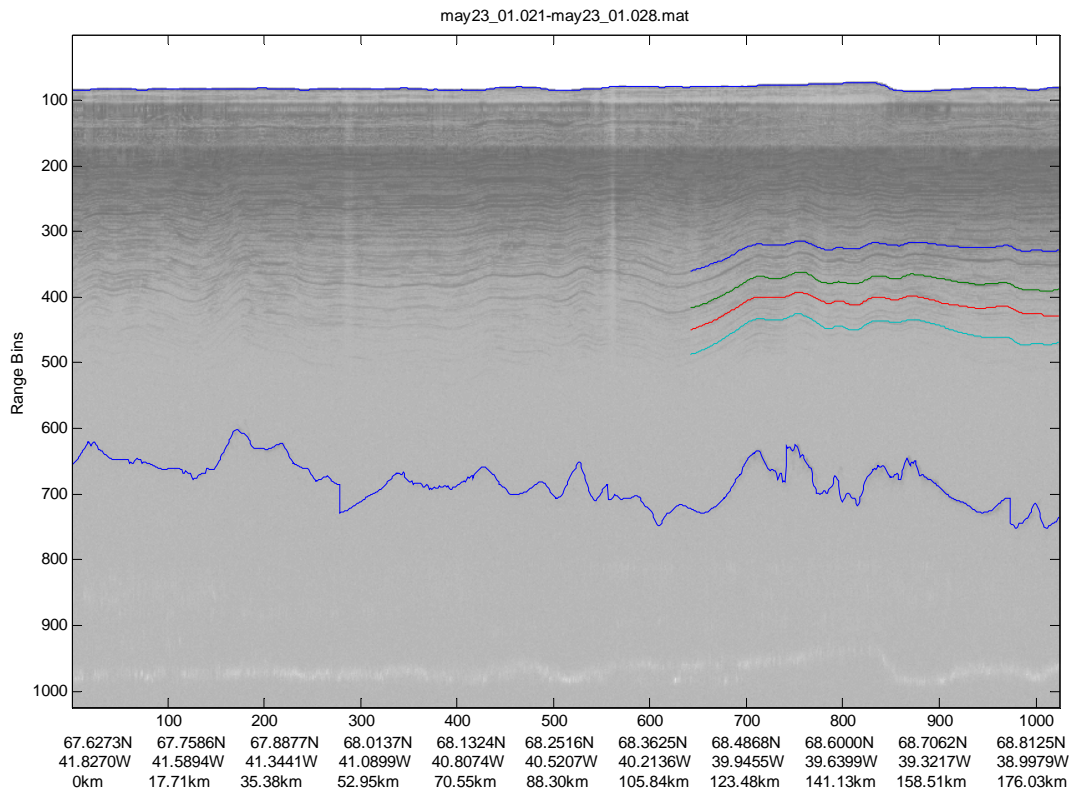
Appendix B The Results of Traced Internal Layers

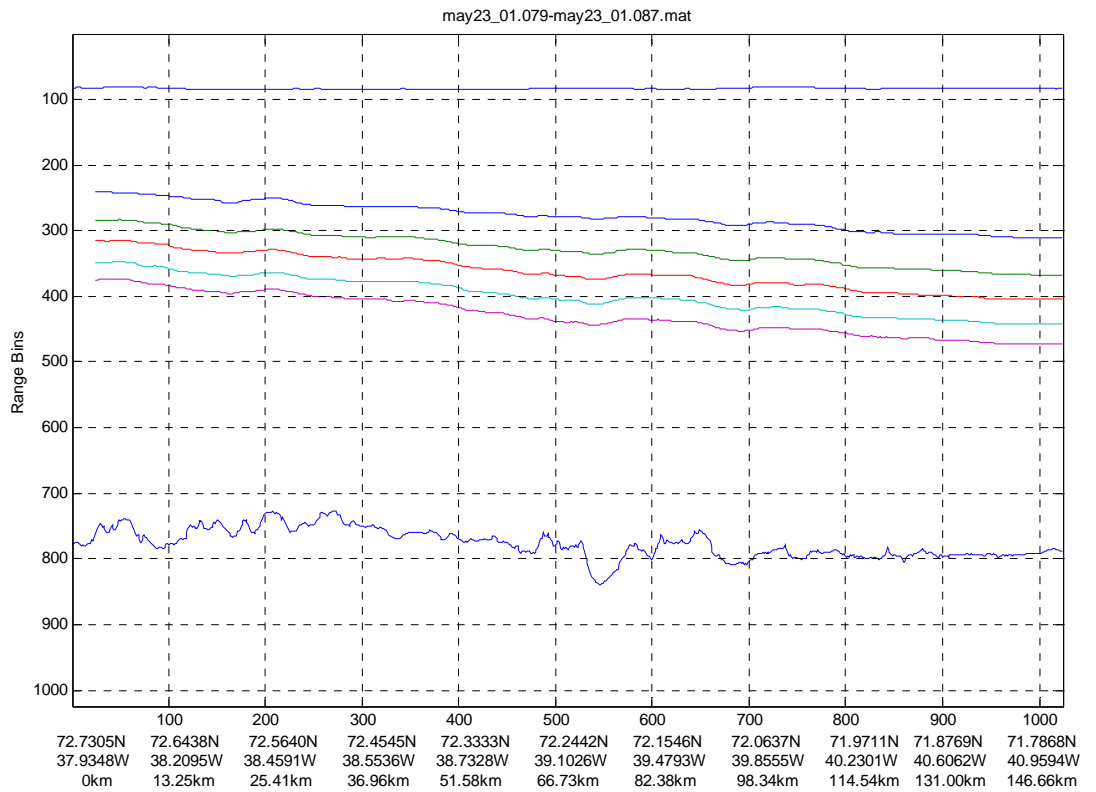
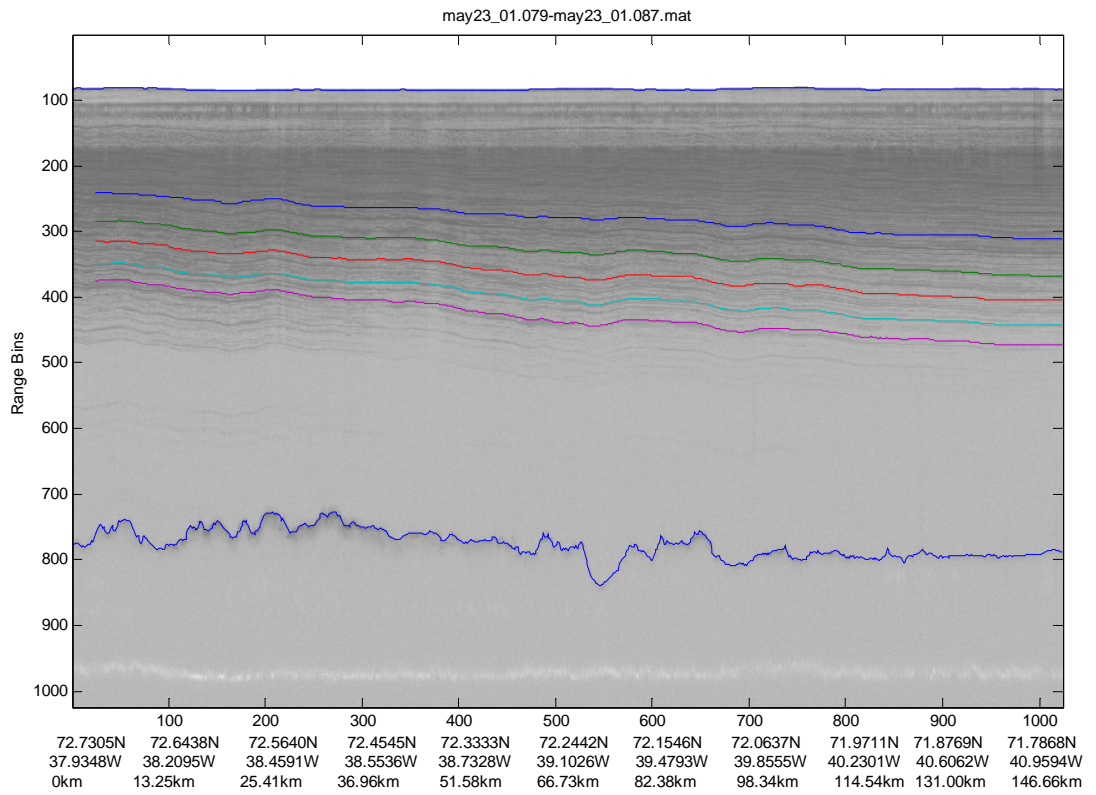


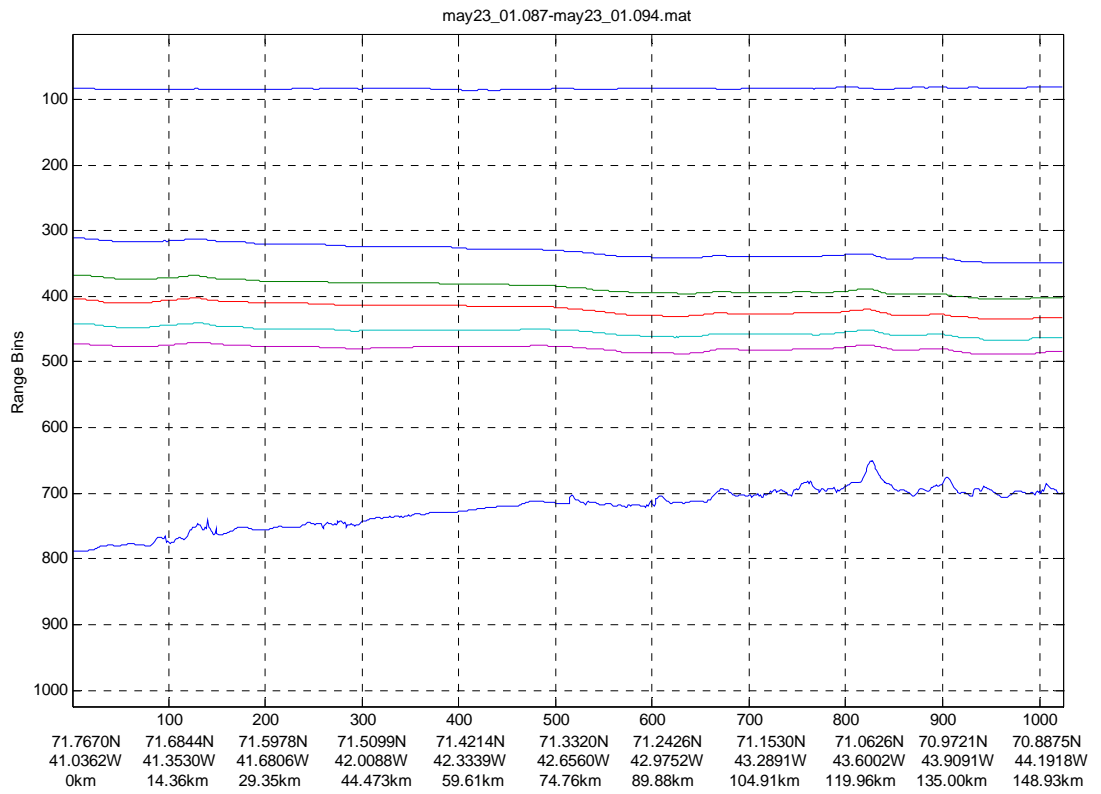
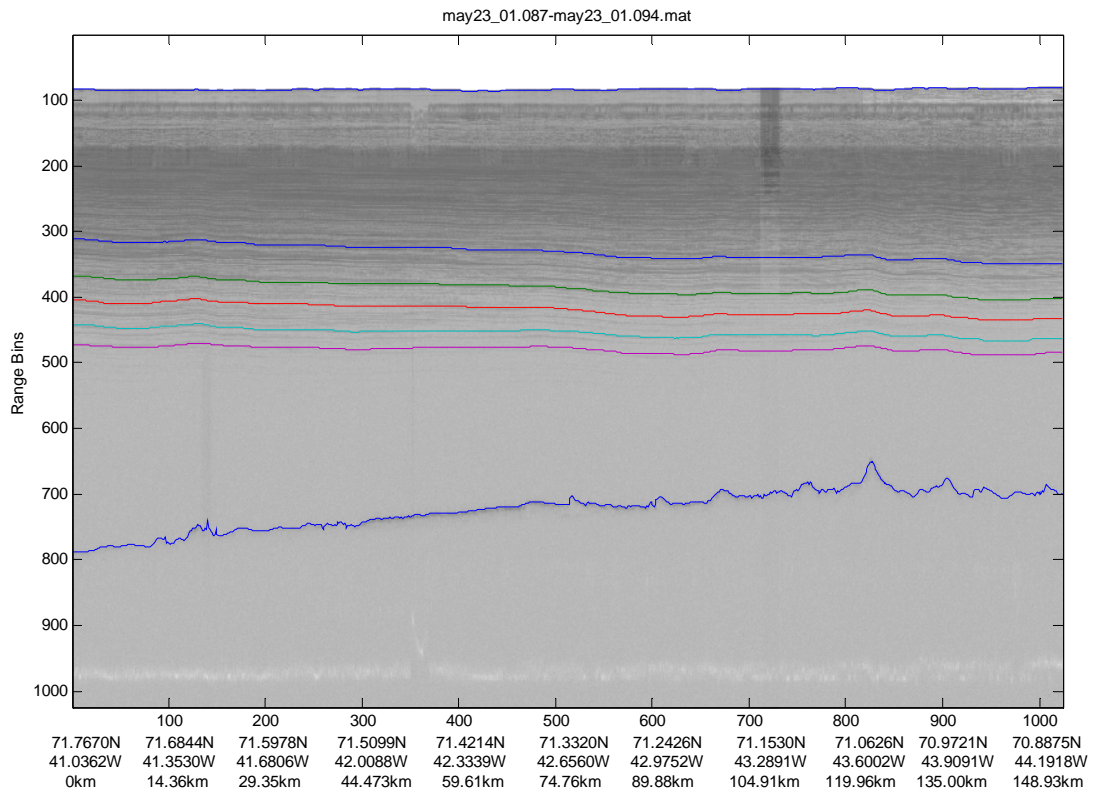


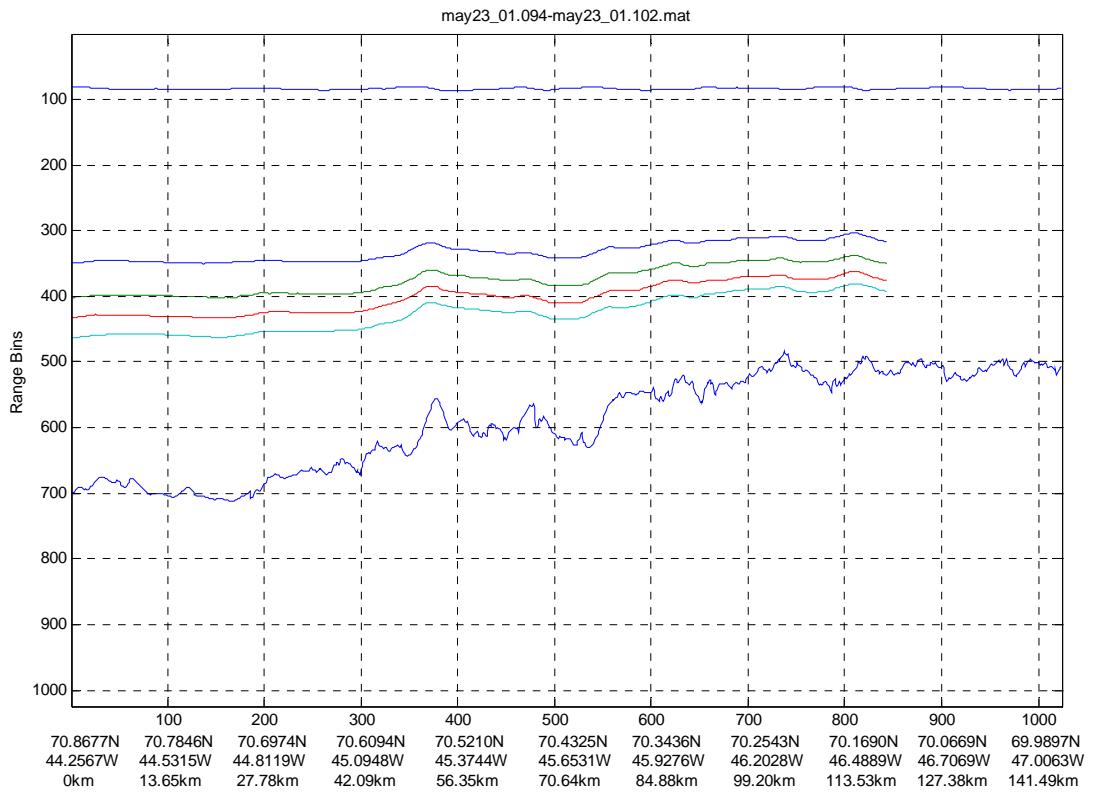
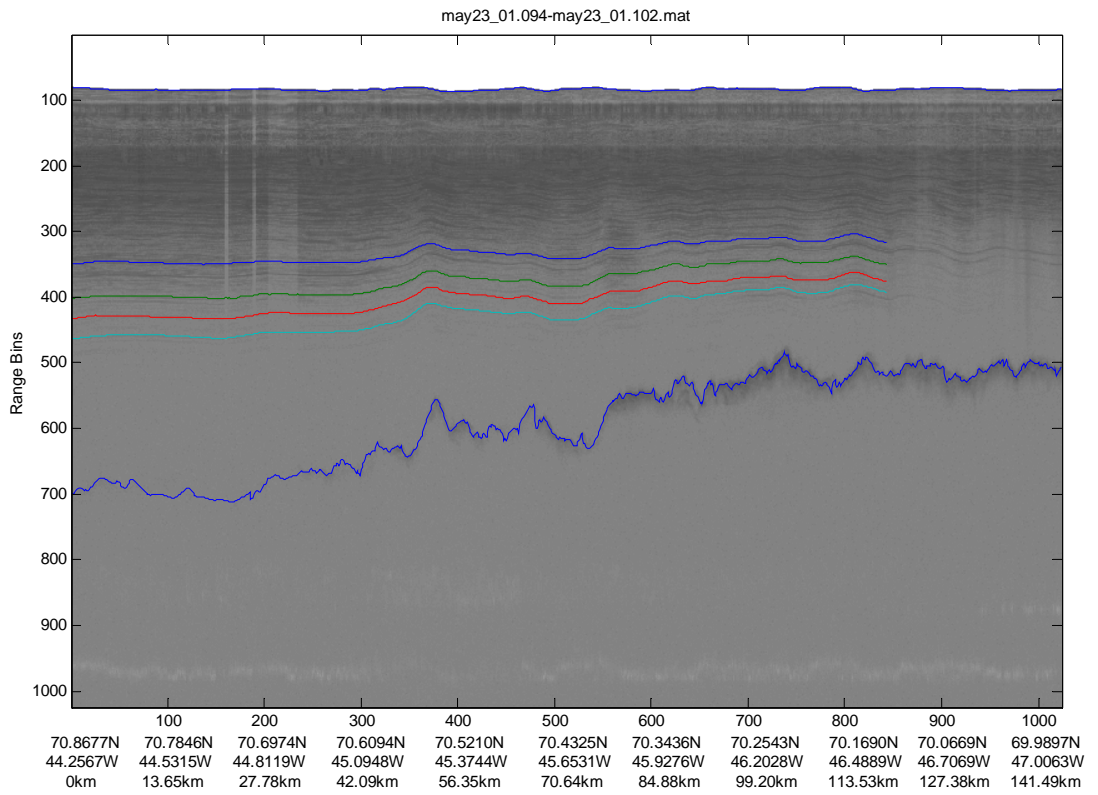


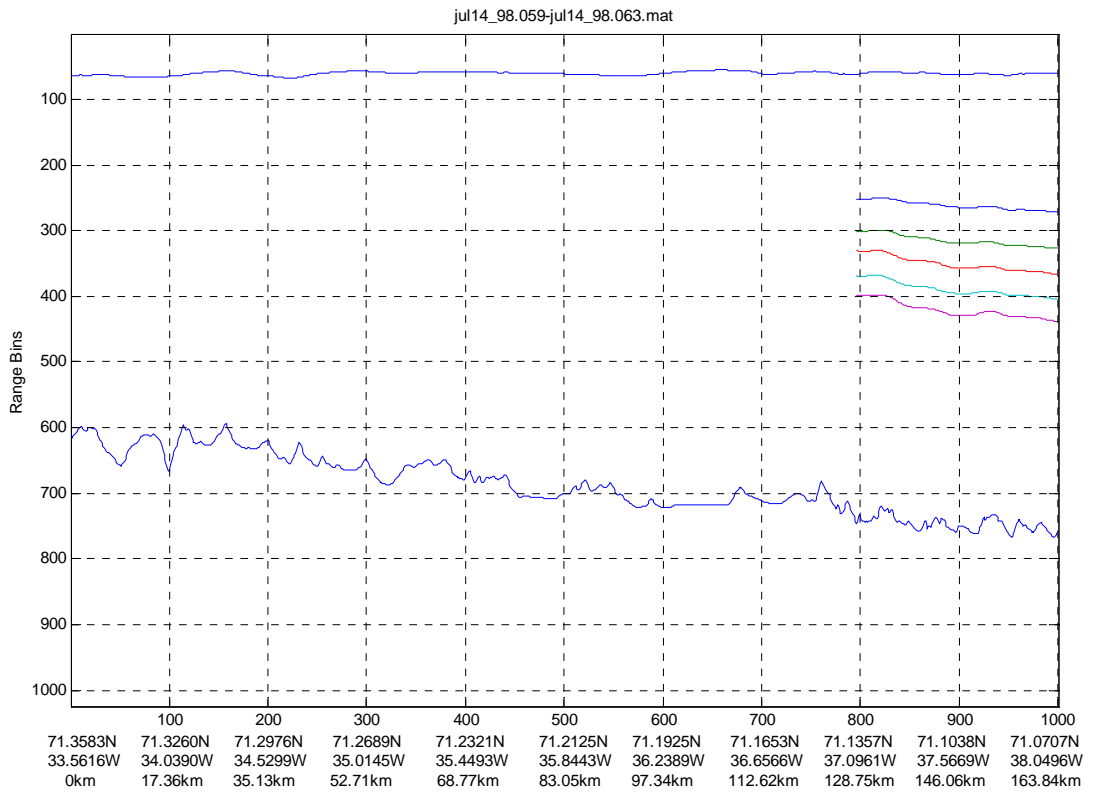
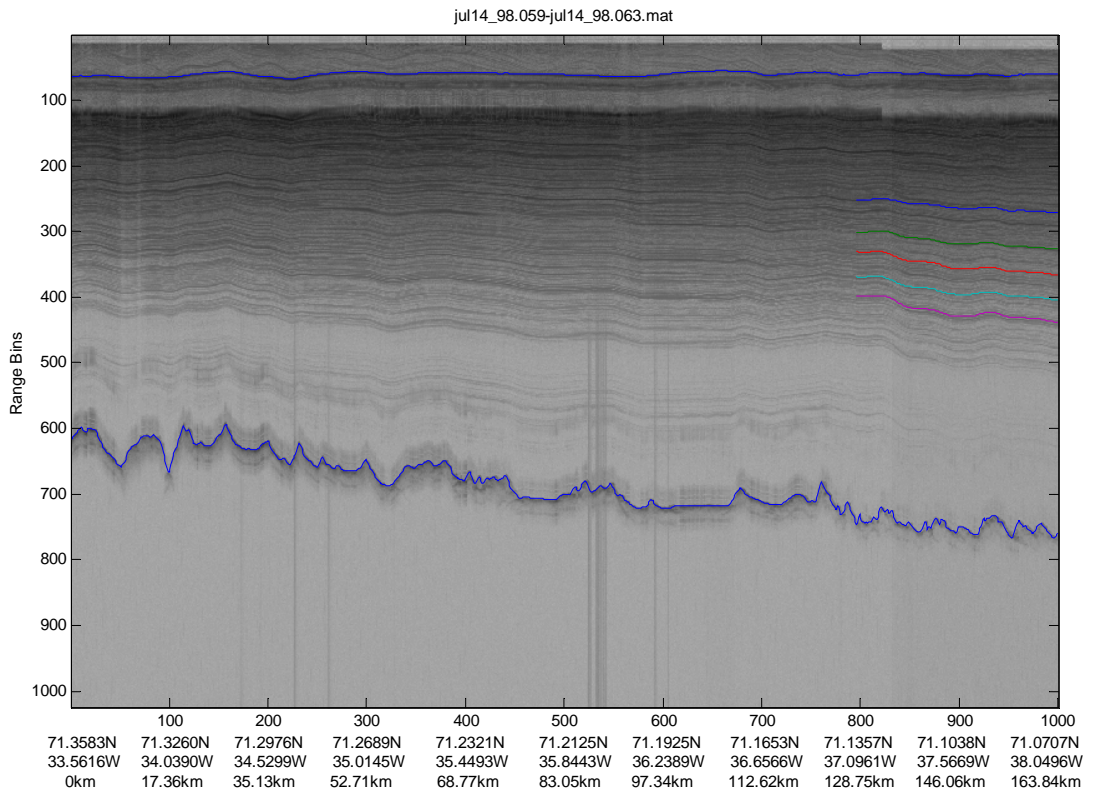


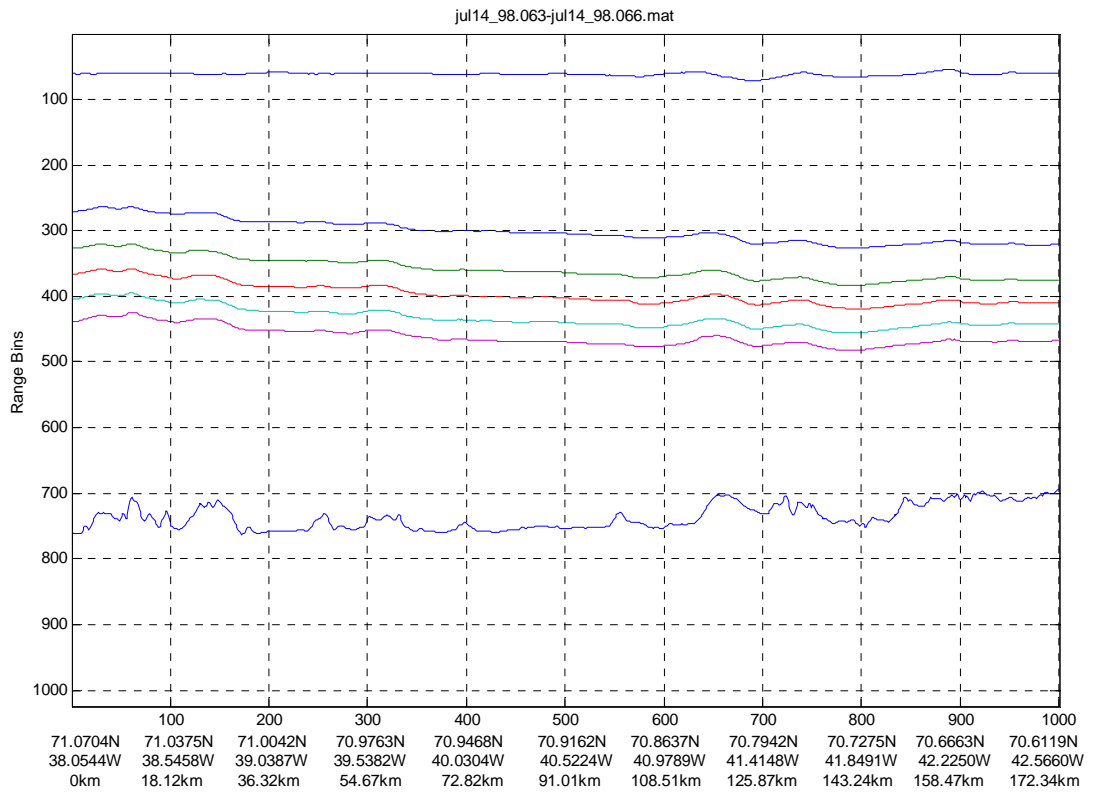
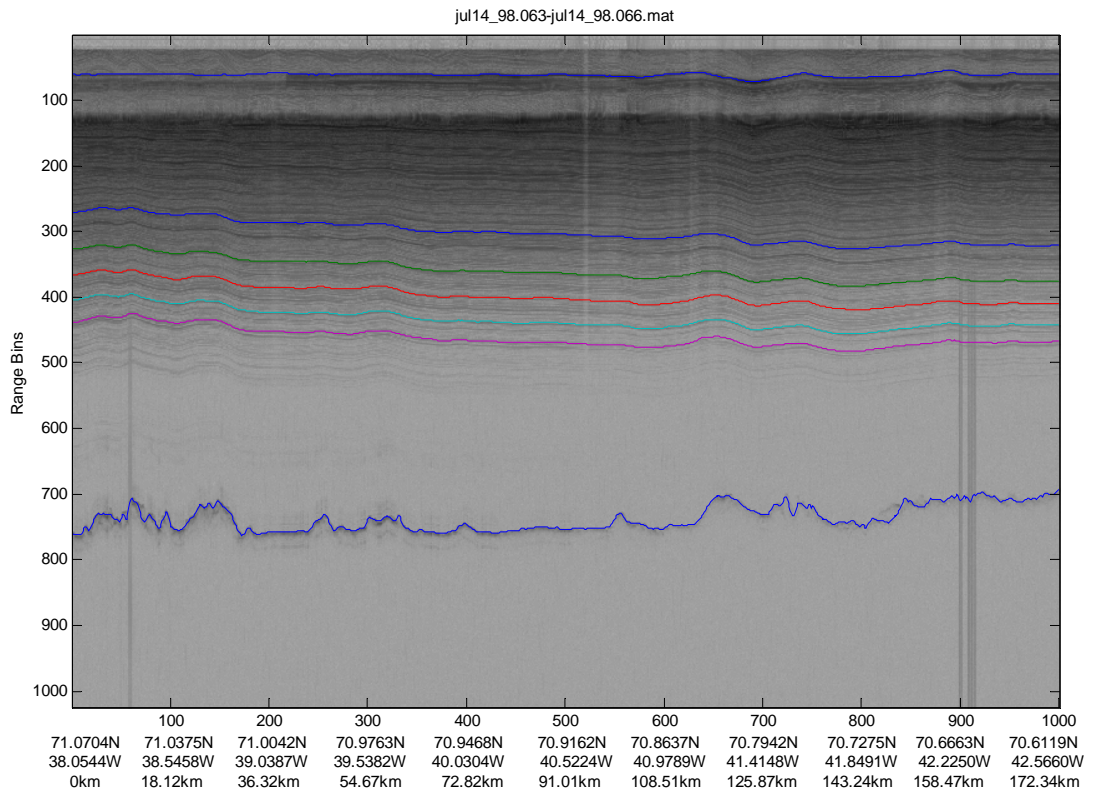


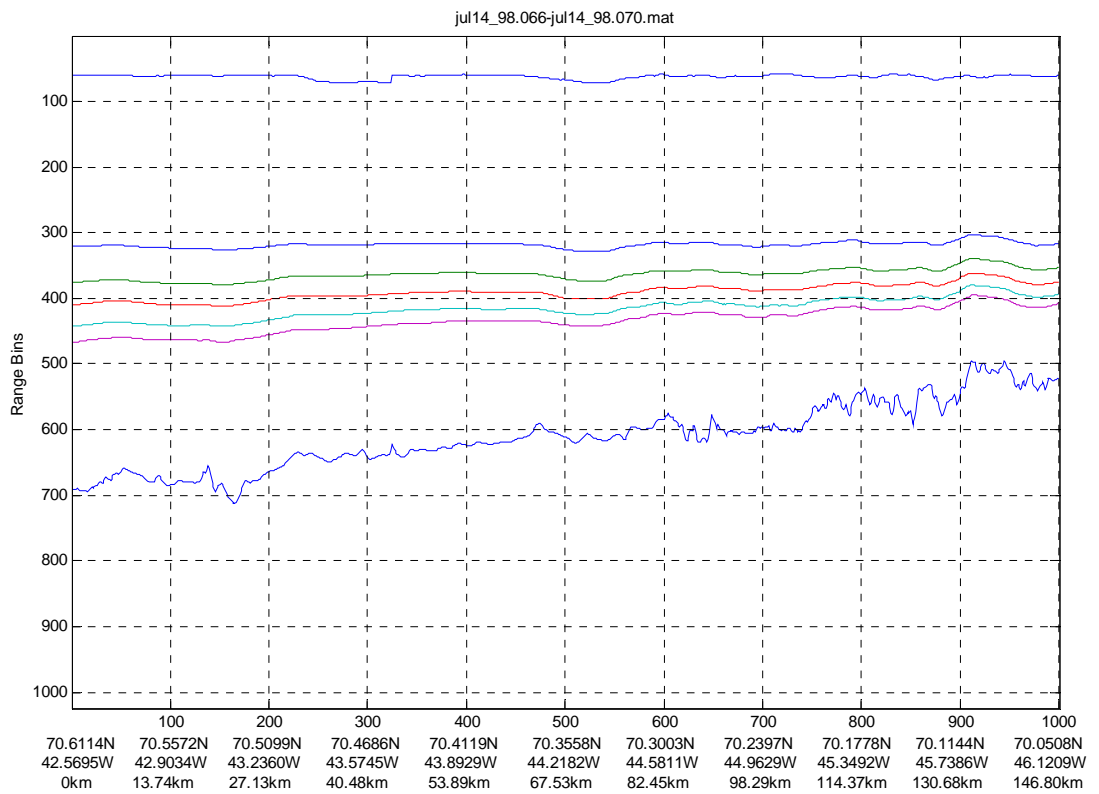
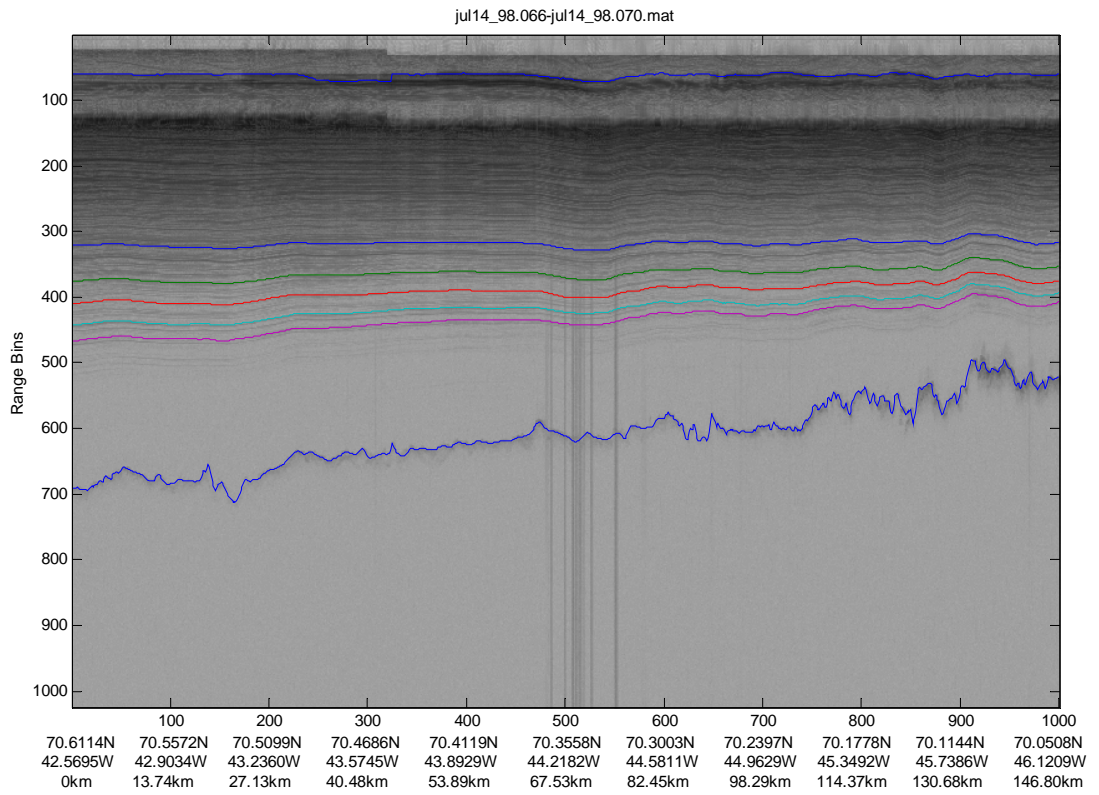


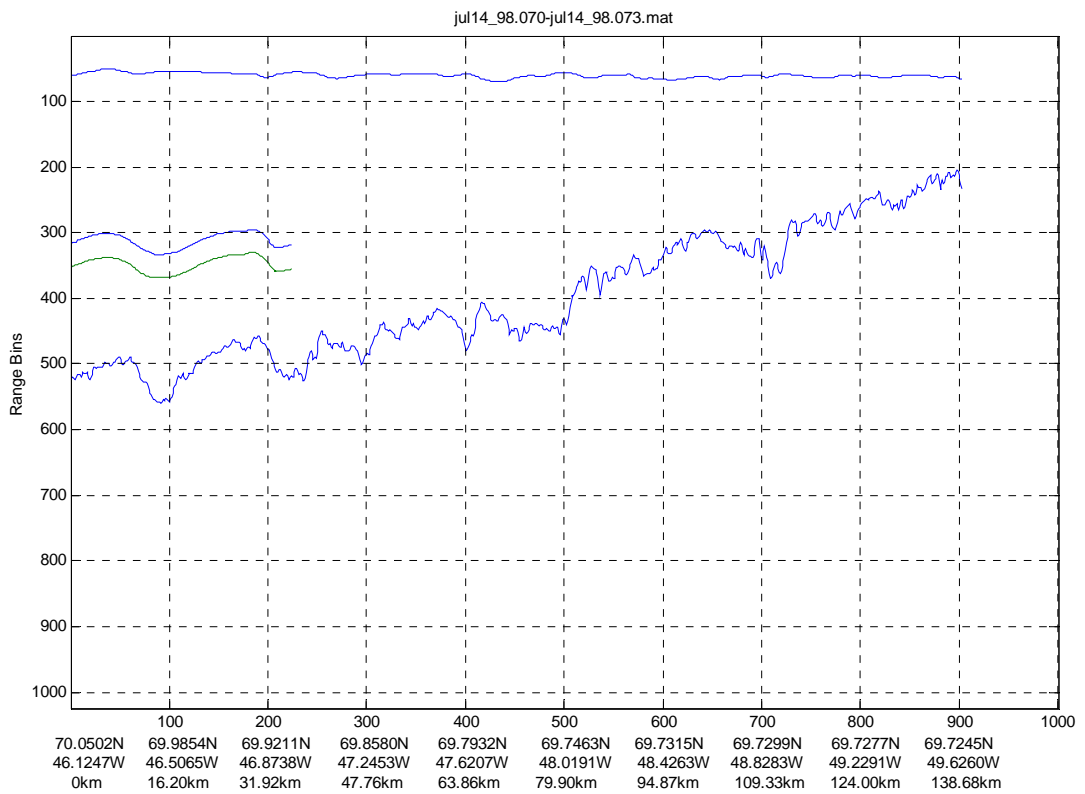
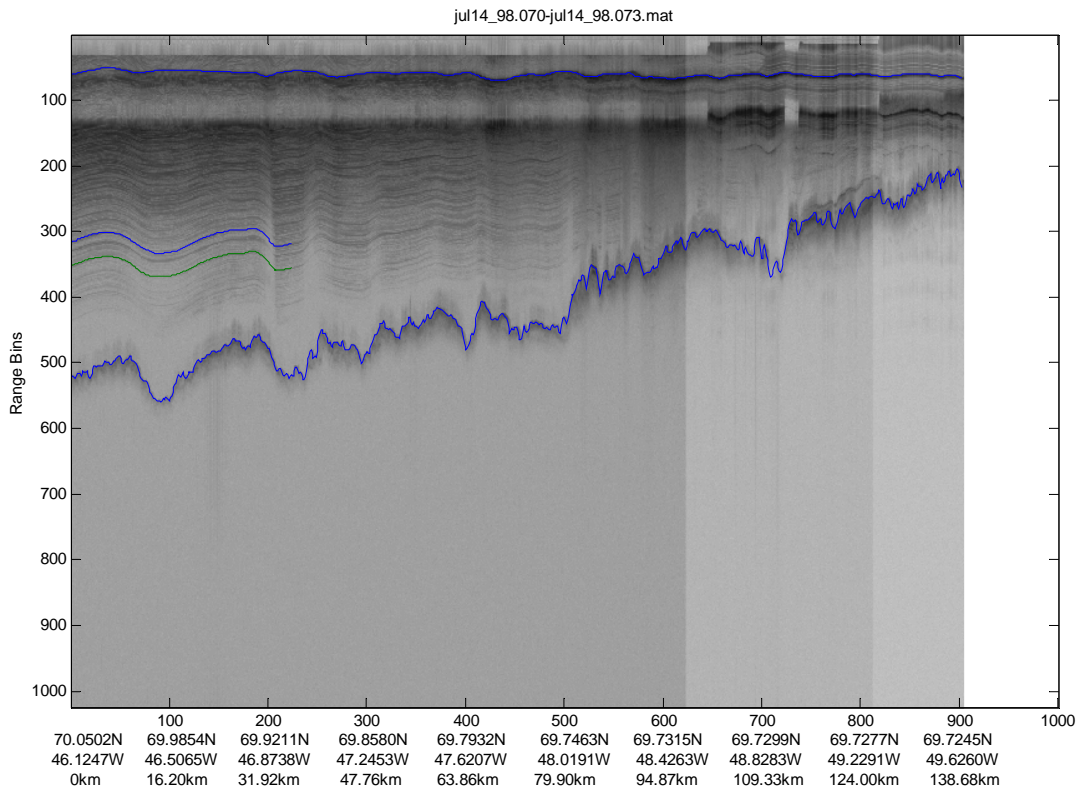




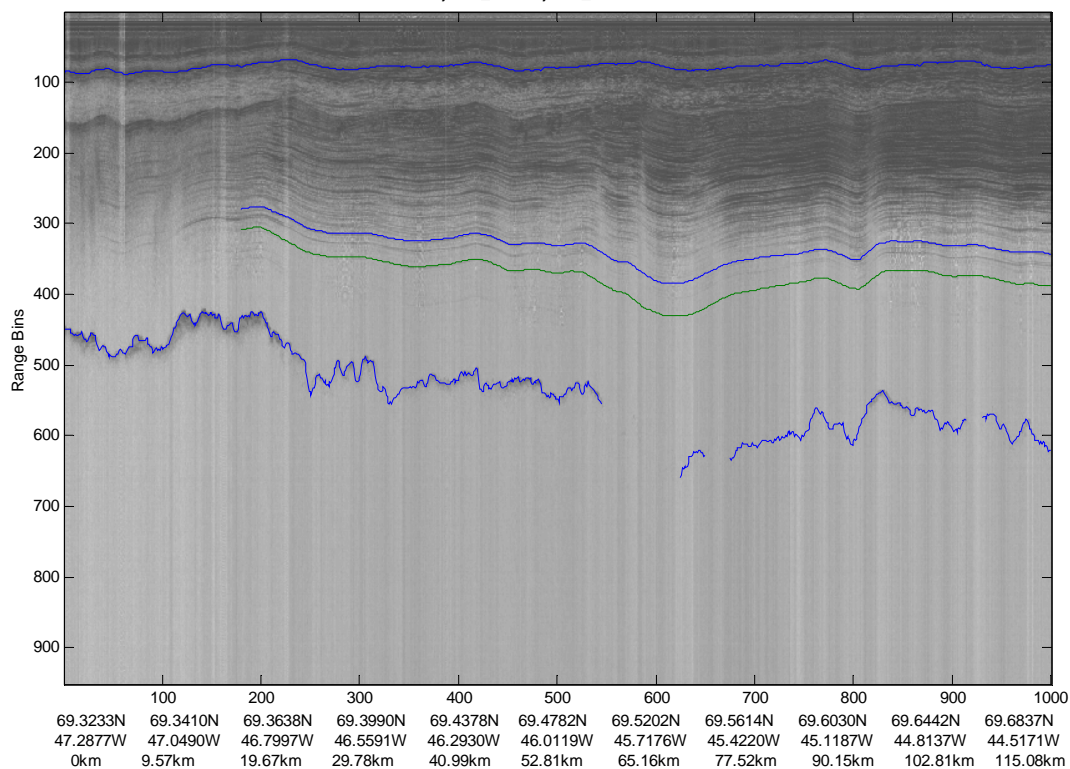




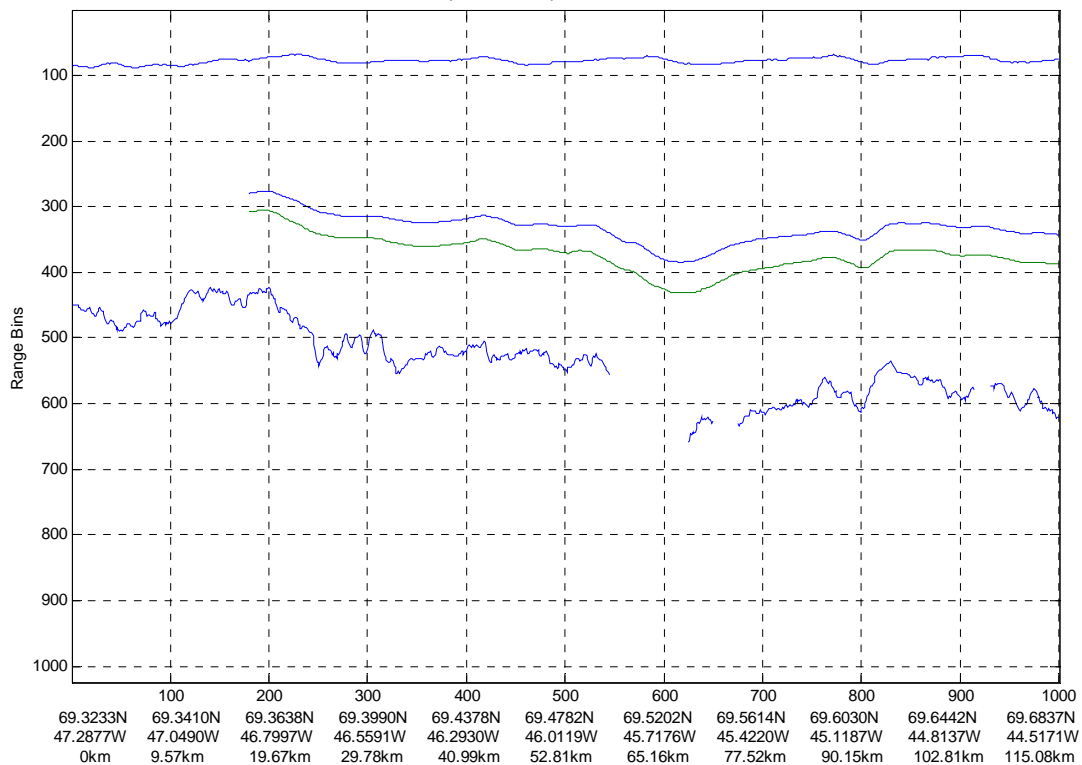




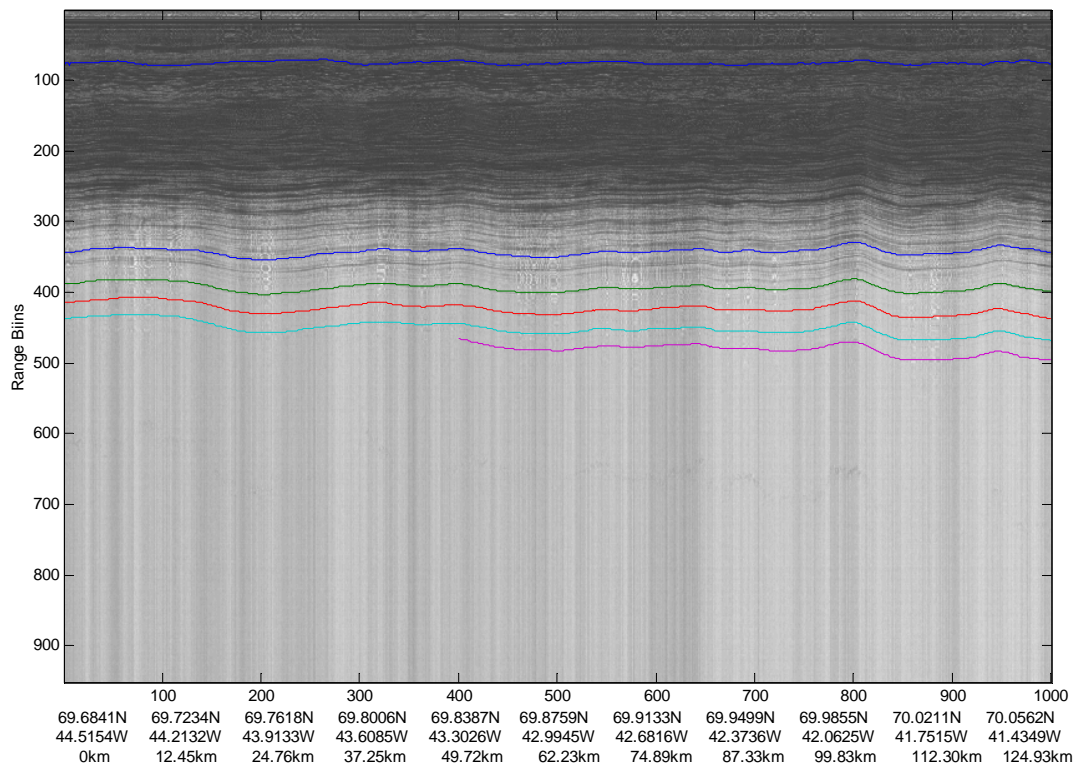
jun24_93.003-jun24_93.003.mat



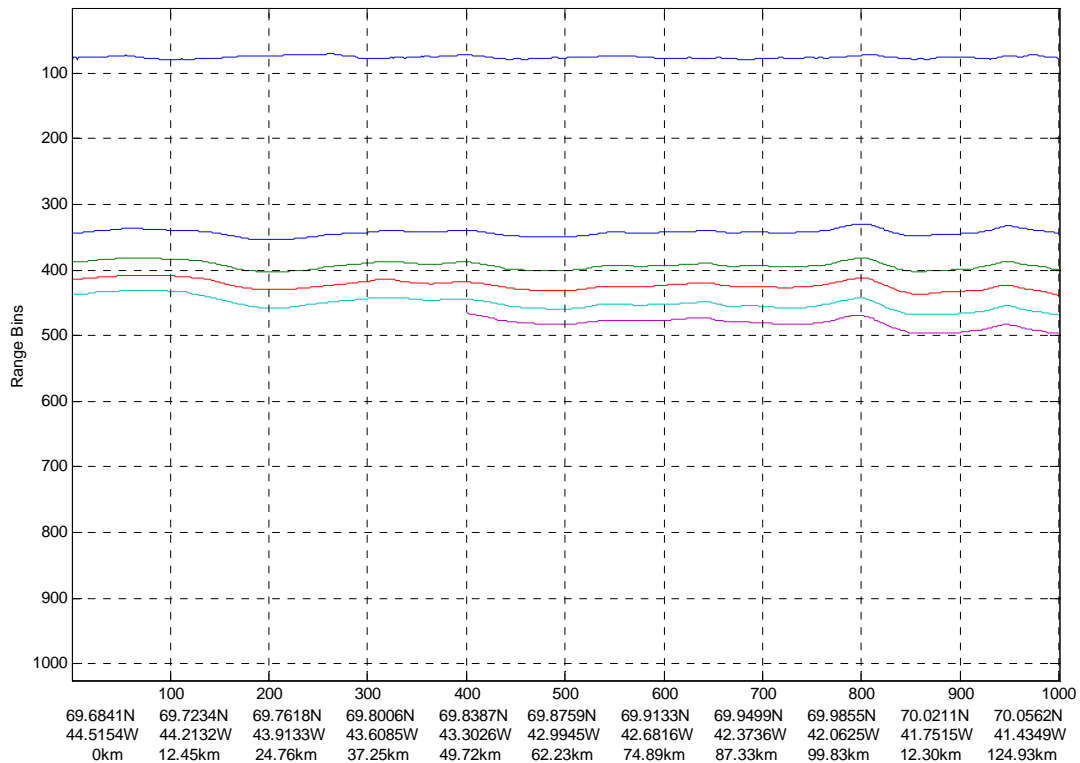
jun24_93.003-jun24_93.003.mat

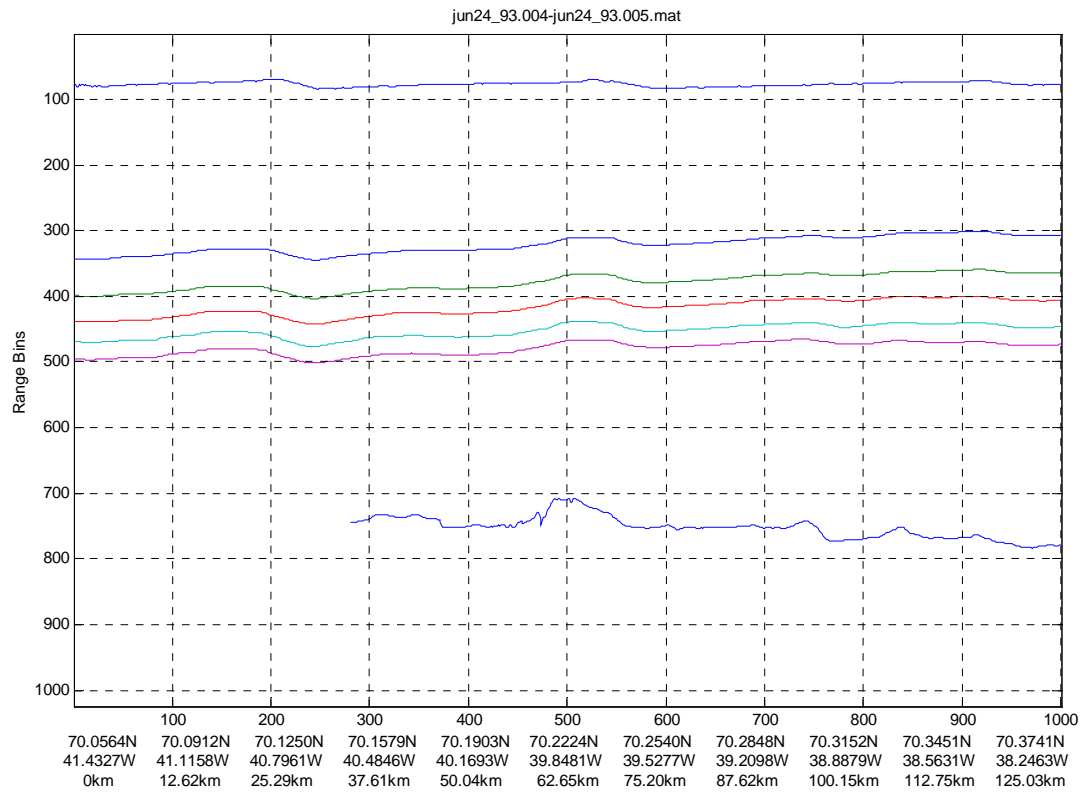
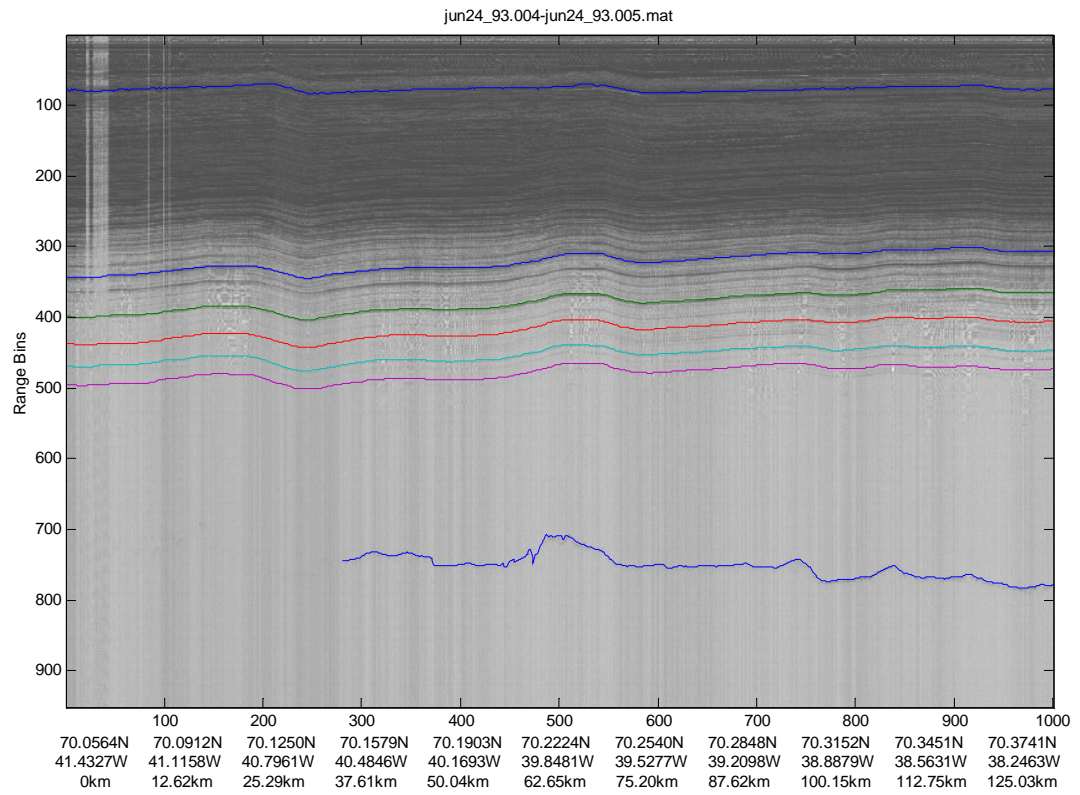


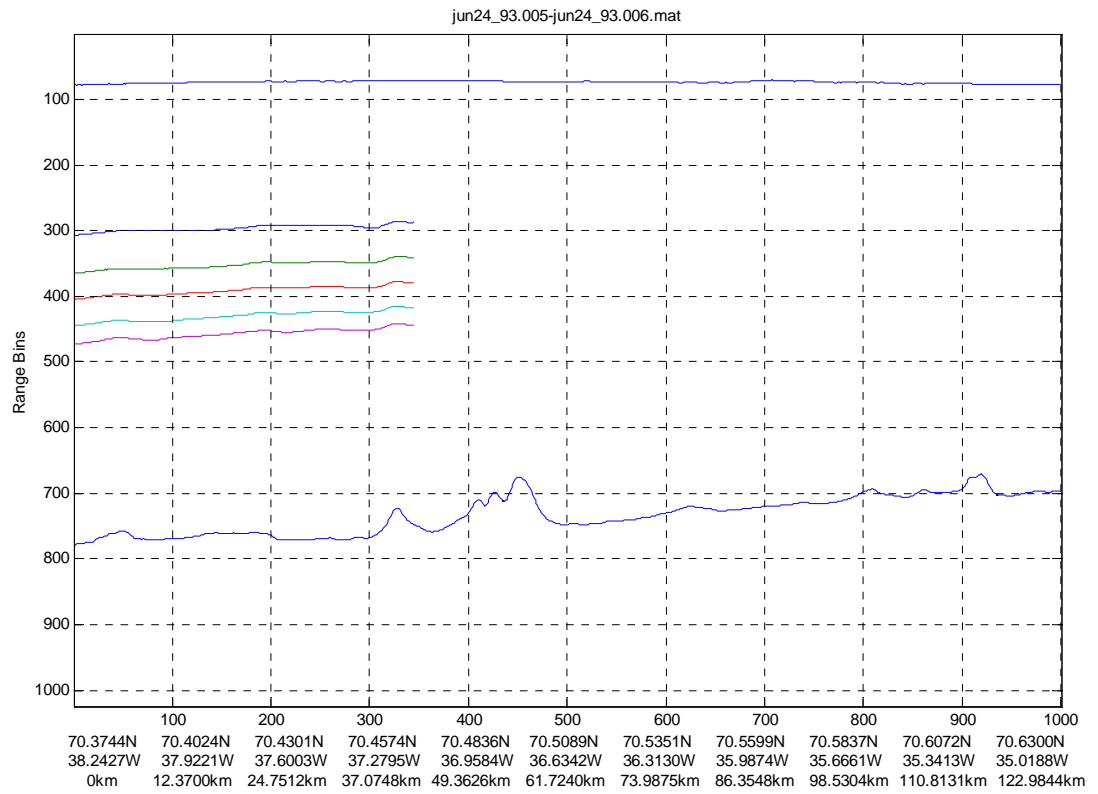
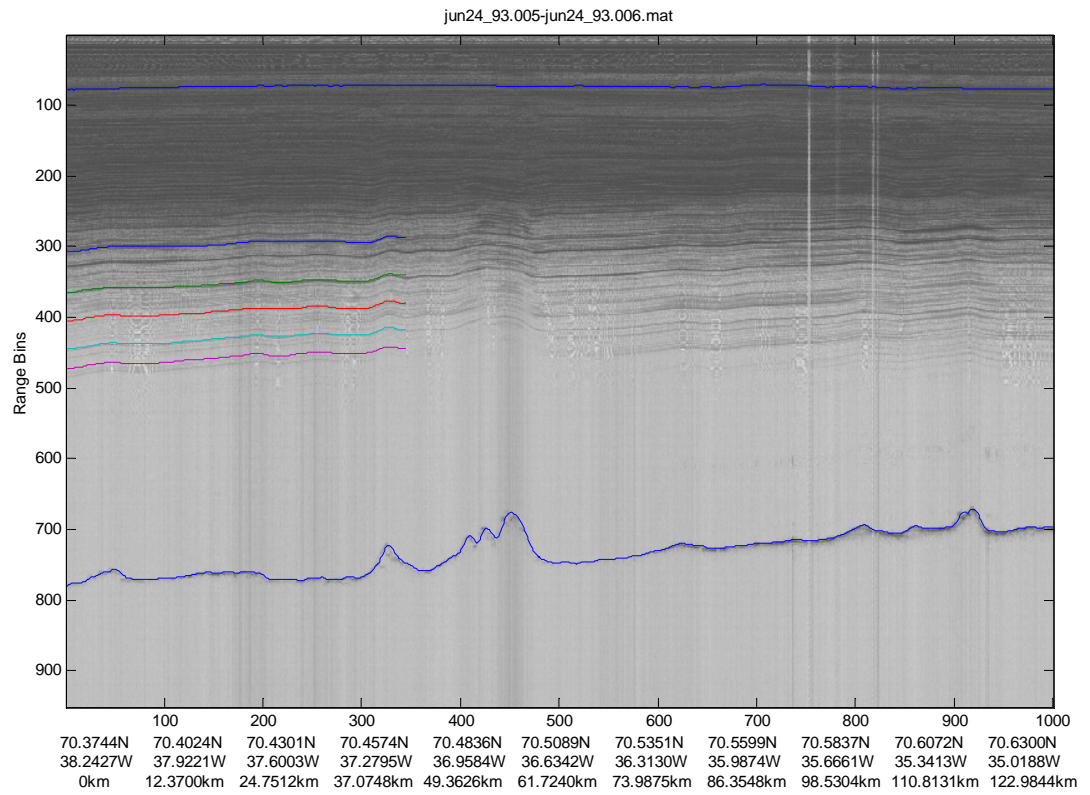
jun24_93.003-jun24_93.004.mat

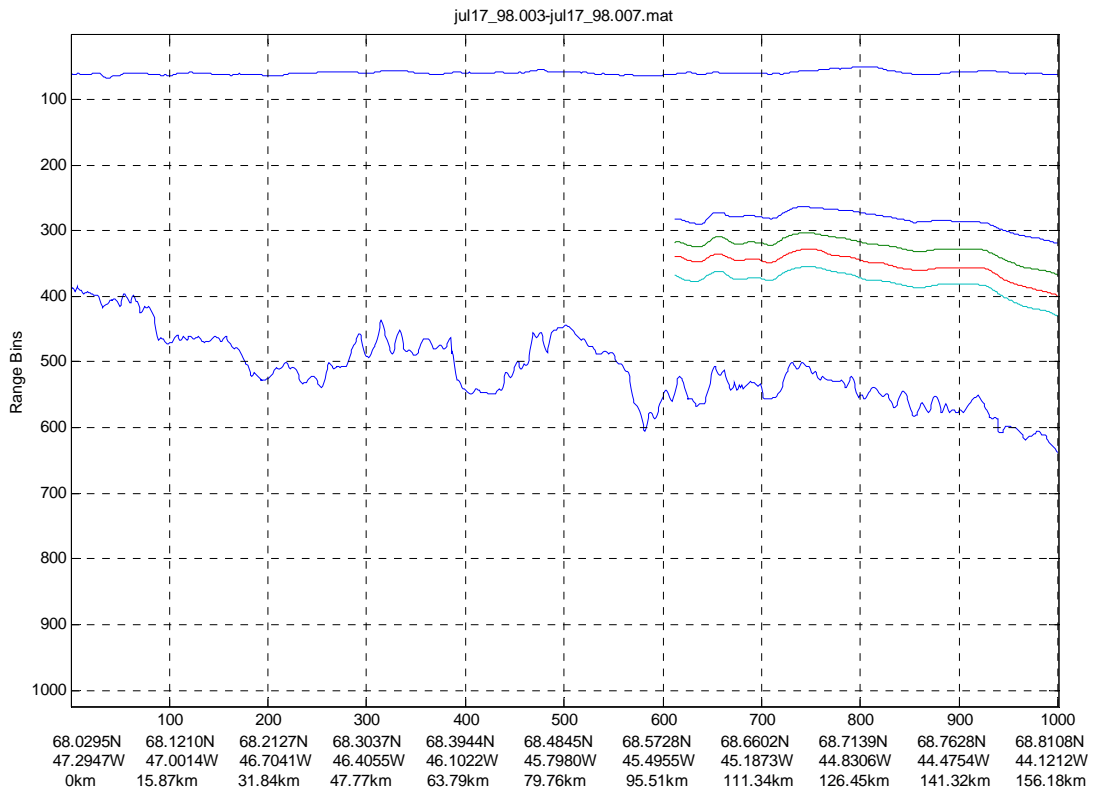
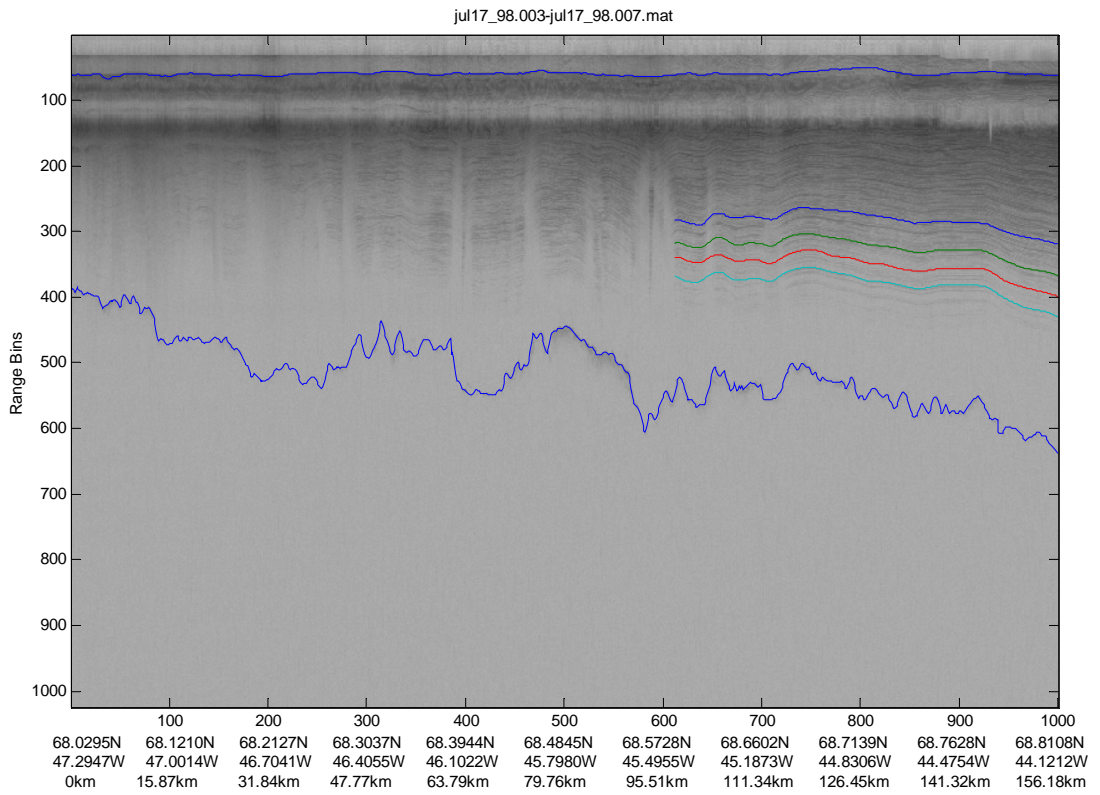


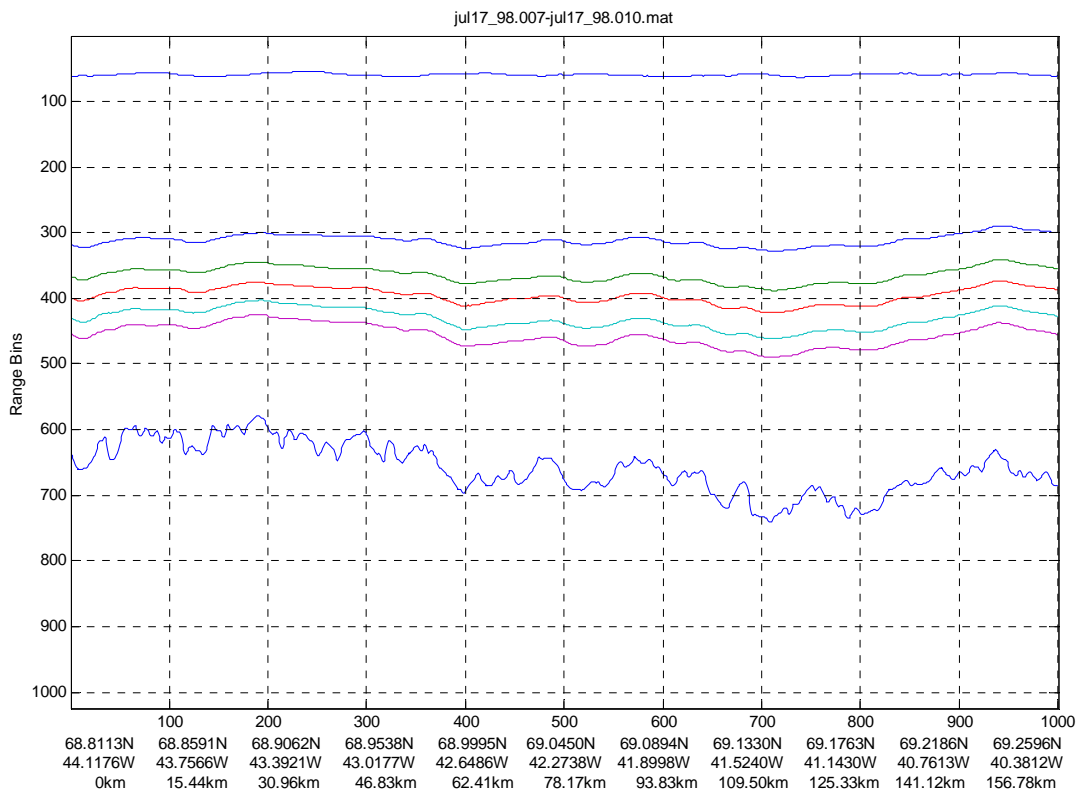
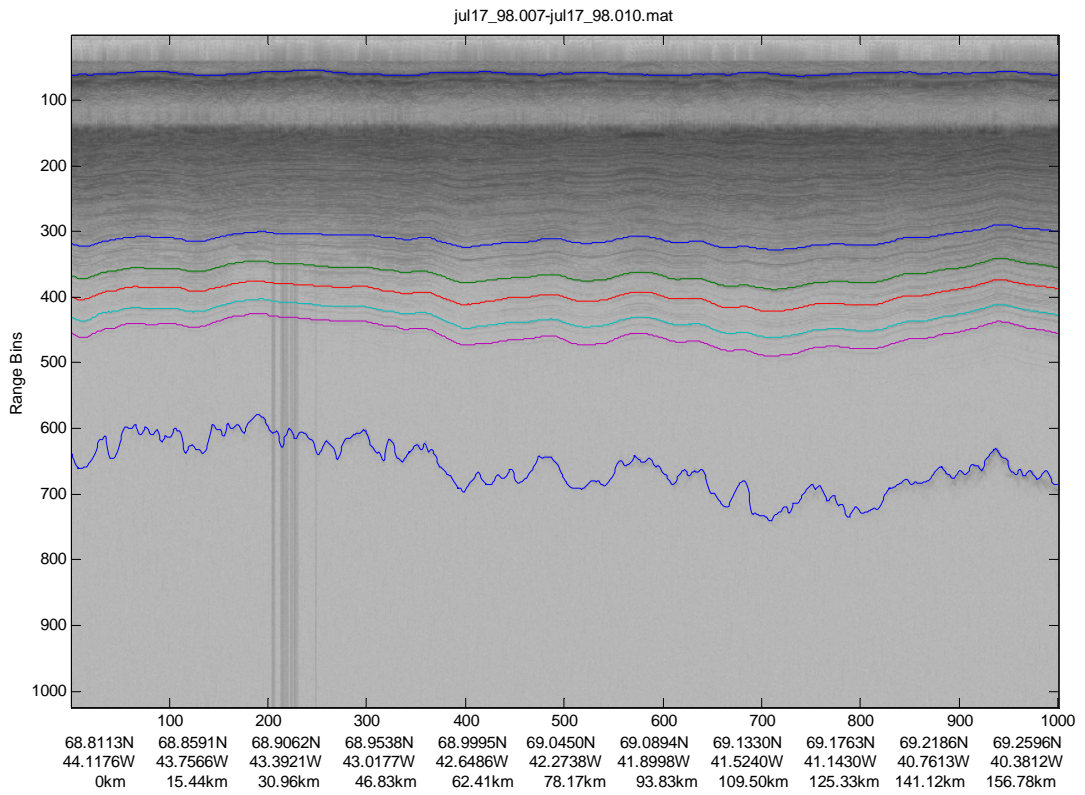
jun24_93.003-jun24_93.004.mat

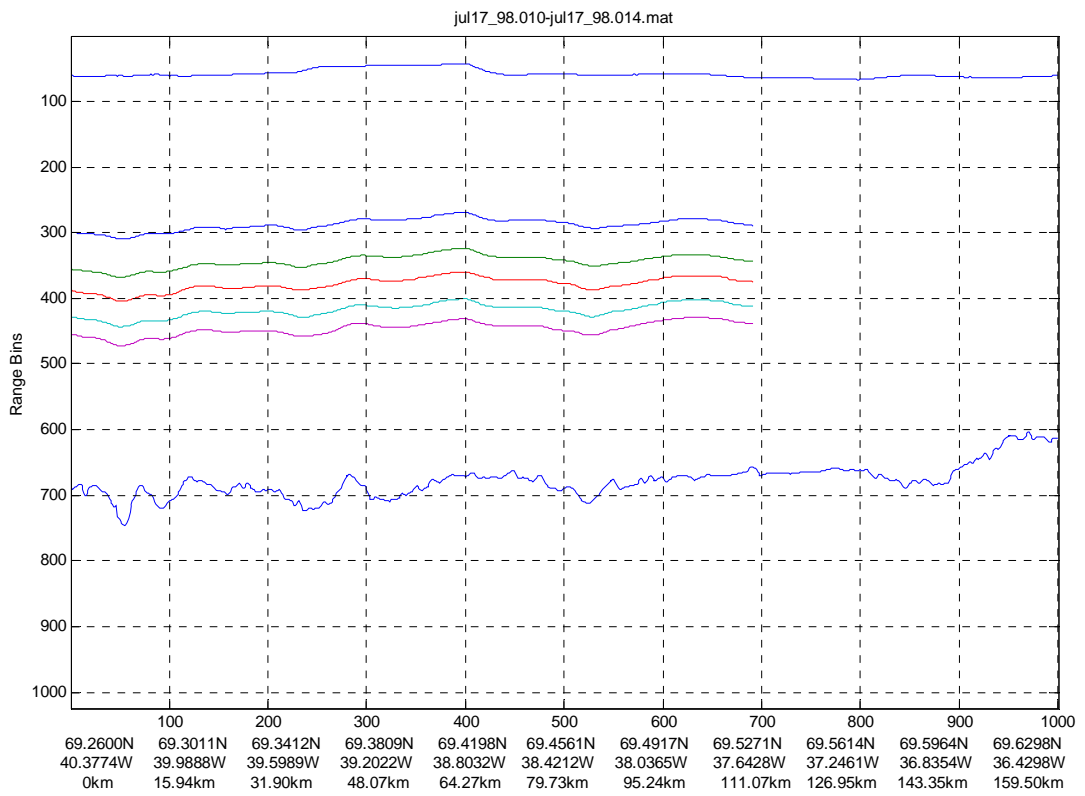
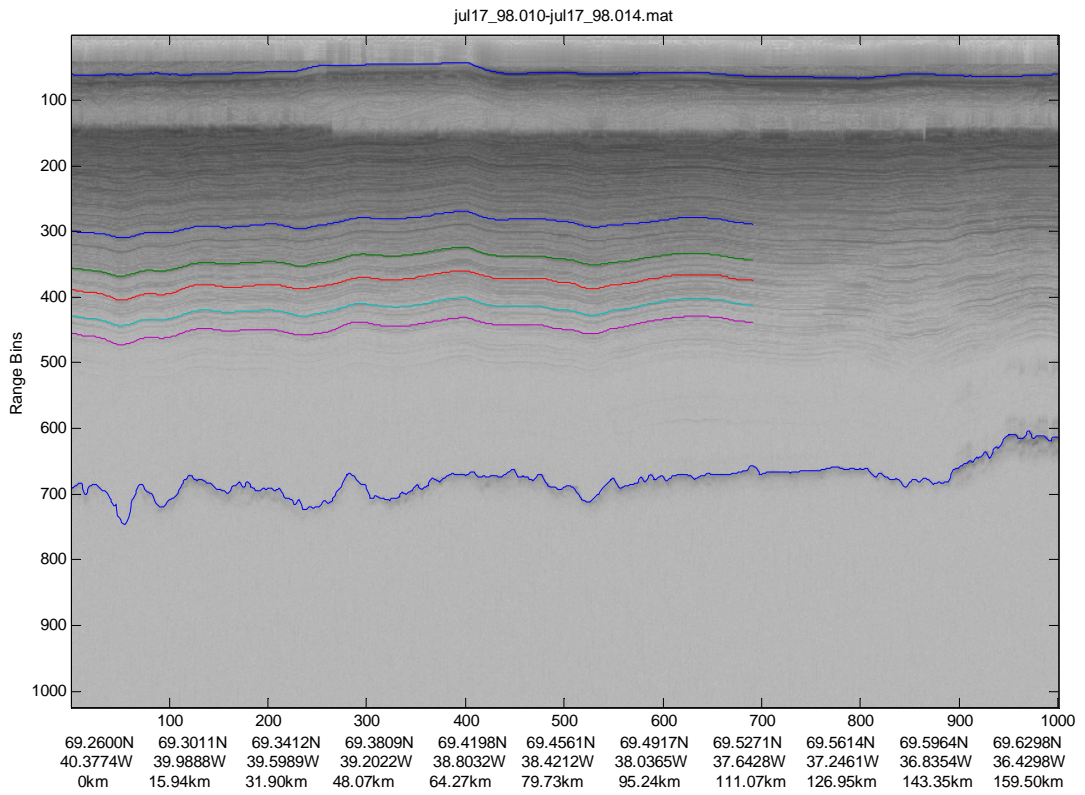


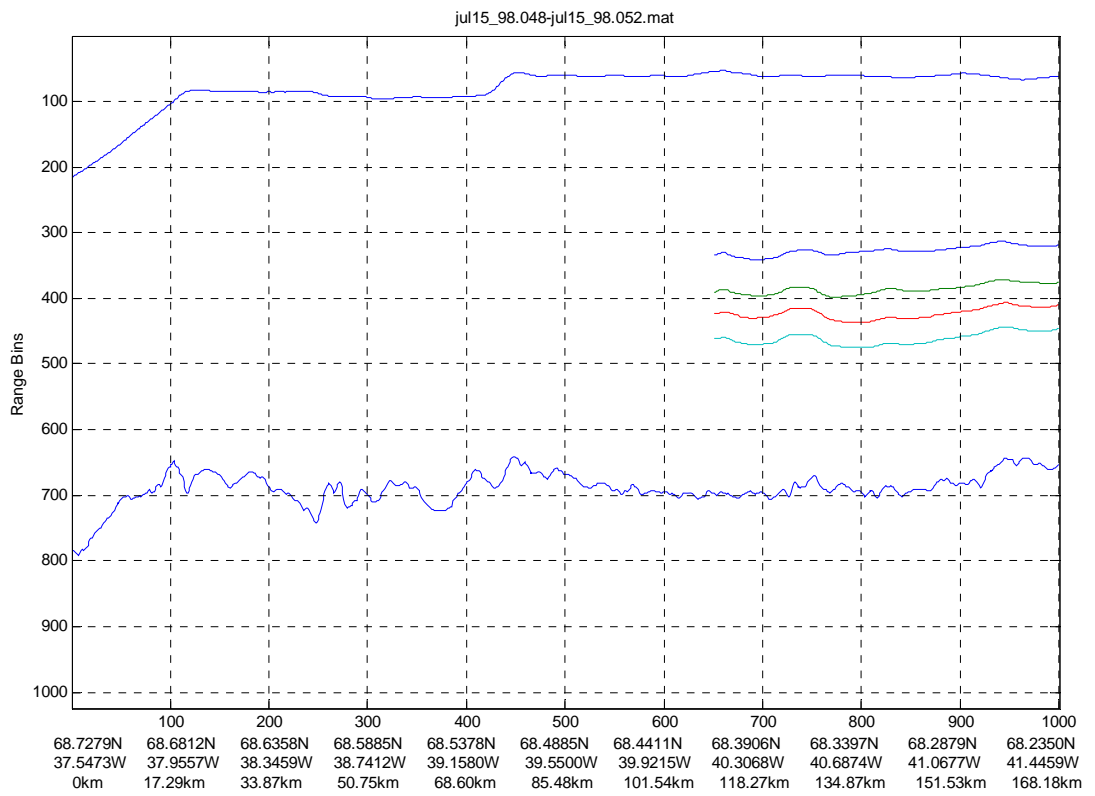
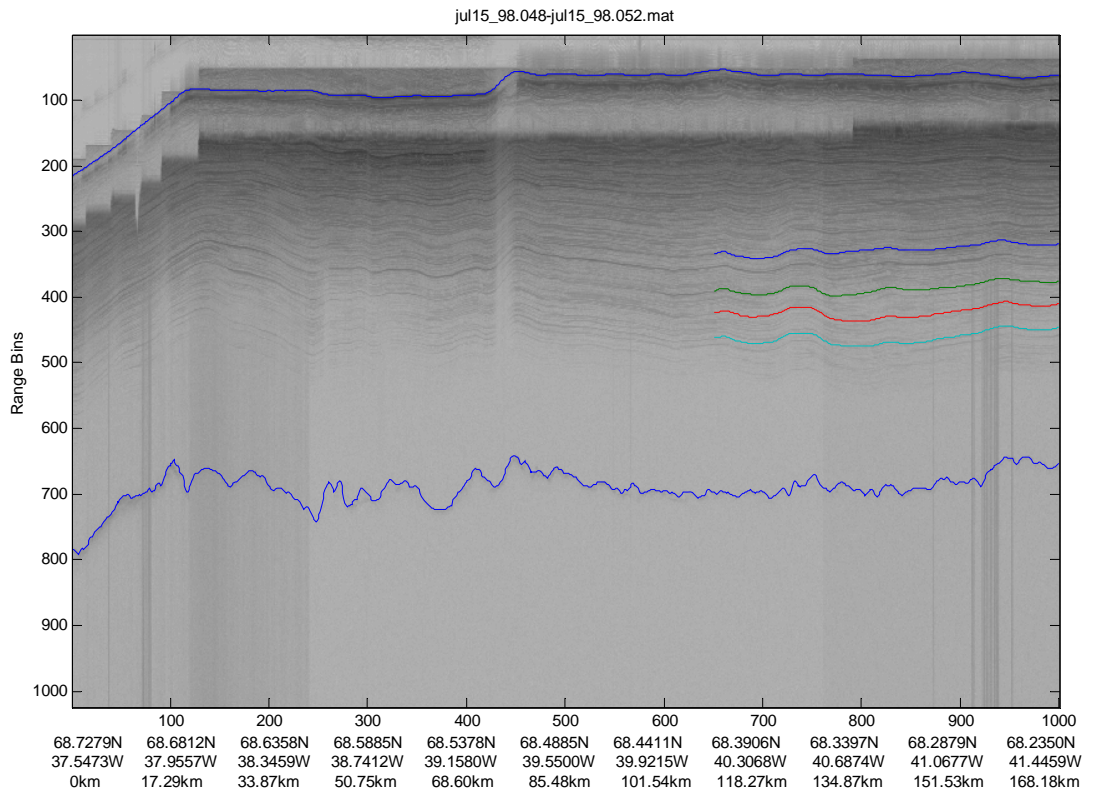


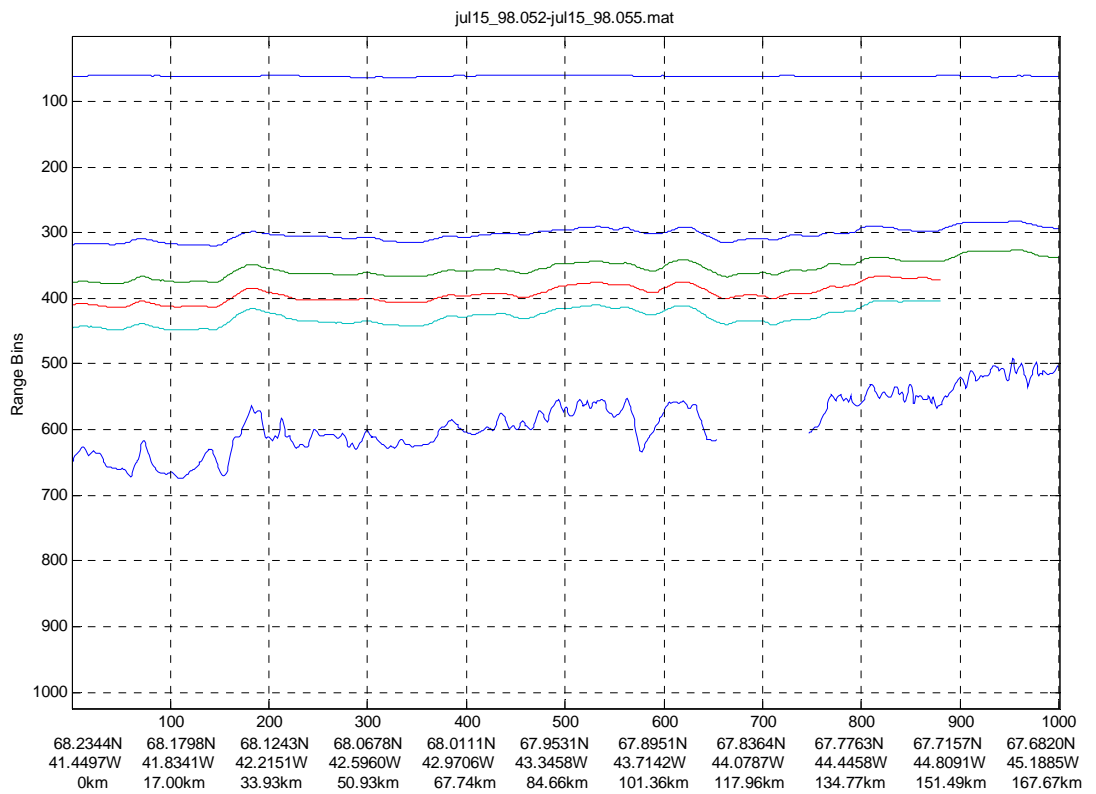
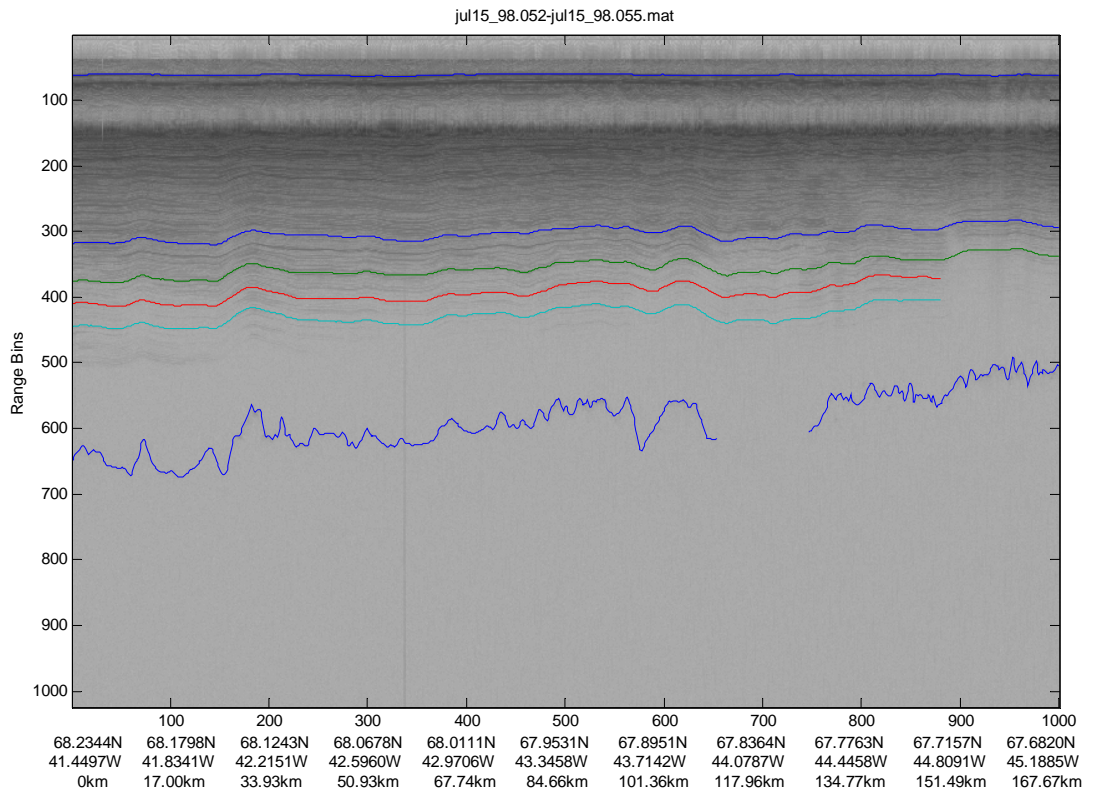


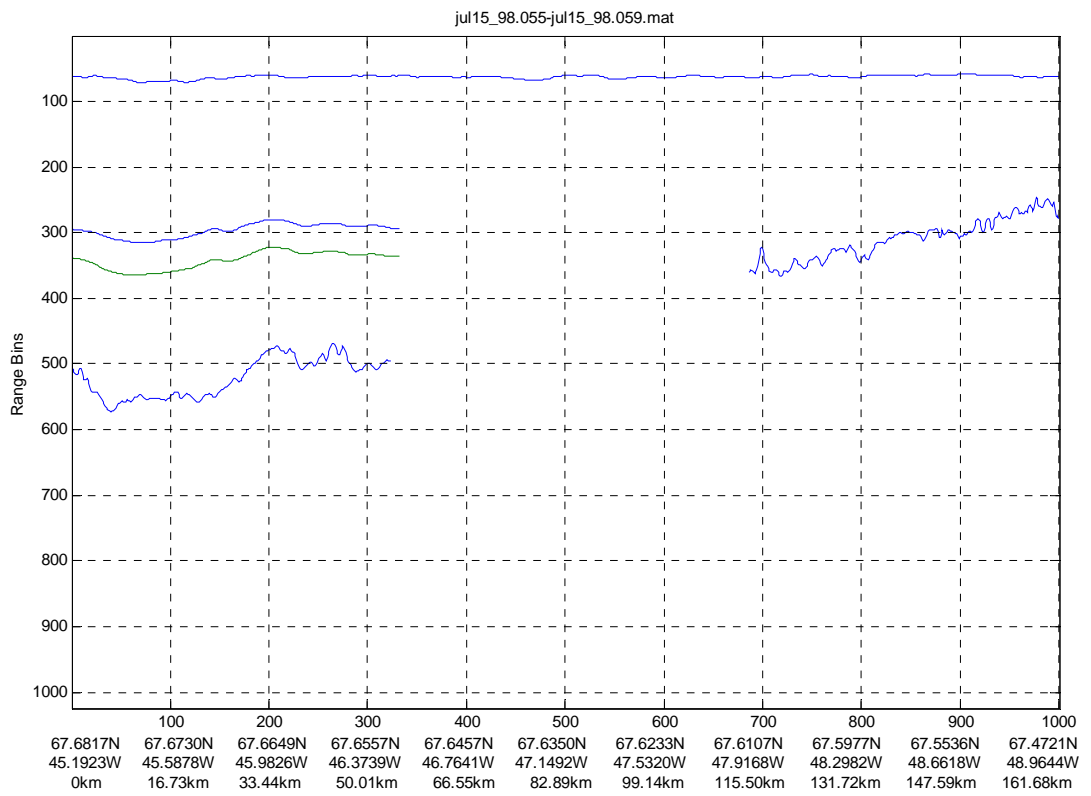
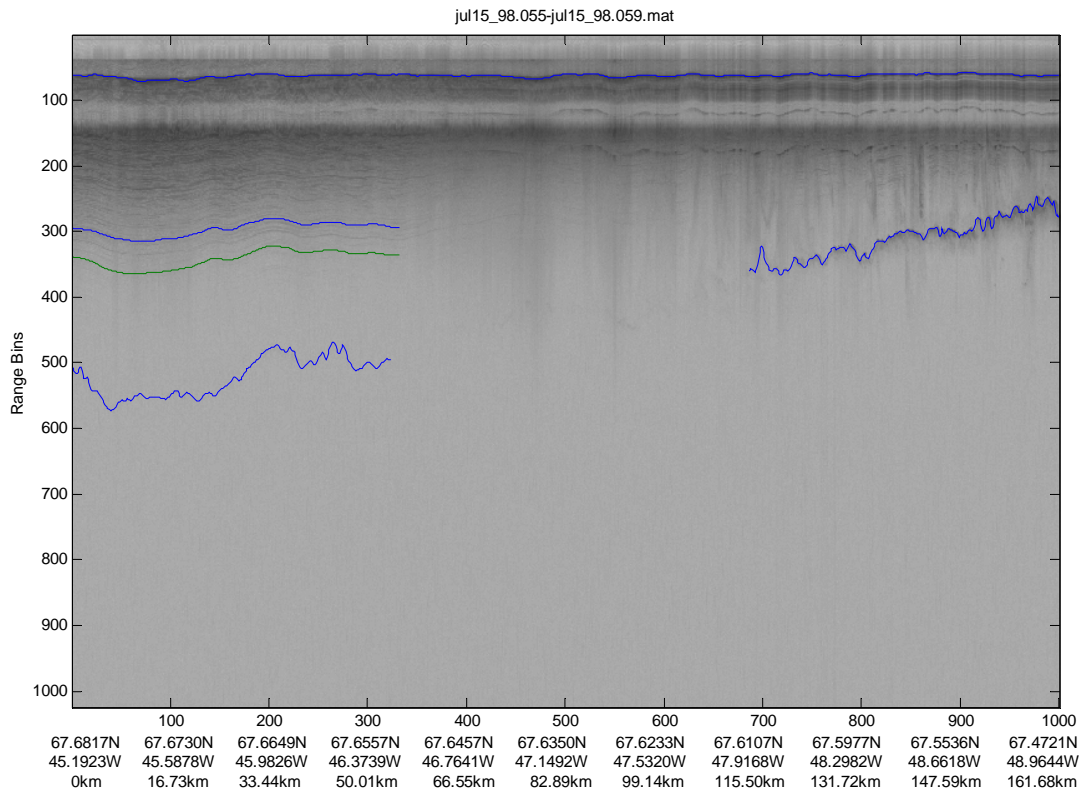


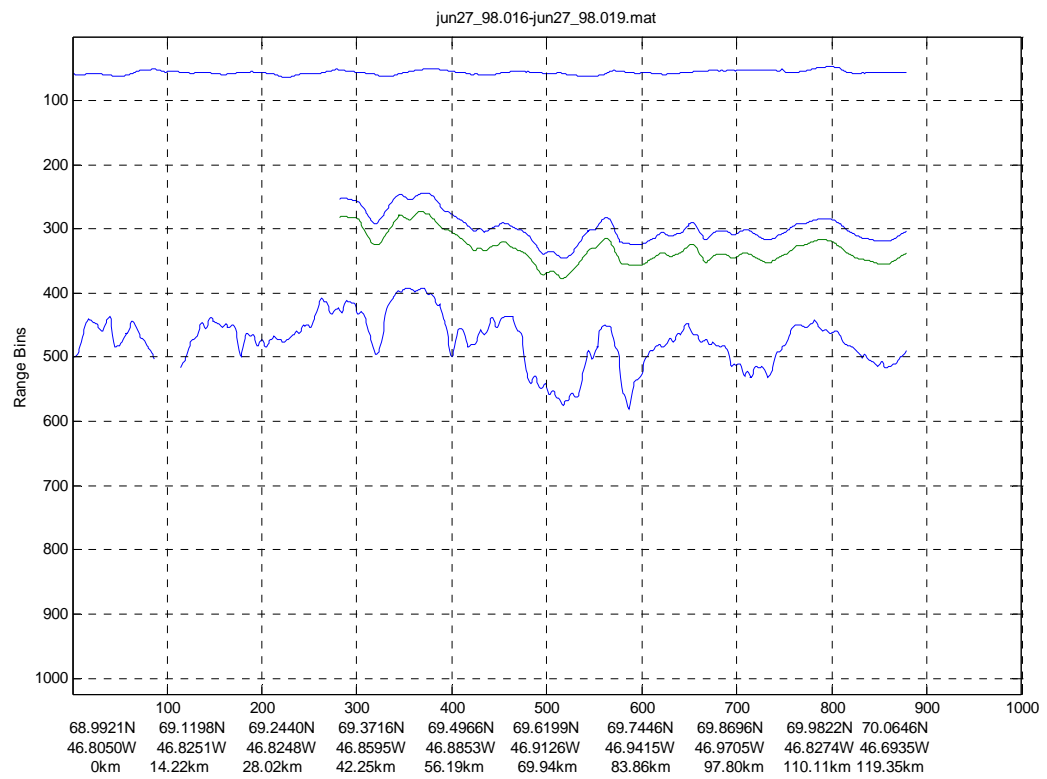
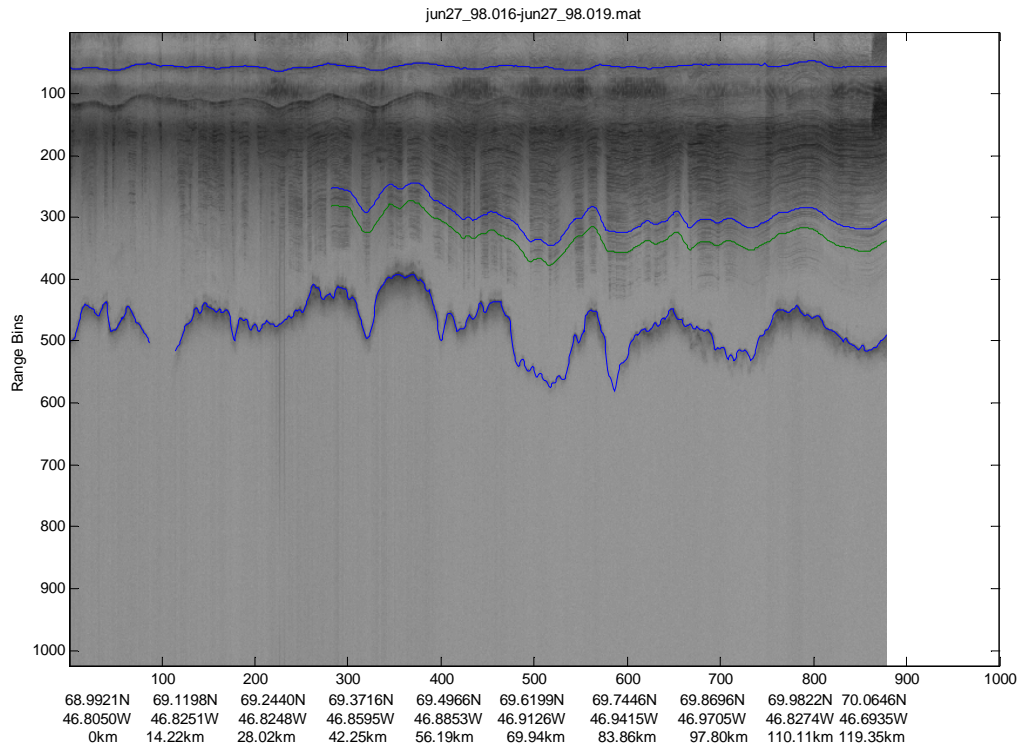


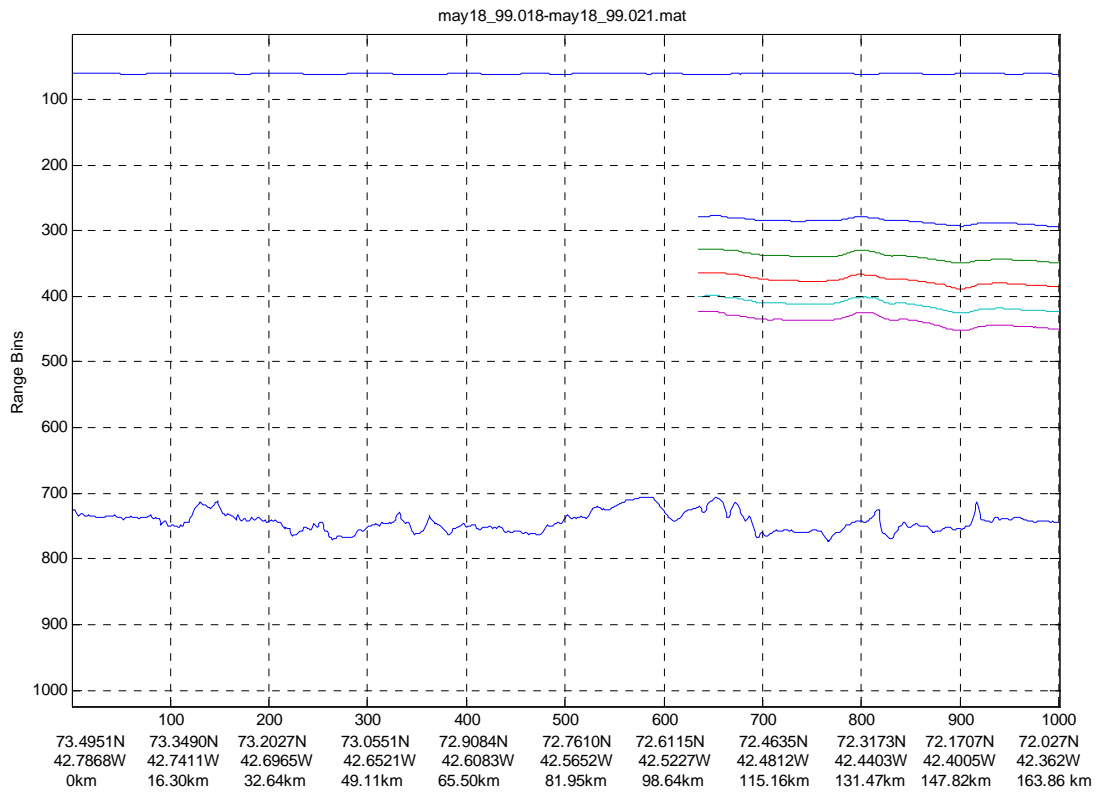
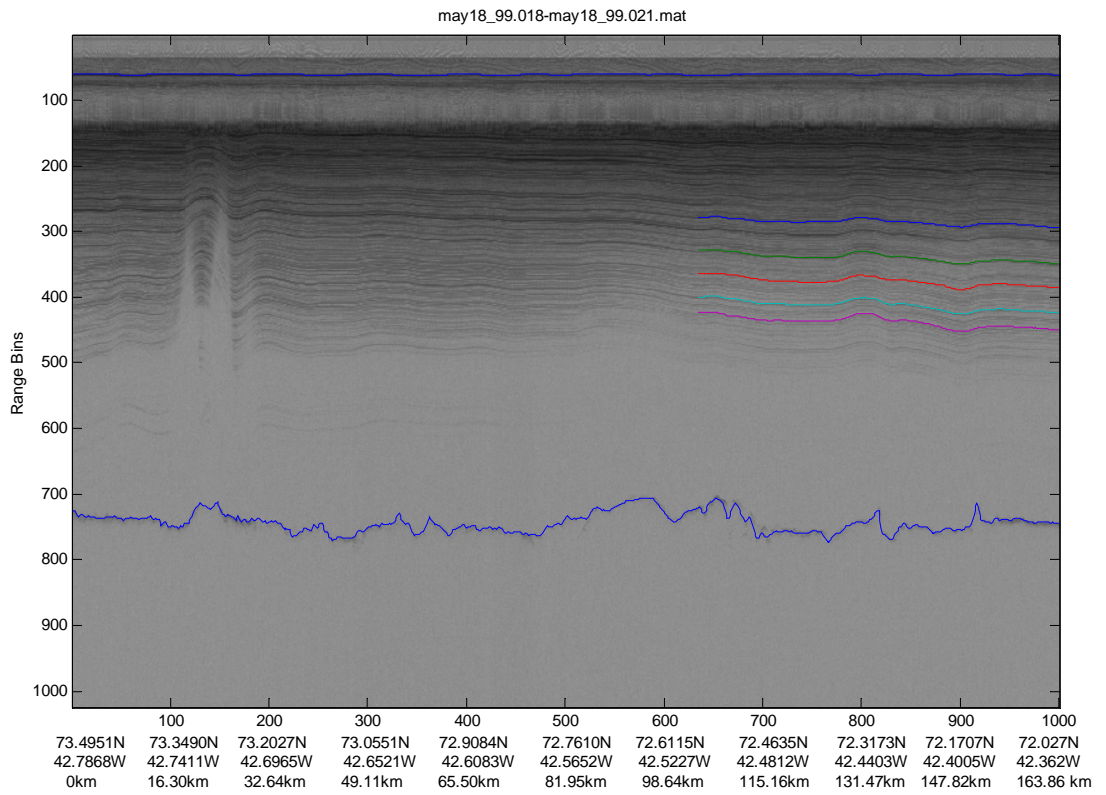


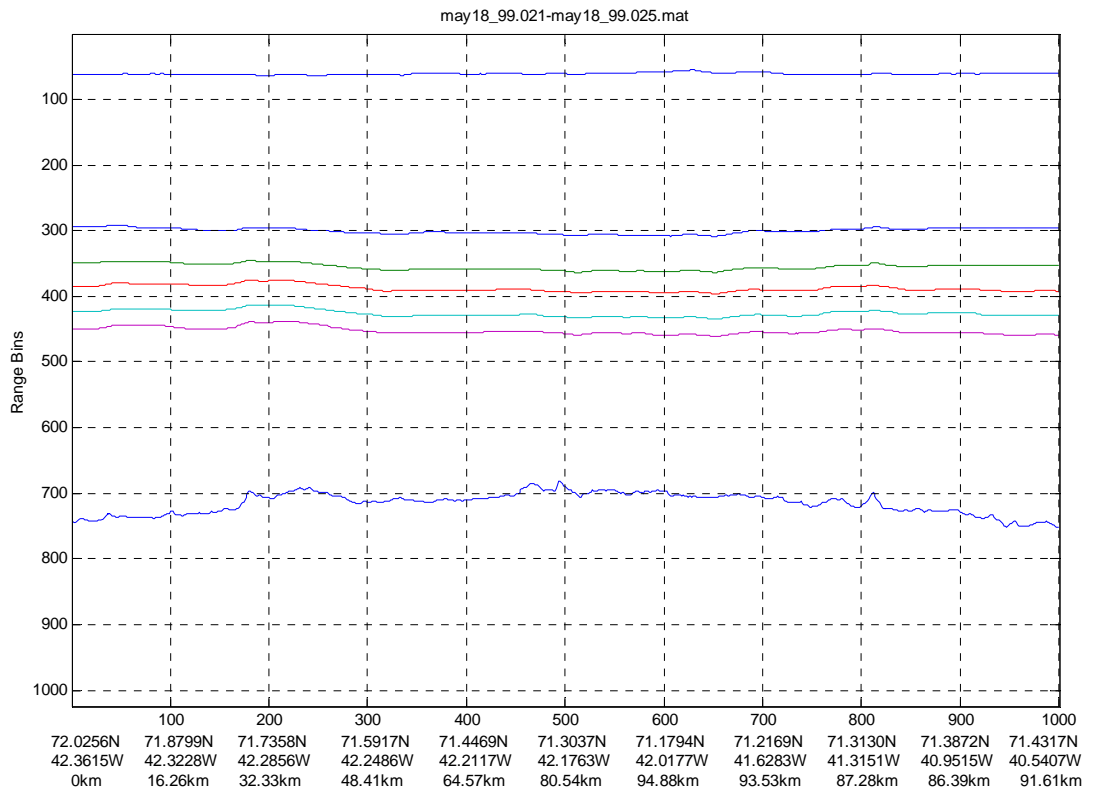
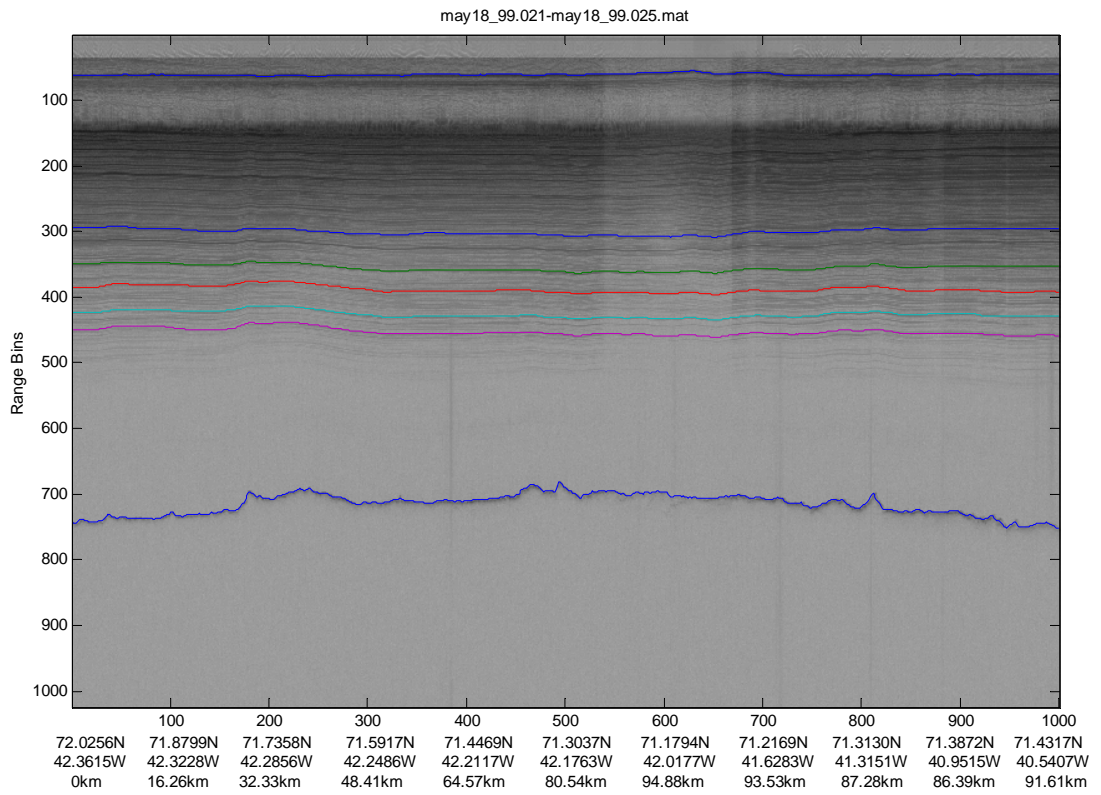


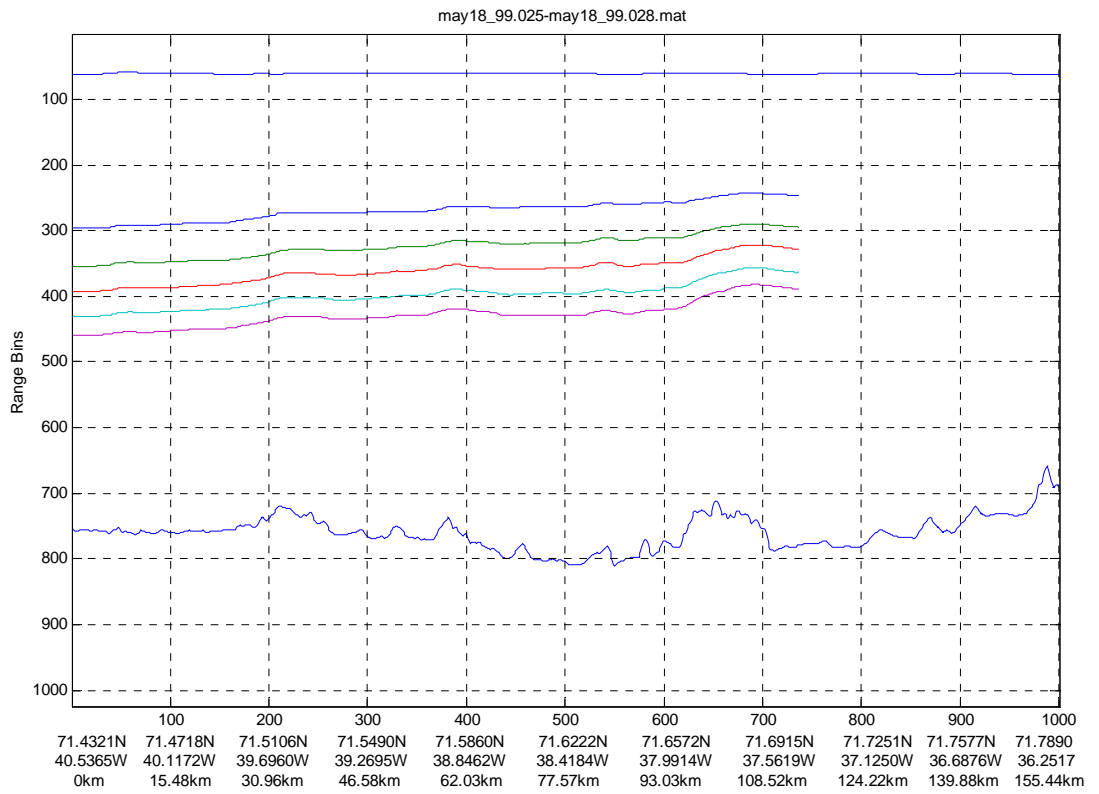
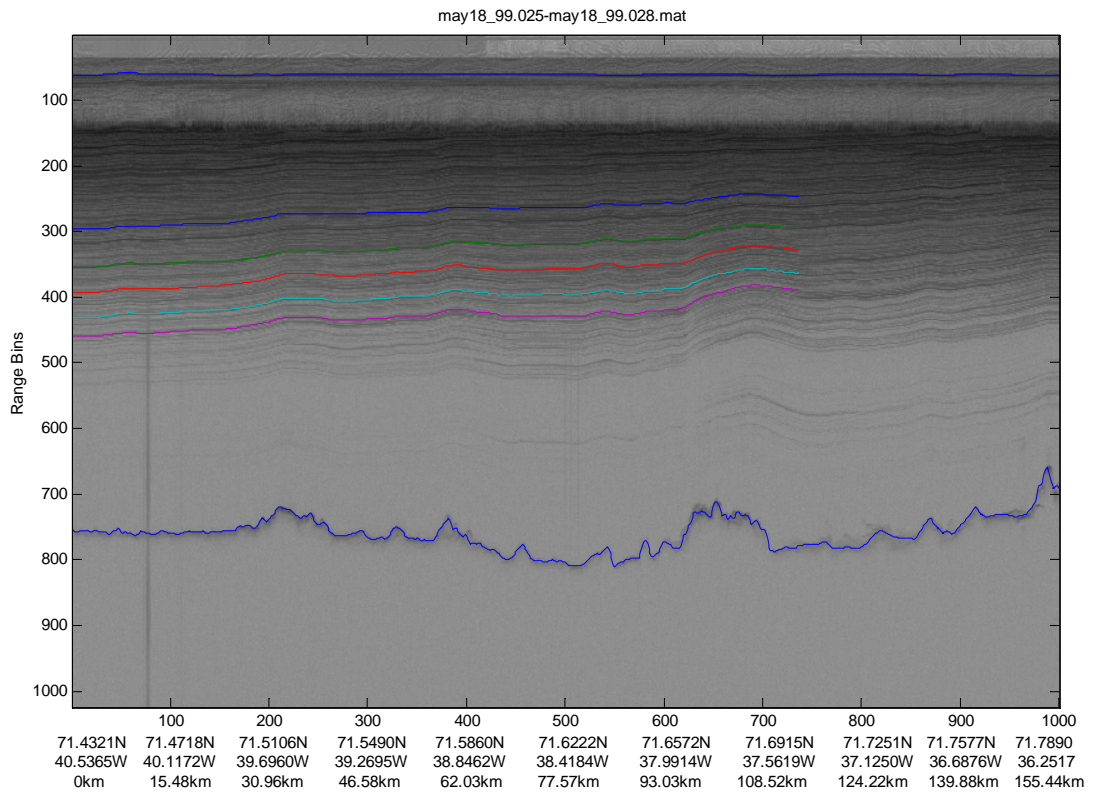


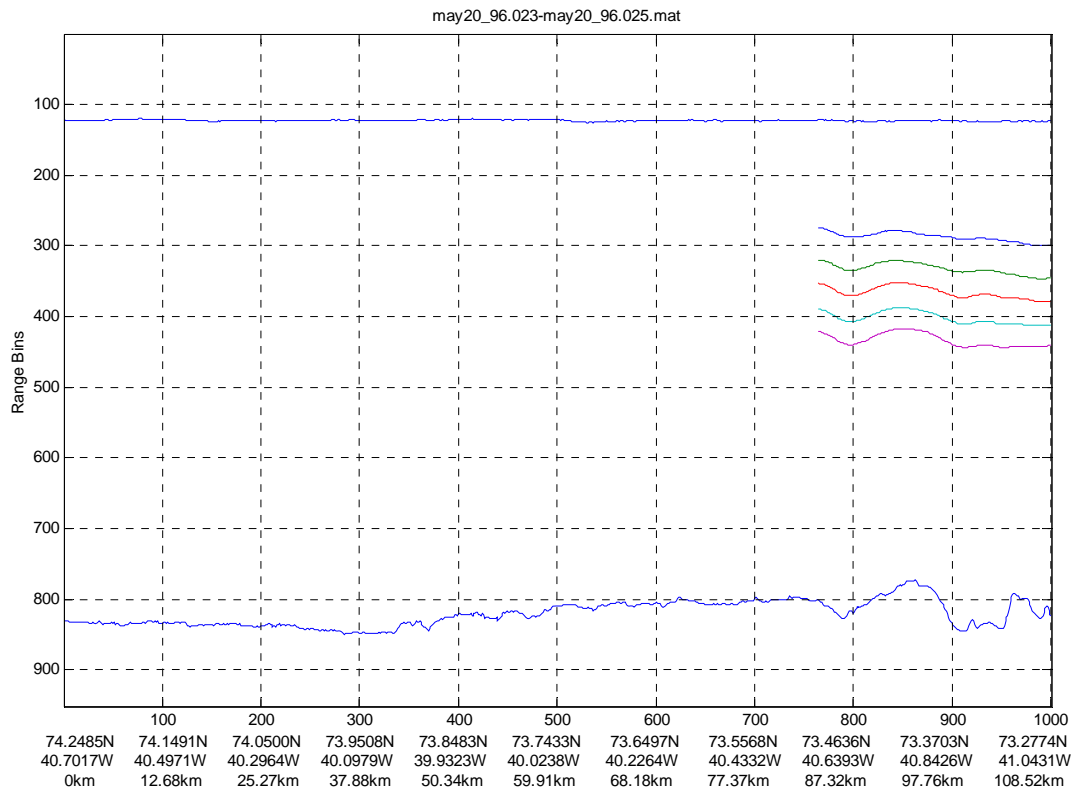
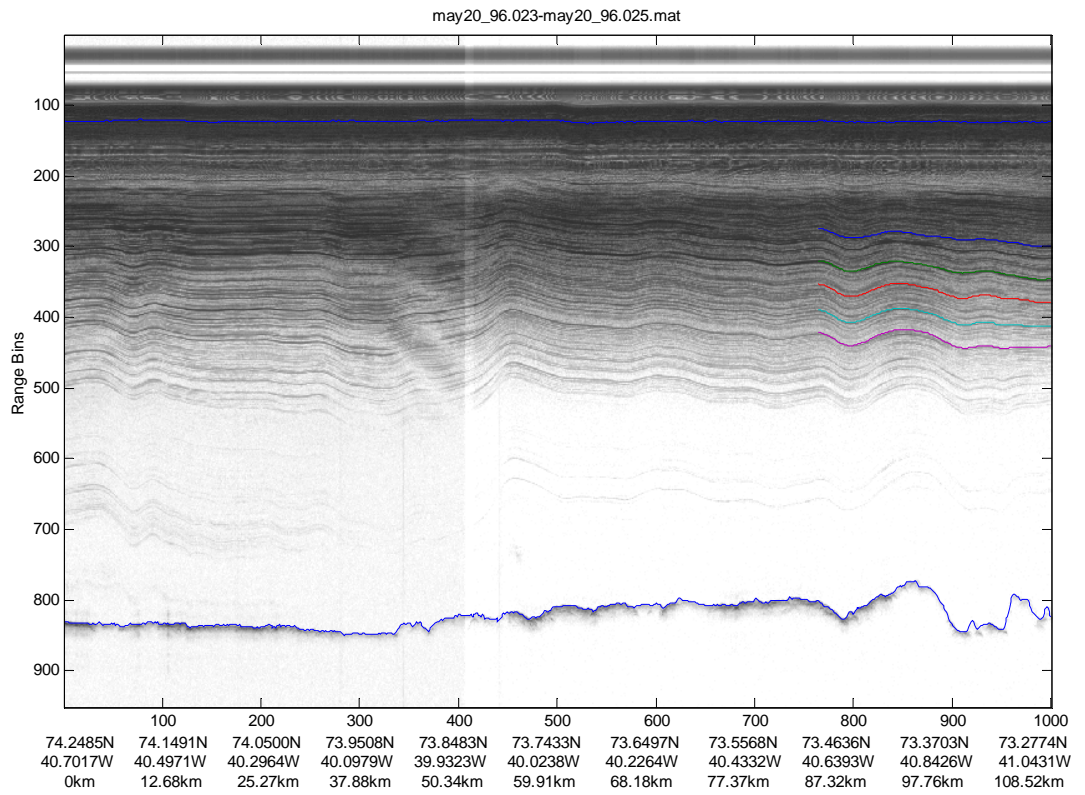


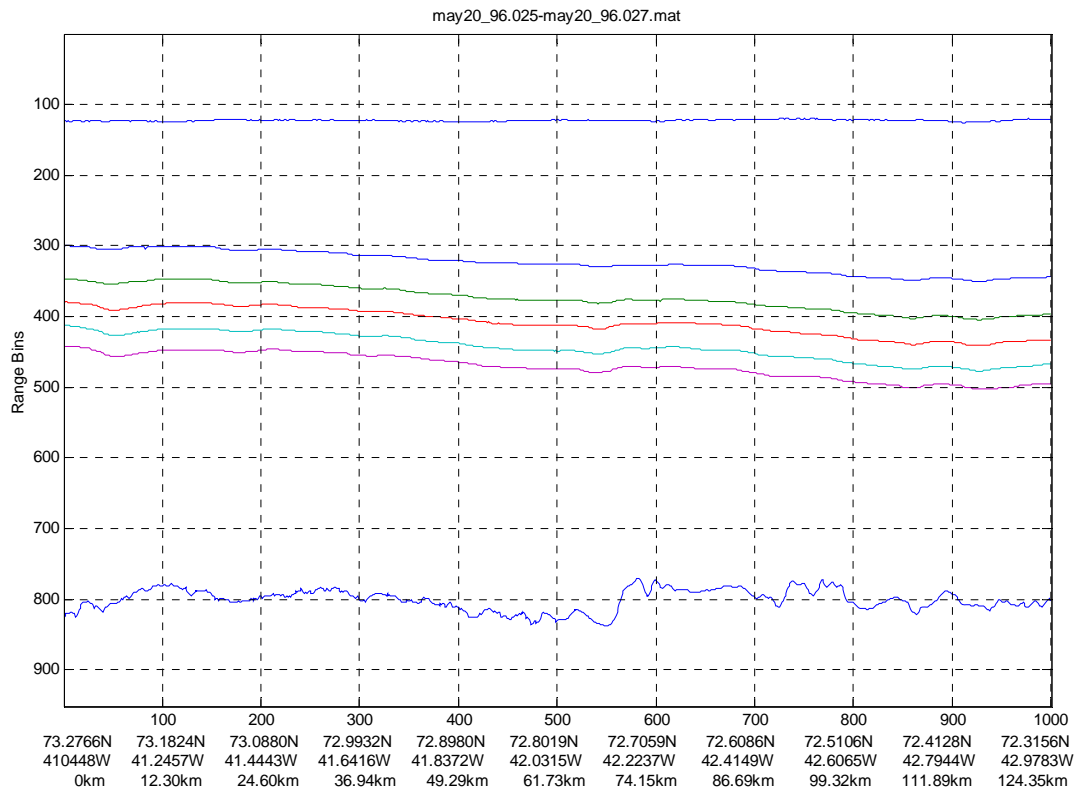
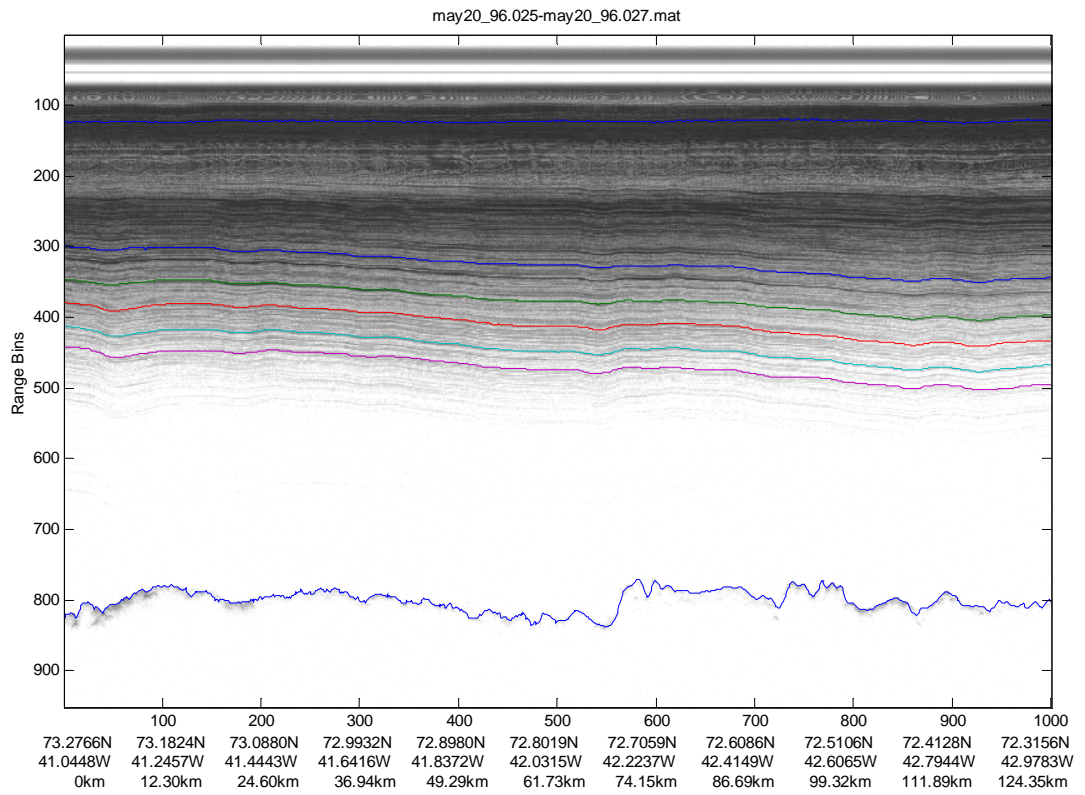


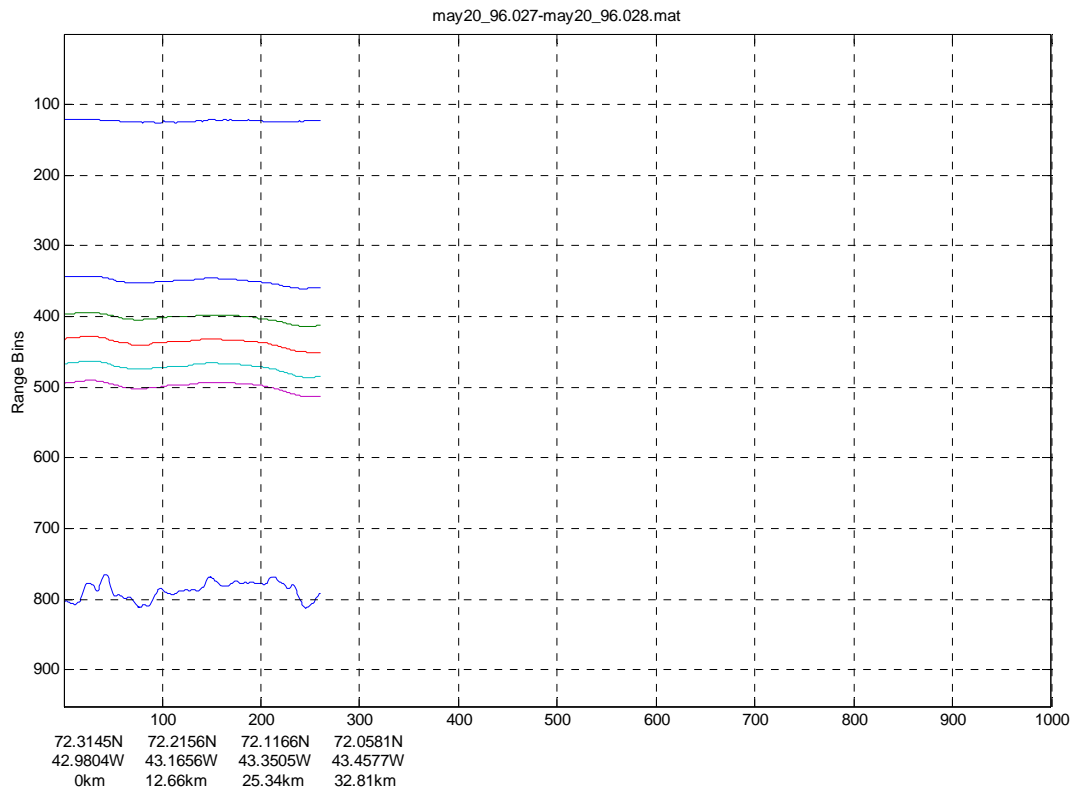
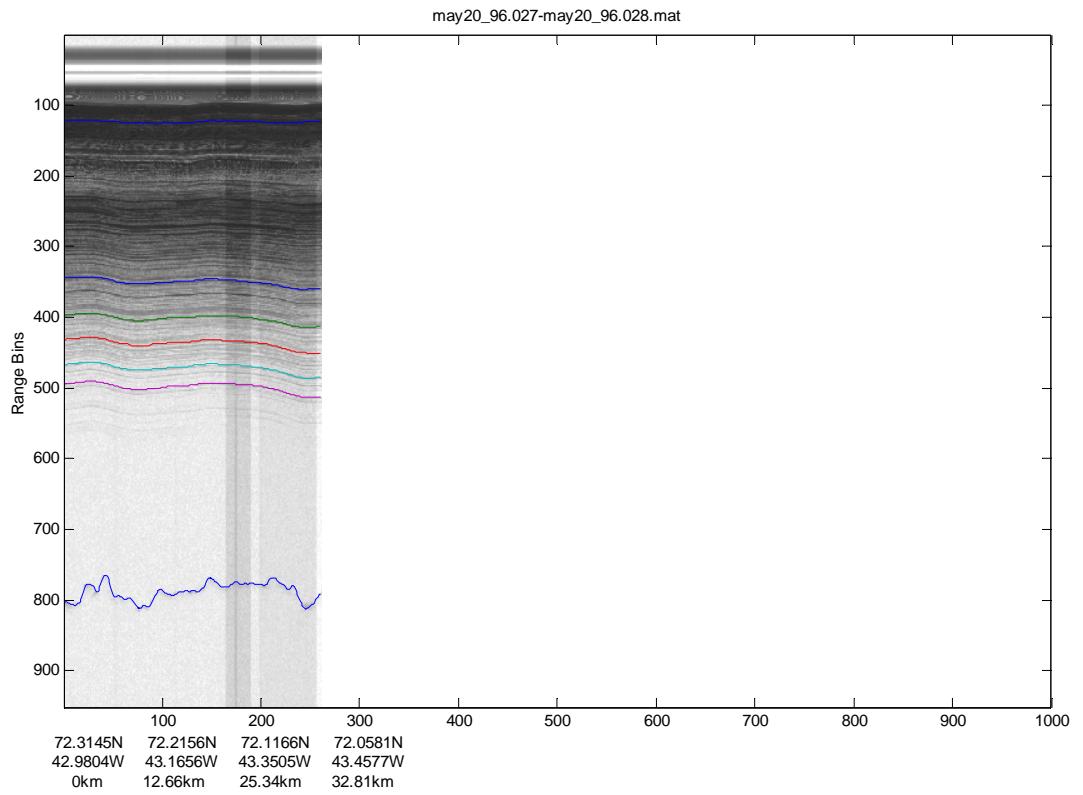


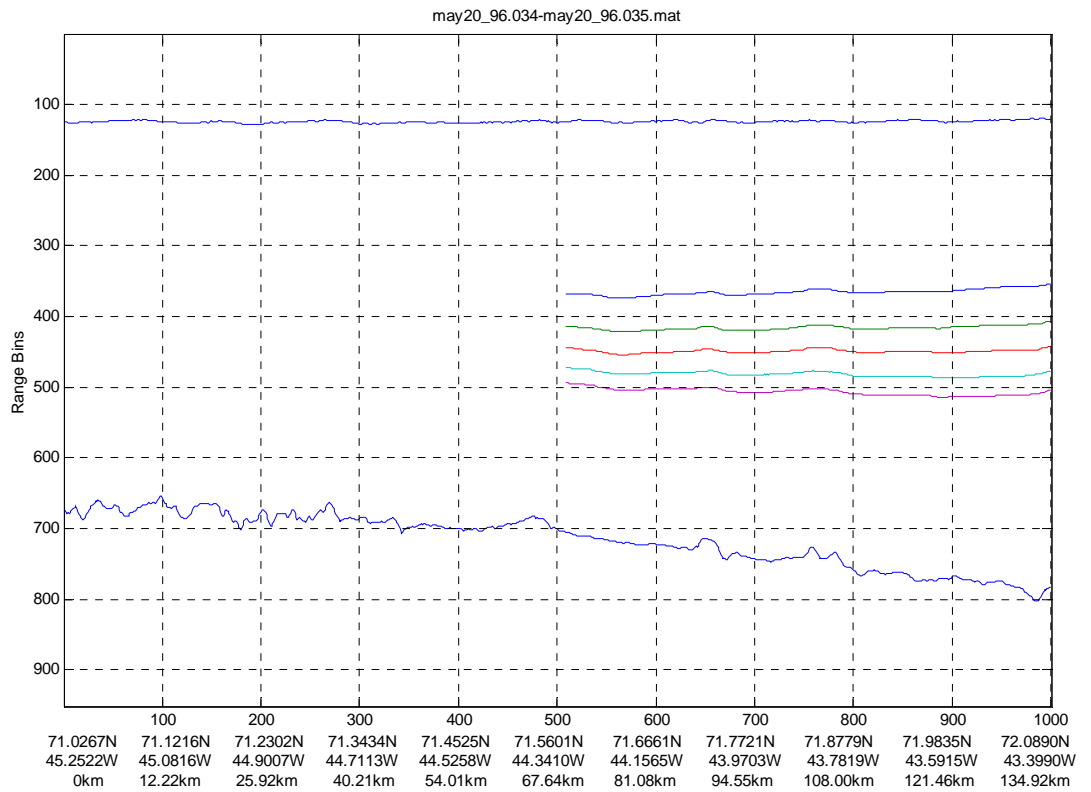
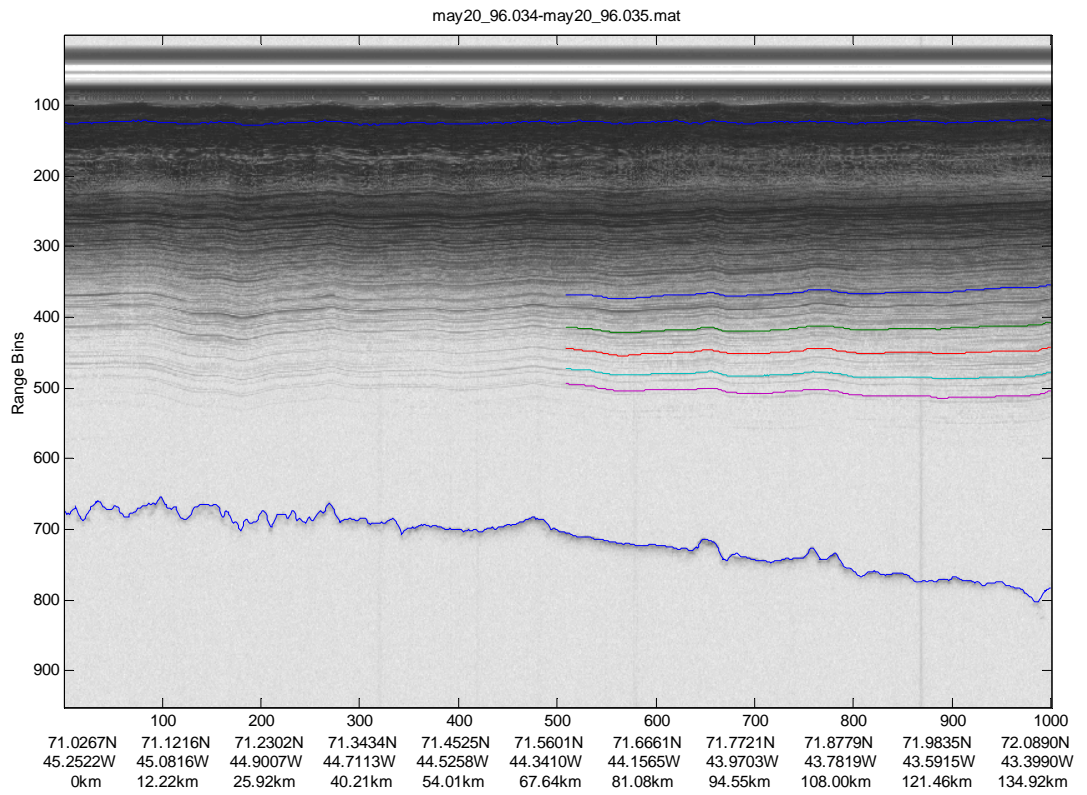


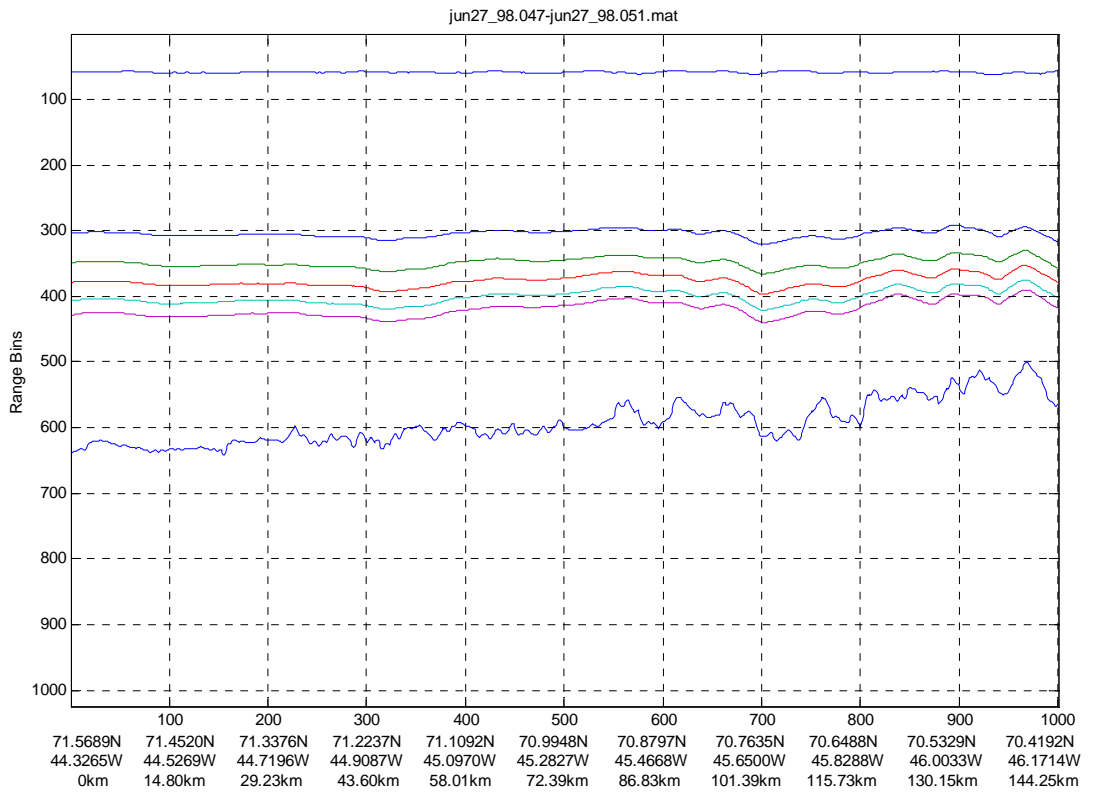
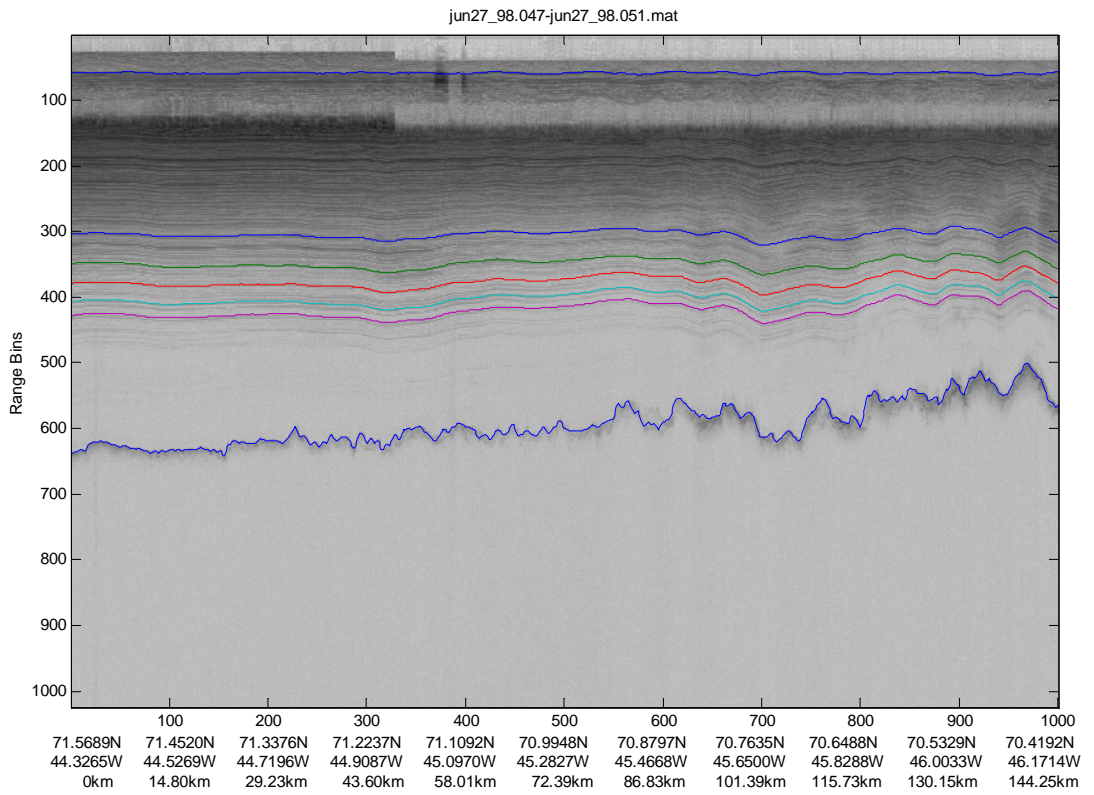


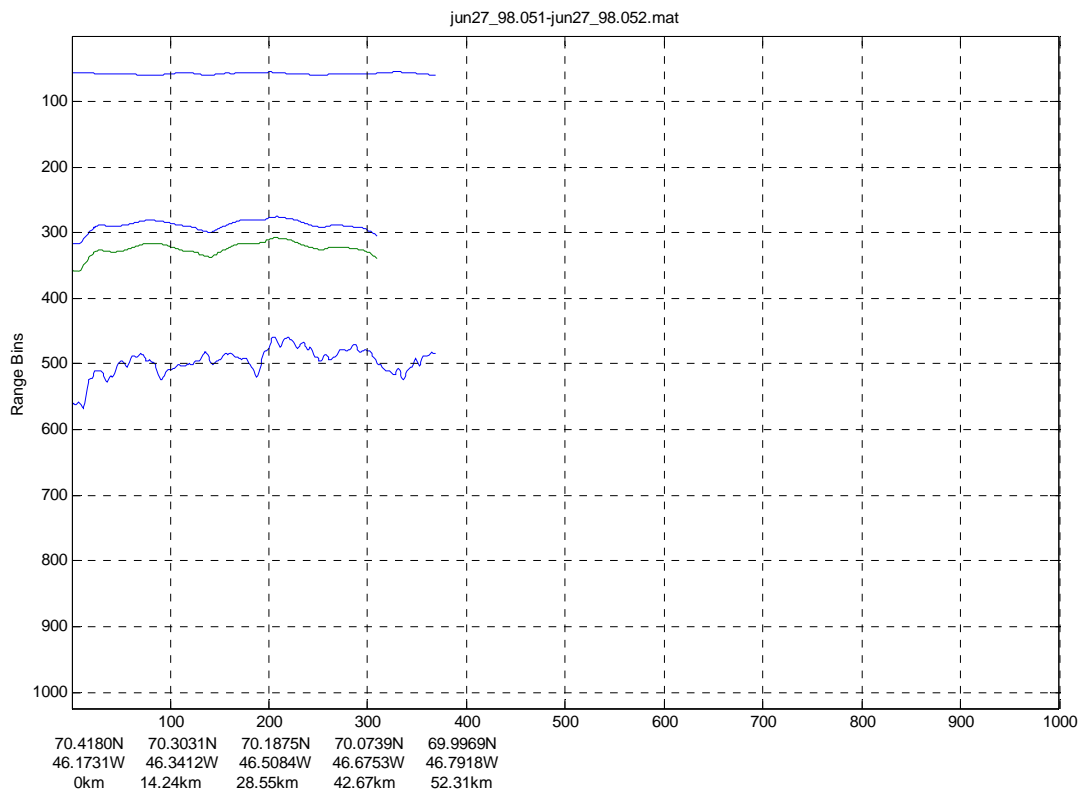
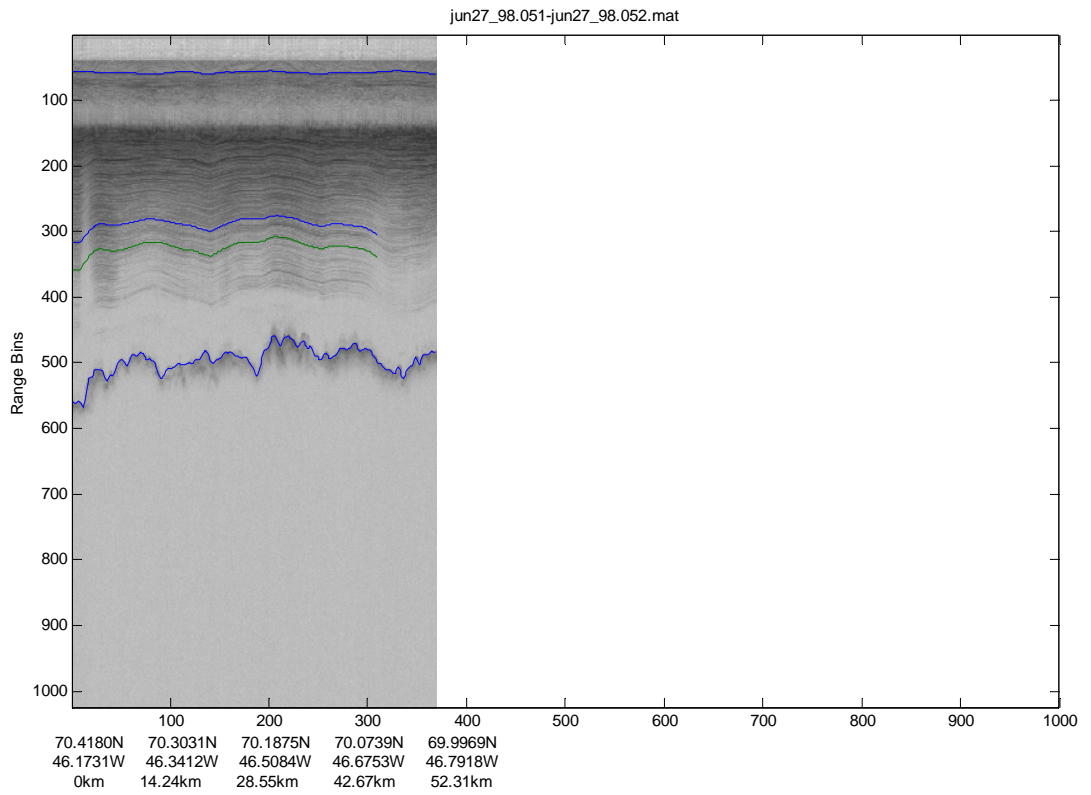


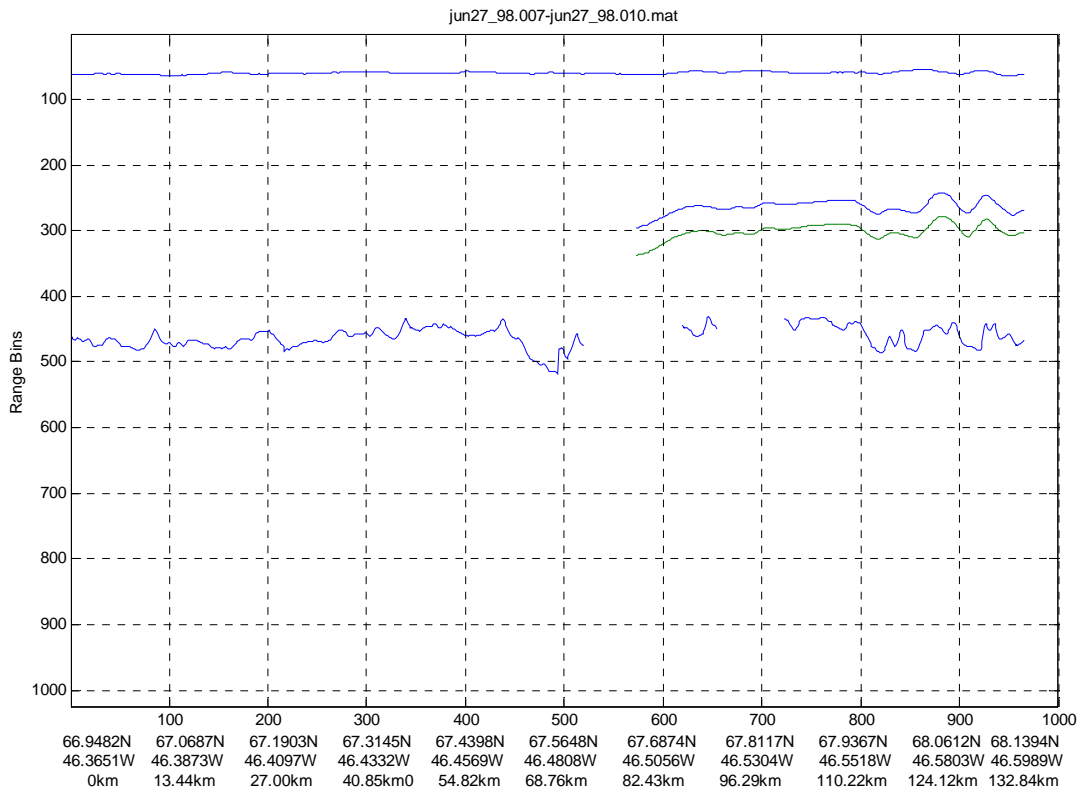
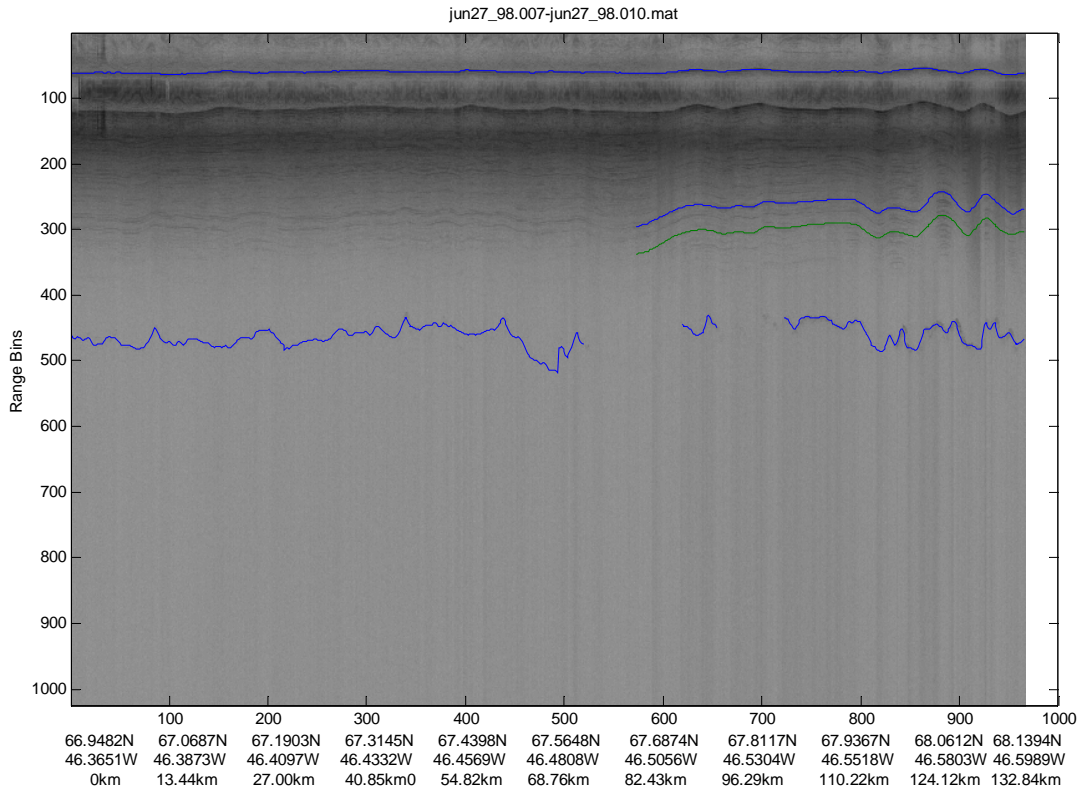


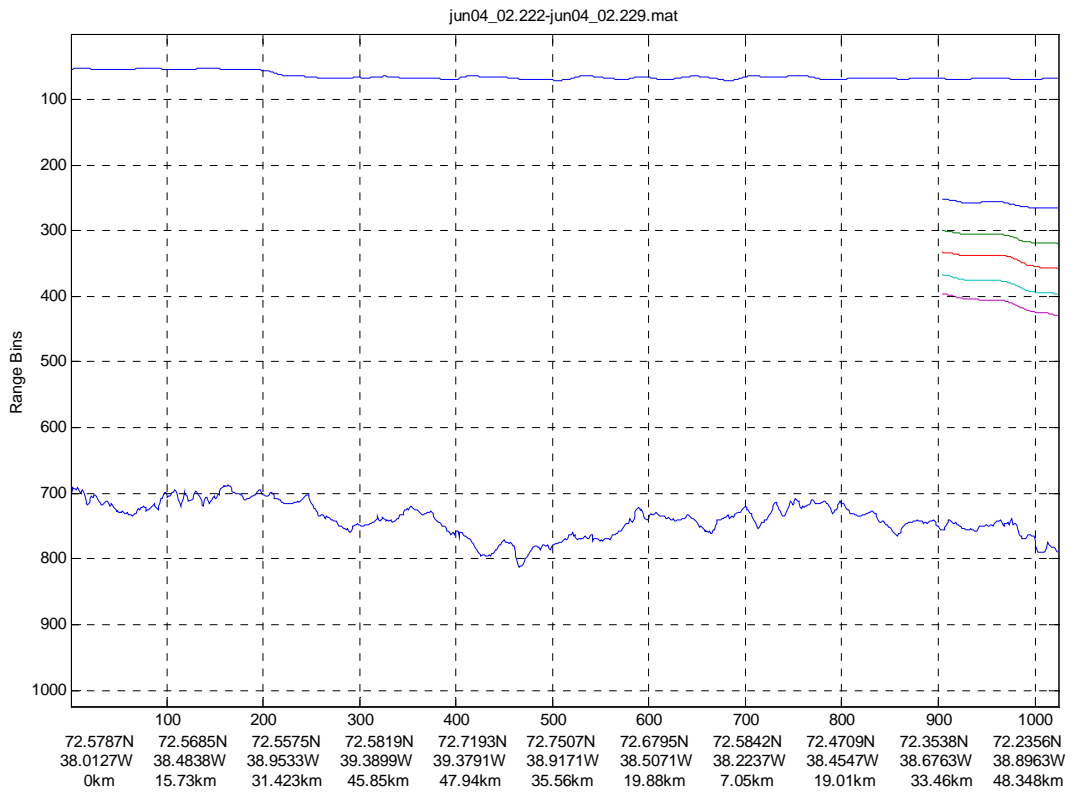
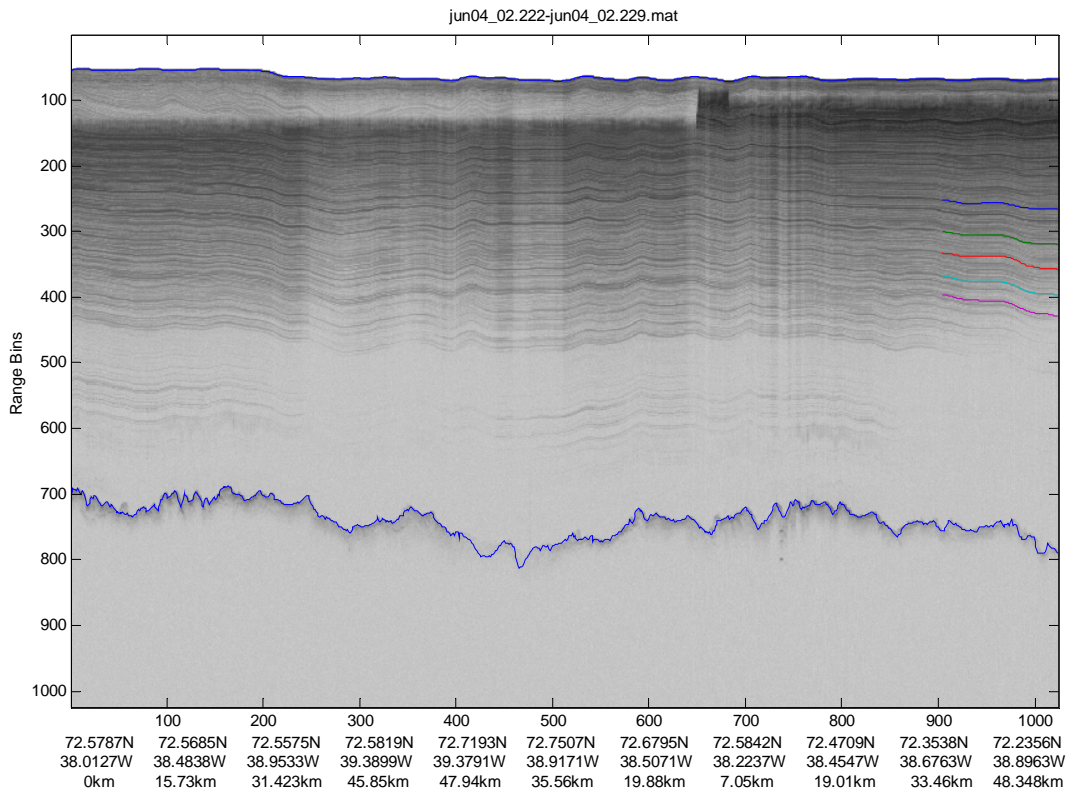


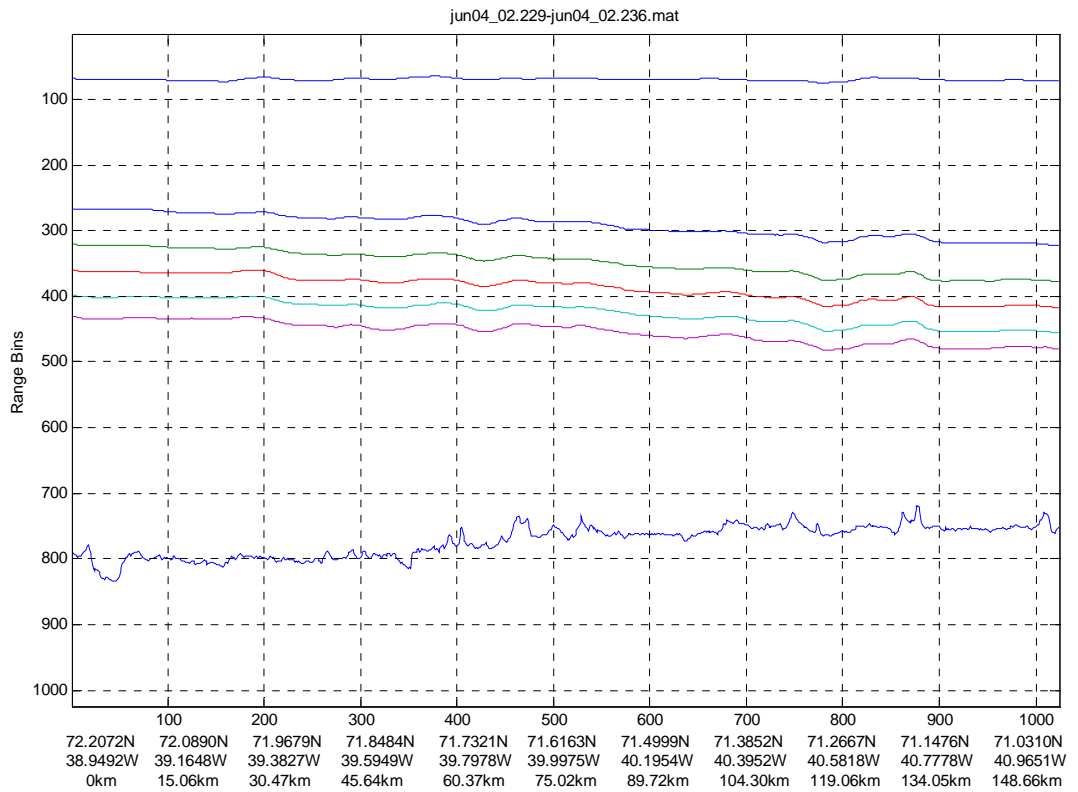
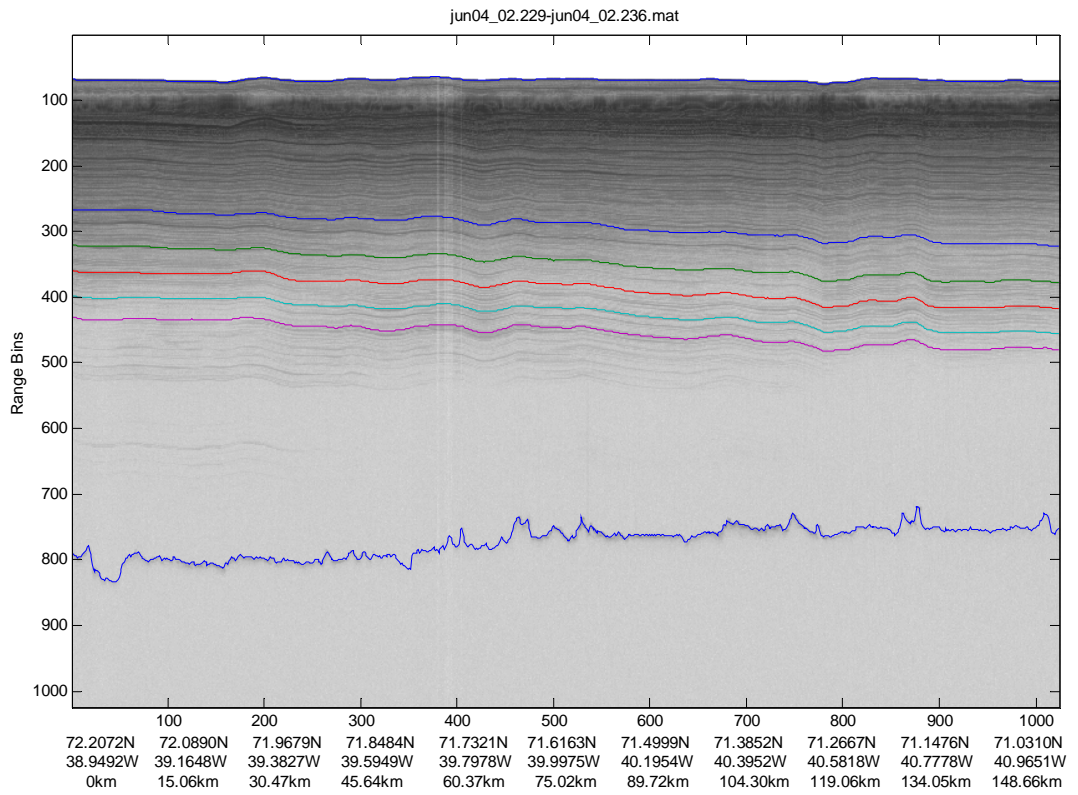


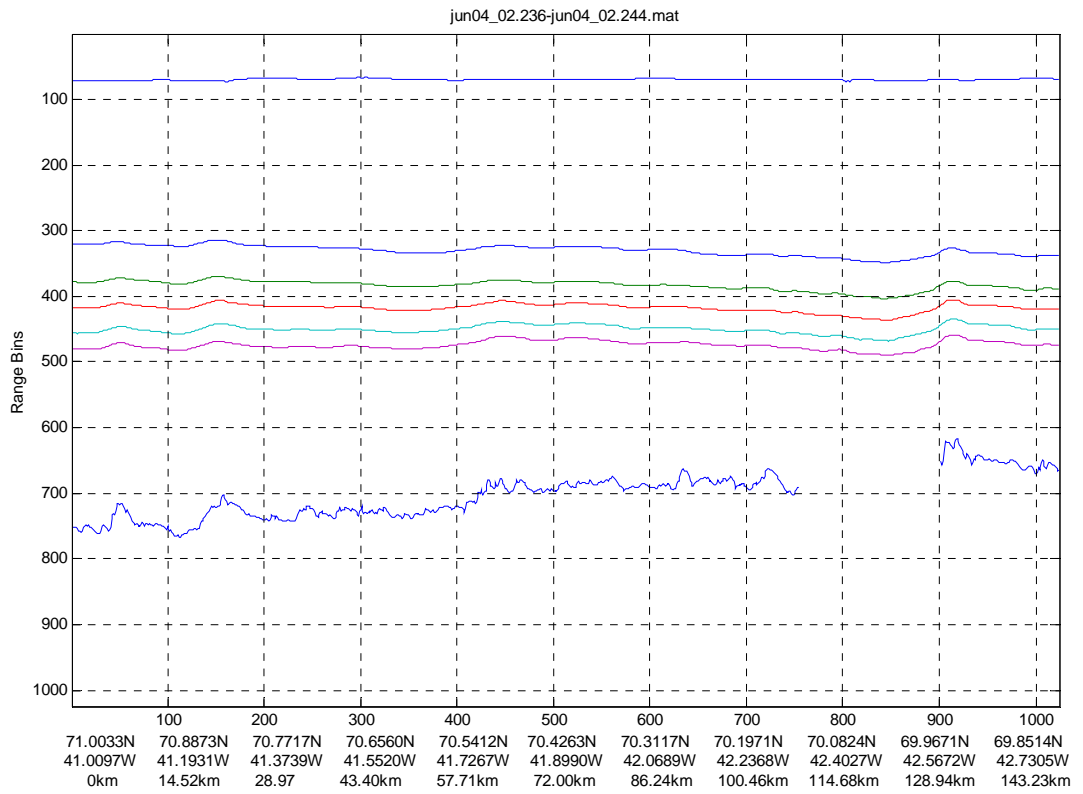
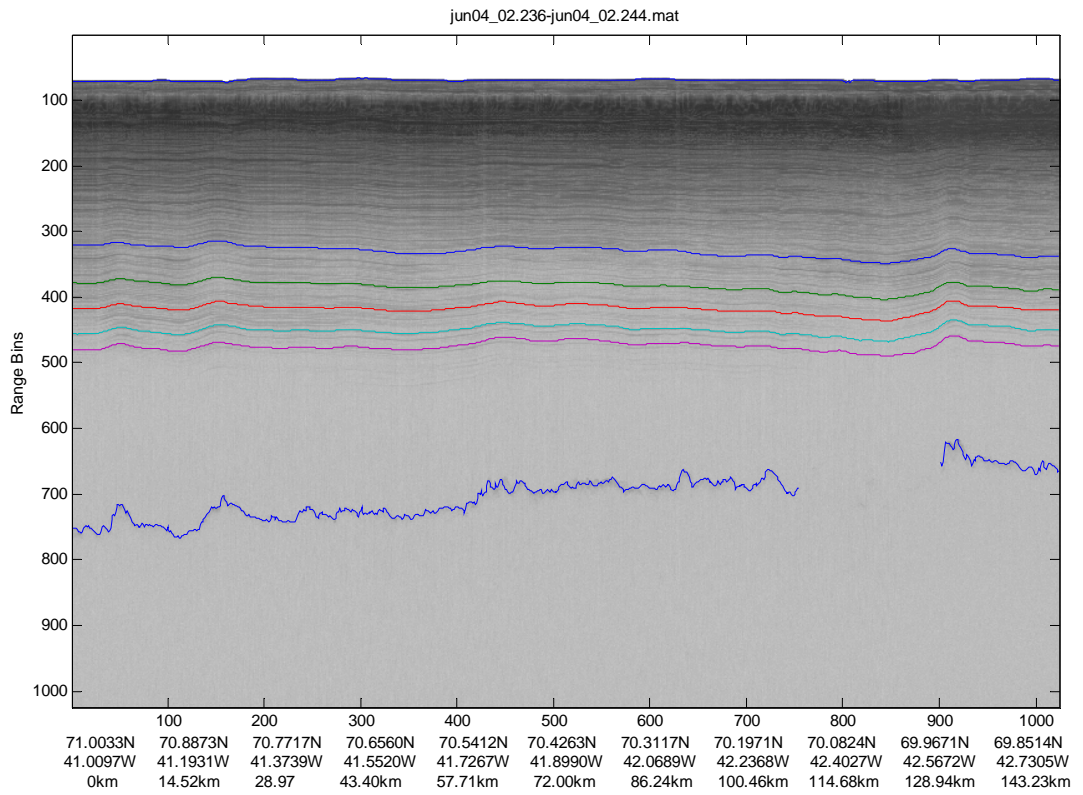


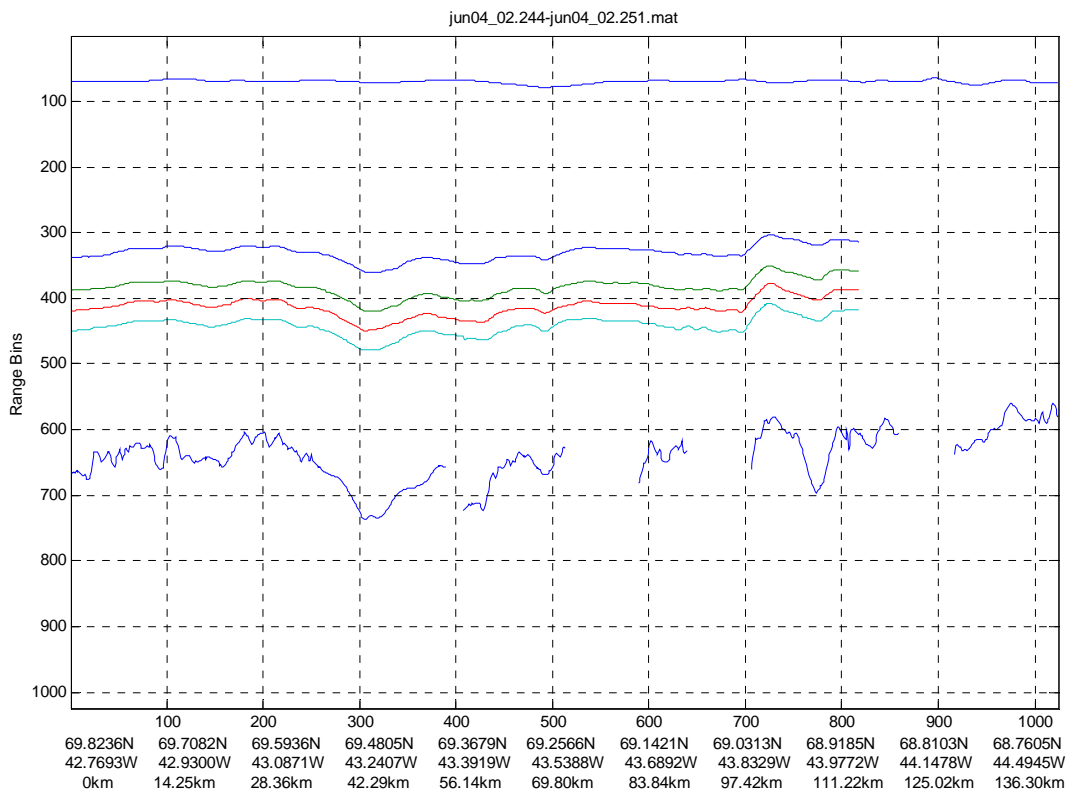
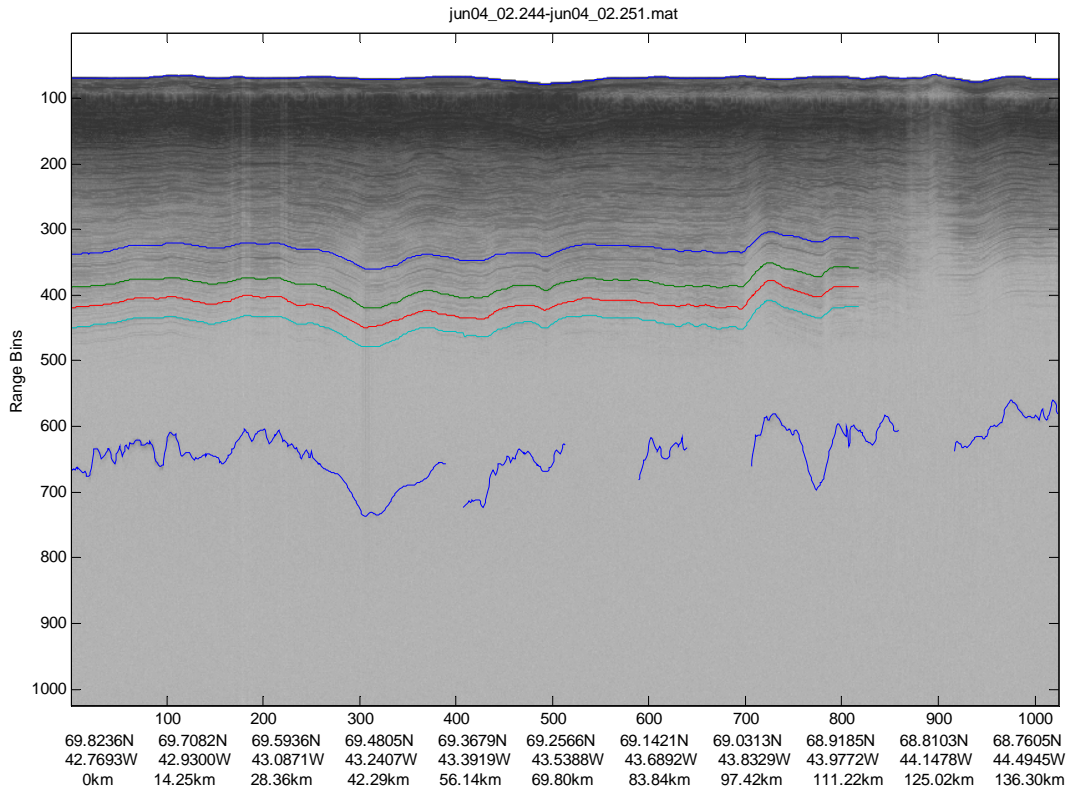


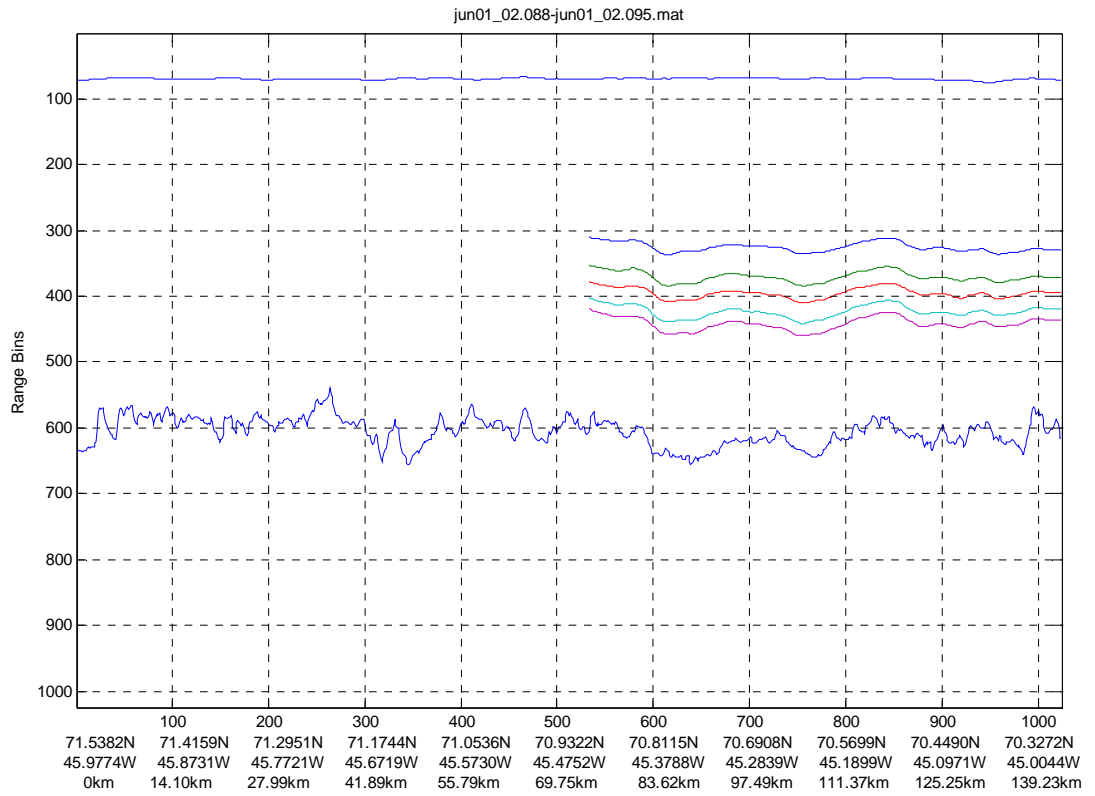
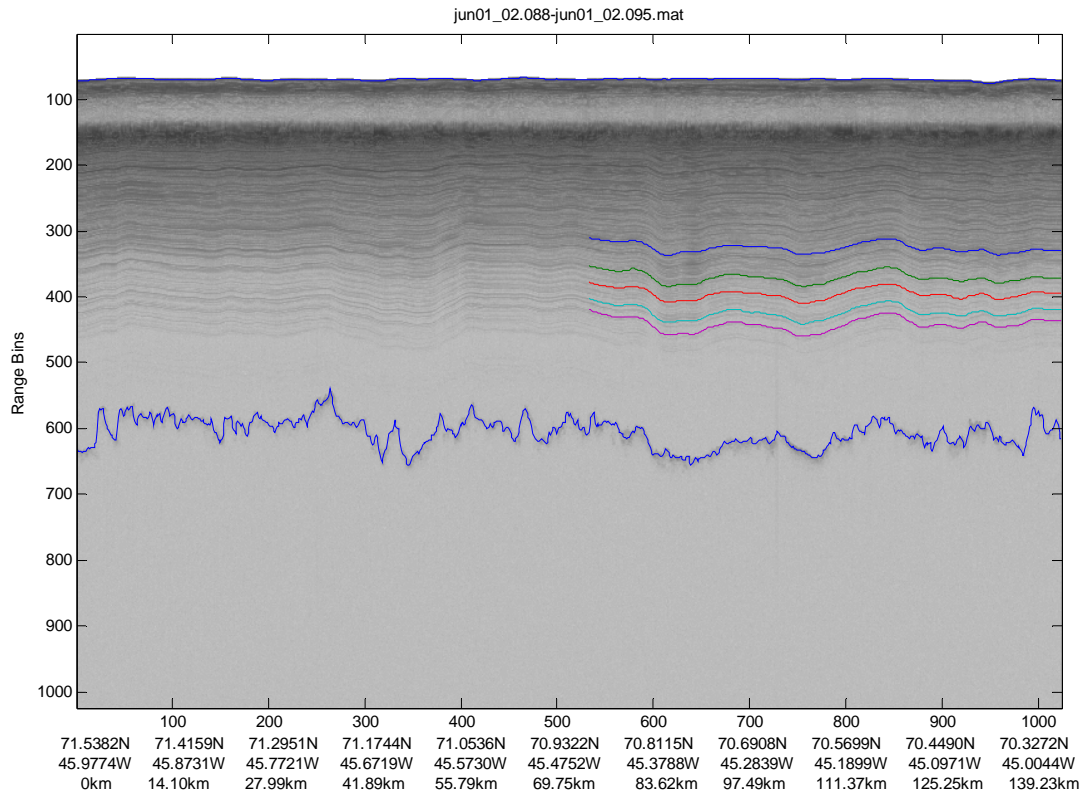


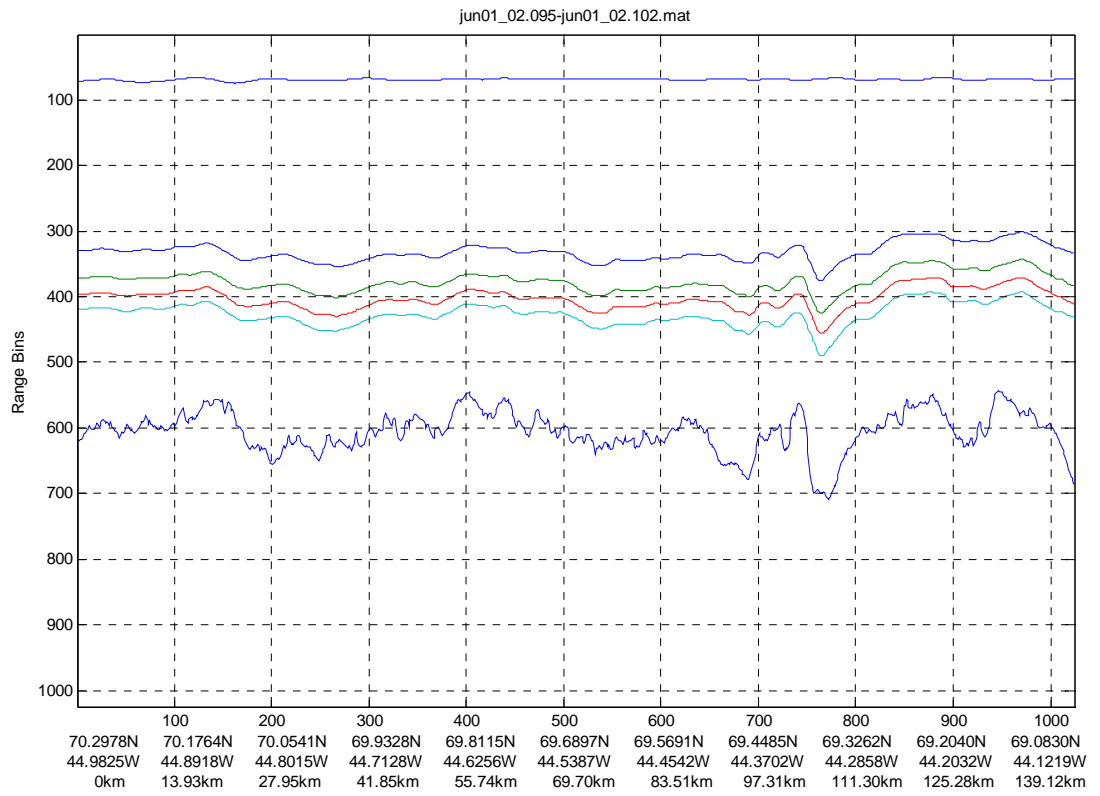
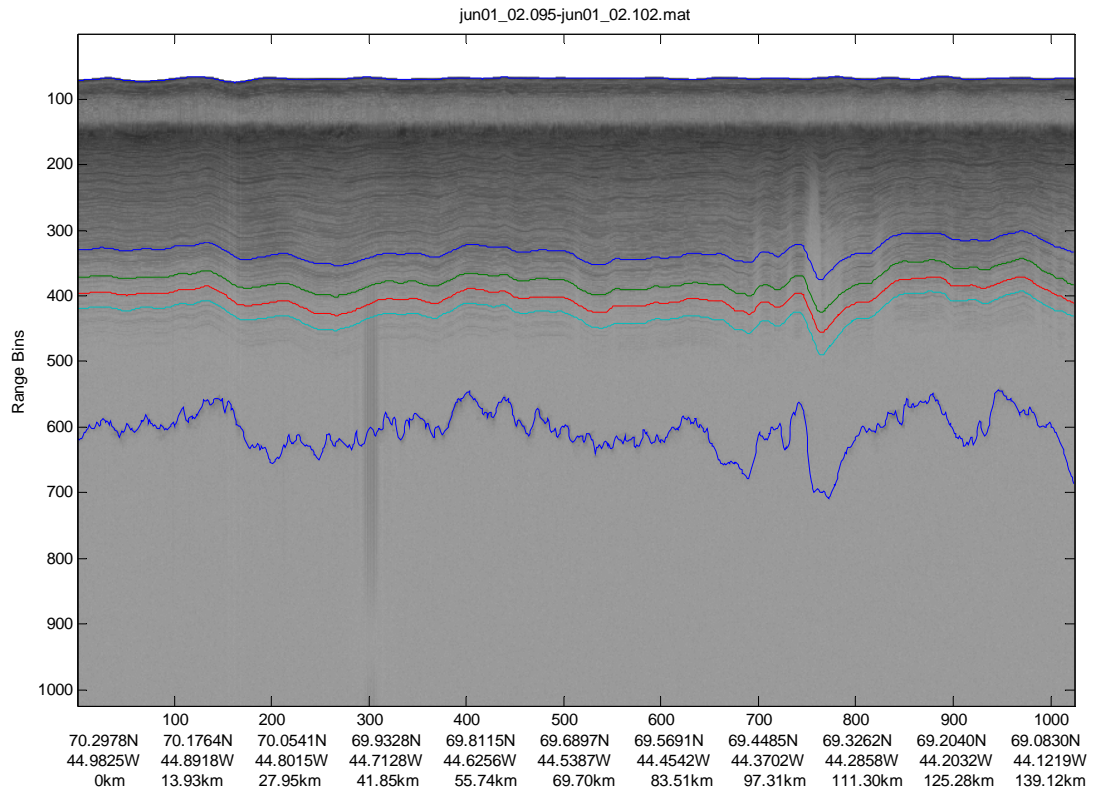


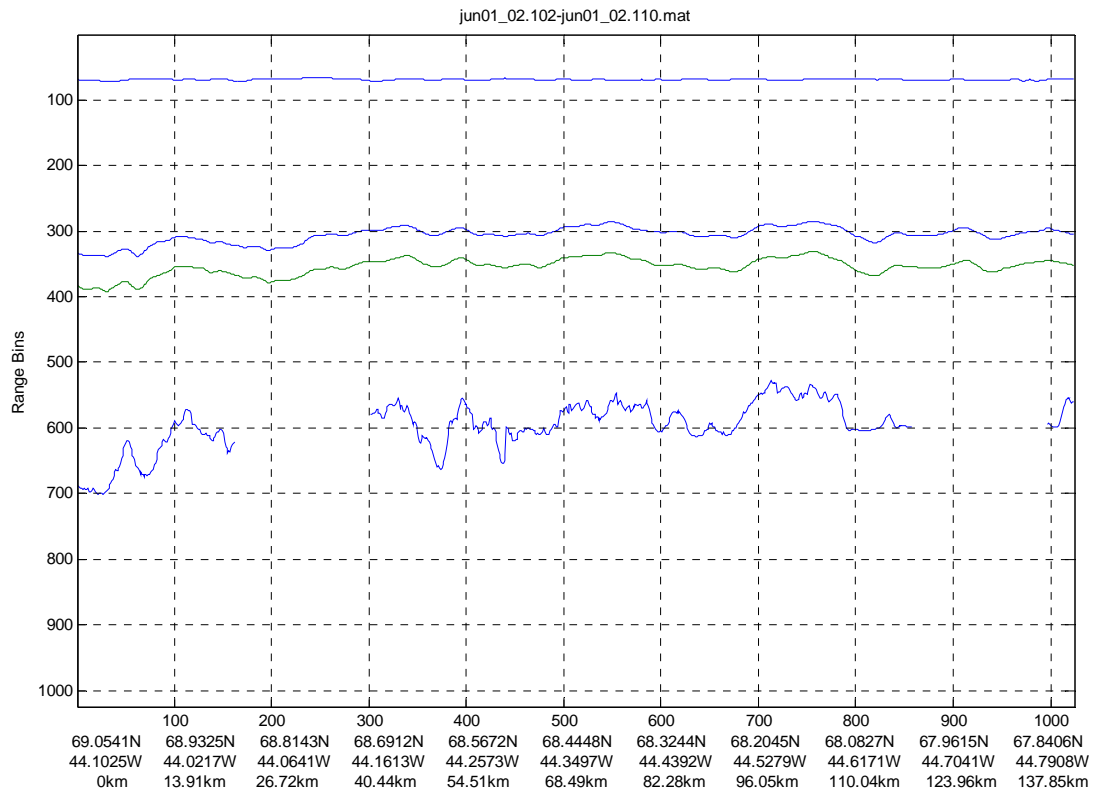
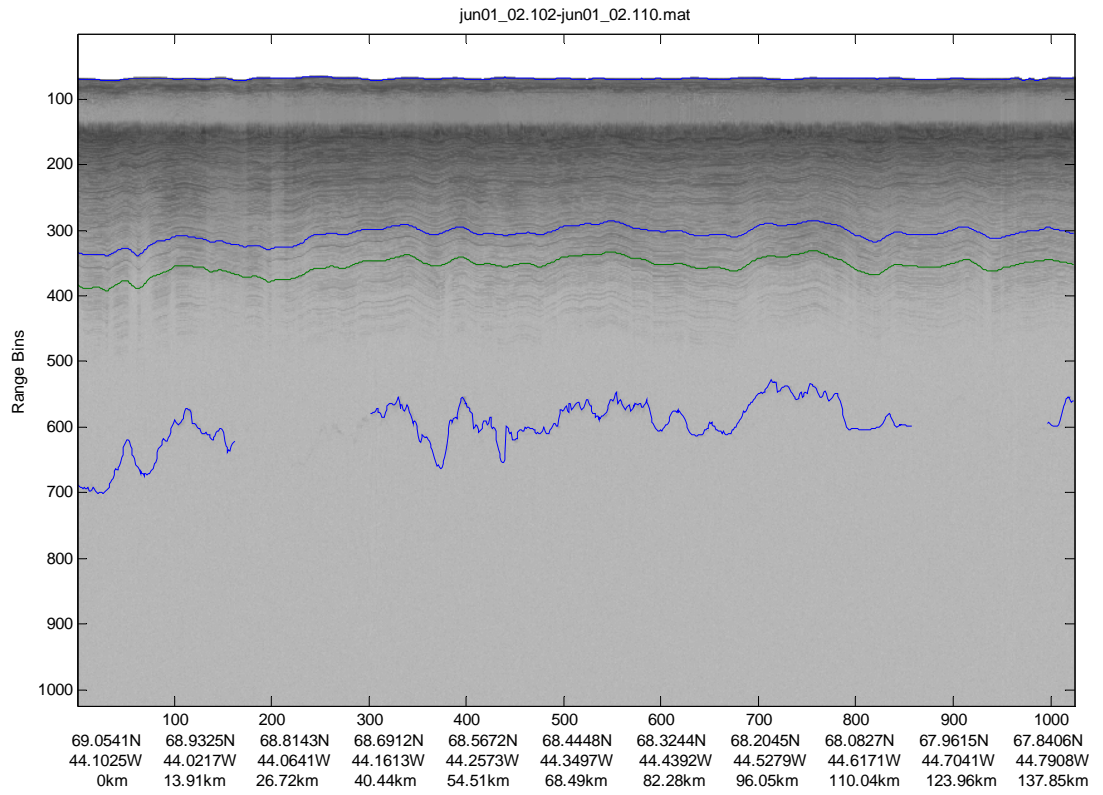


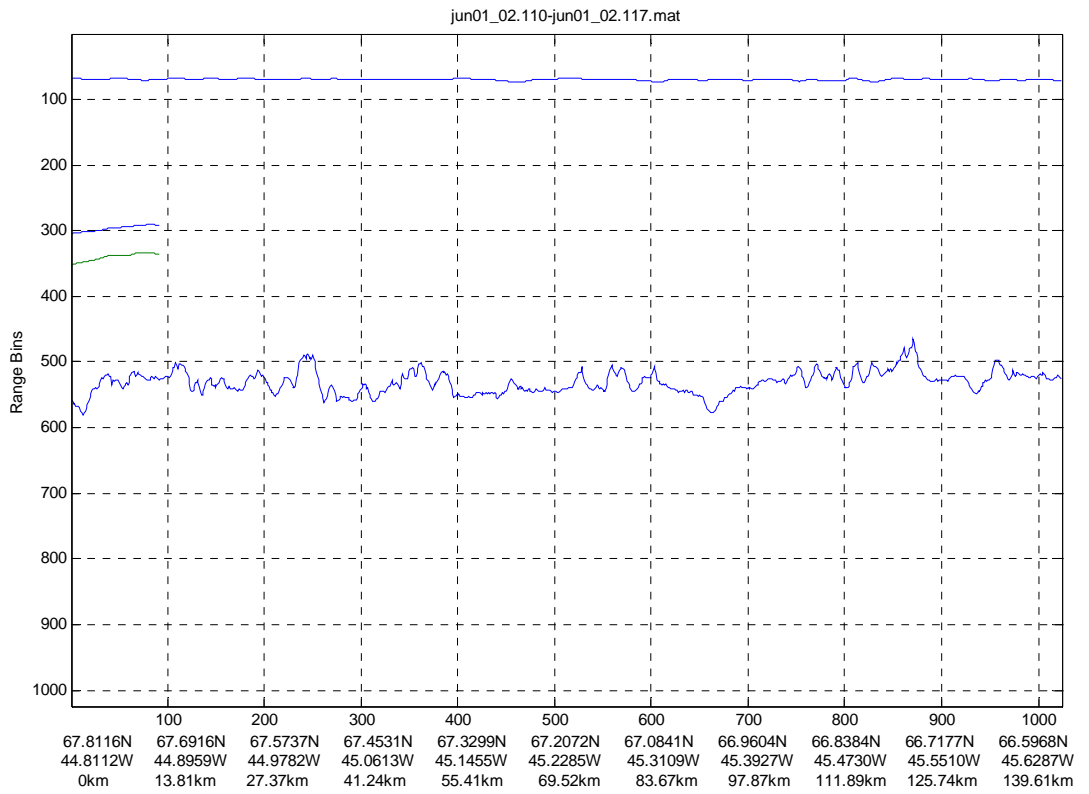
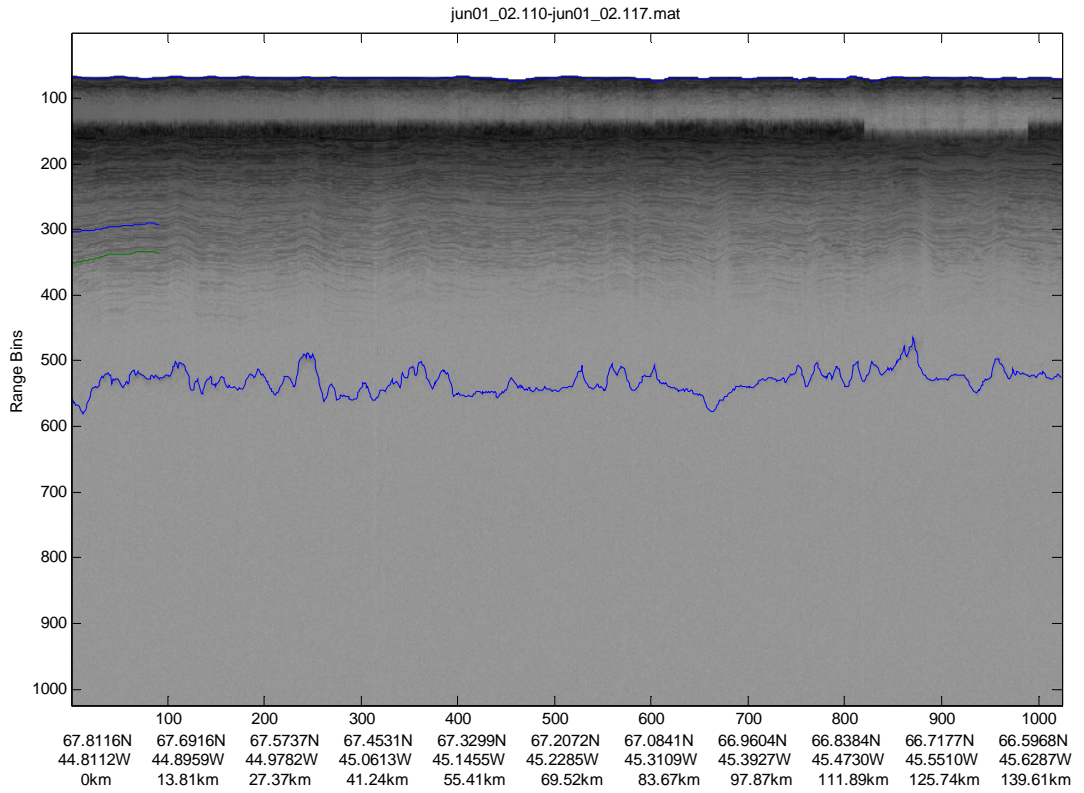


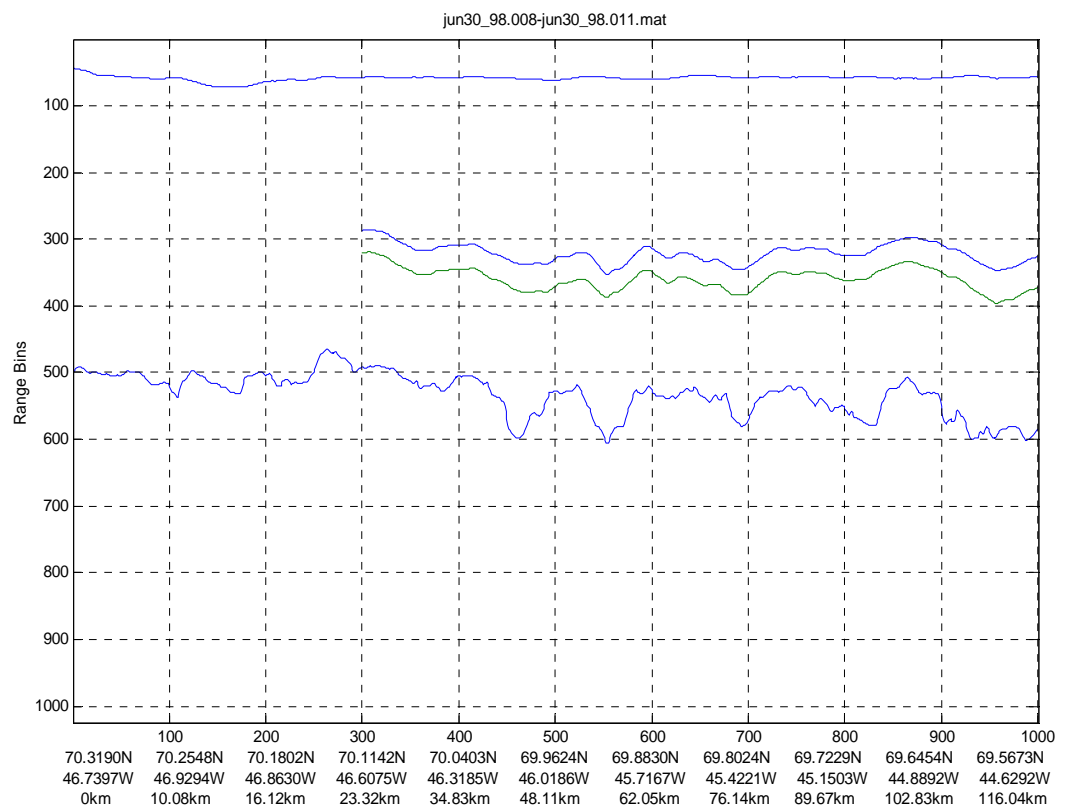
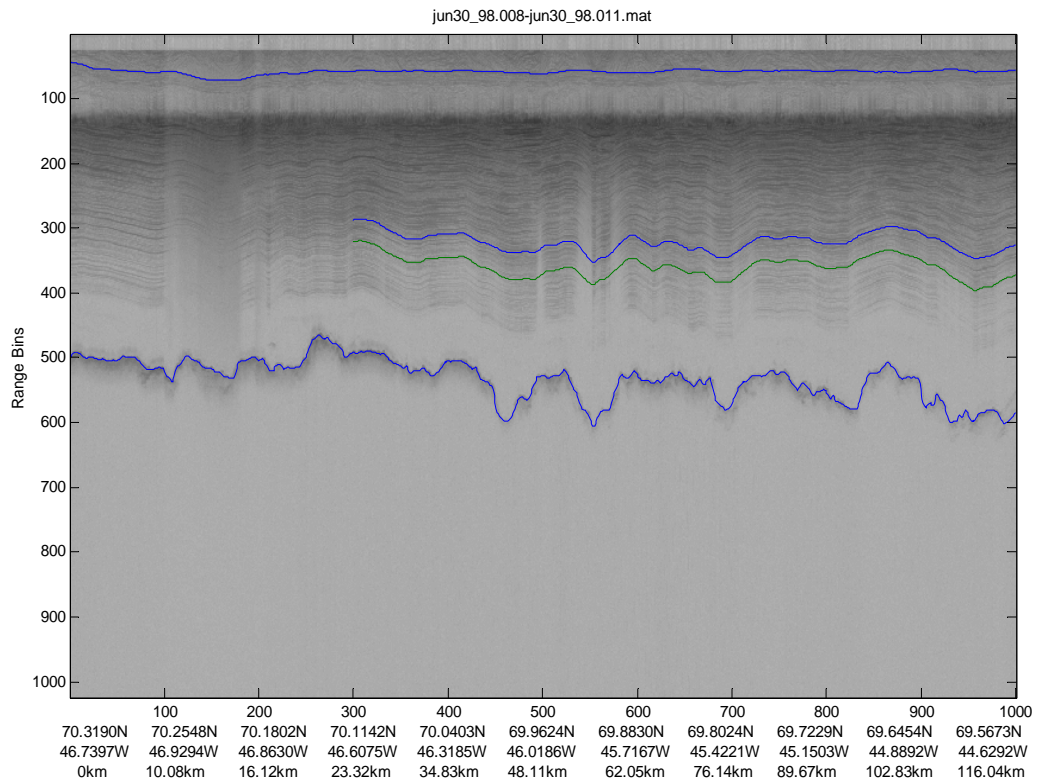


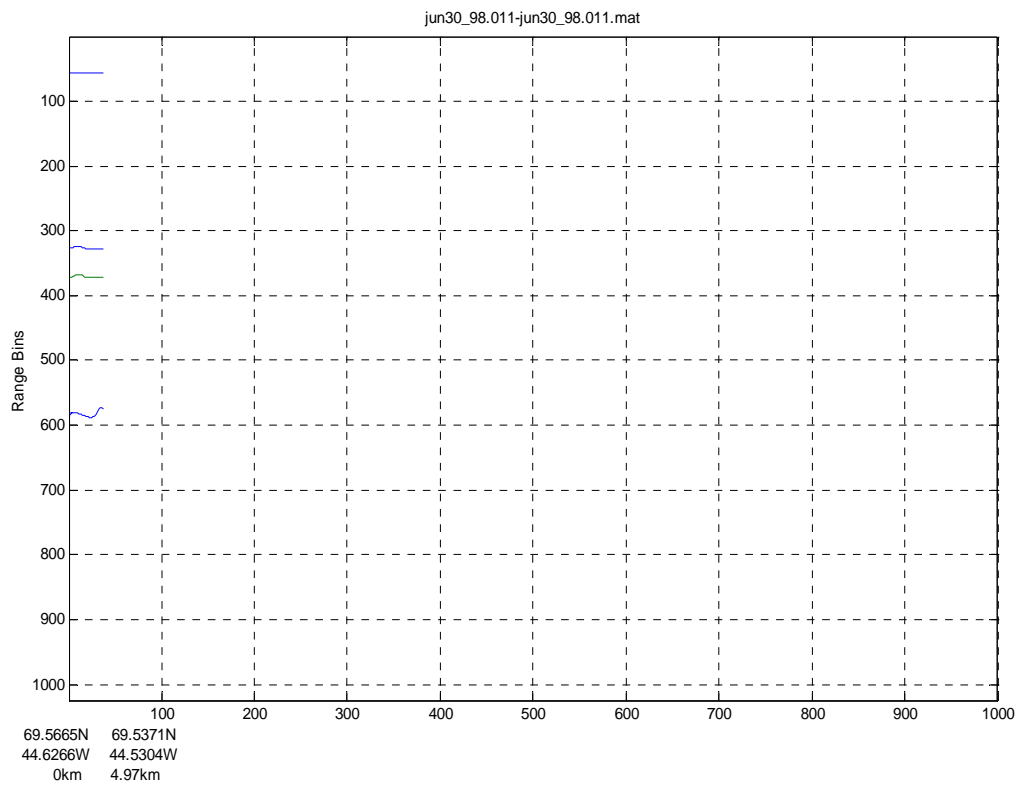
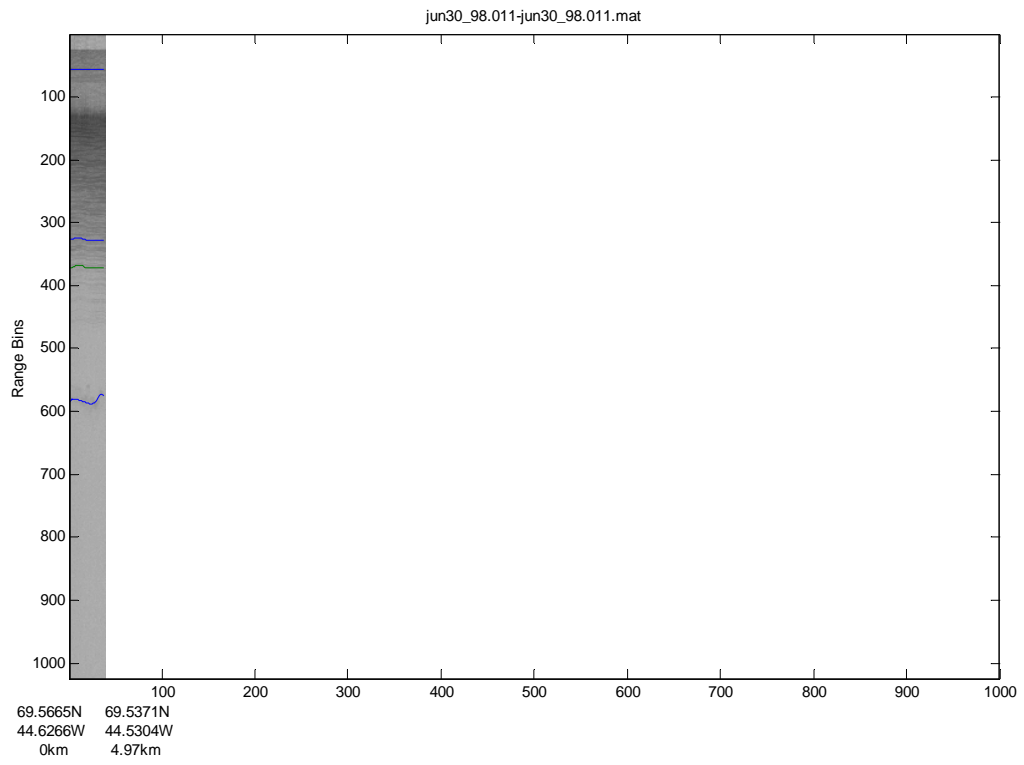




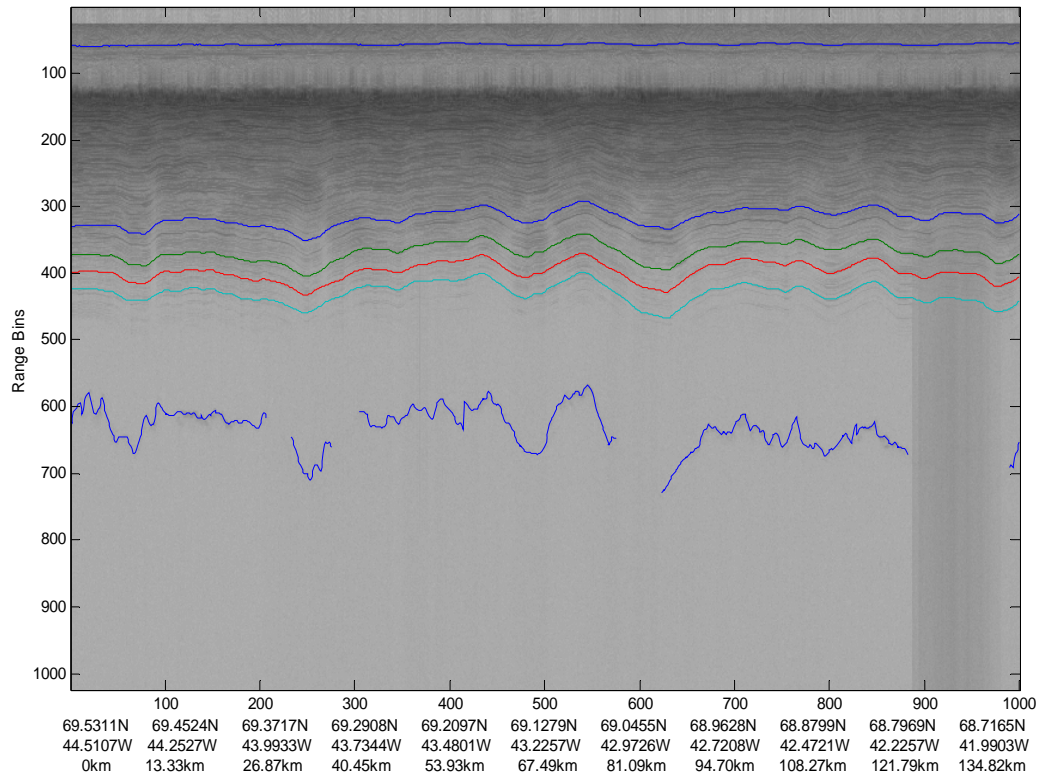




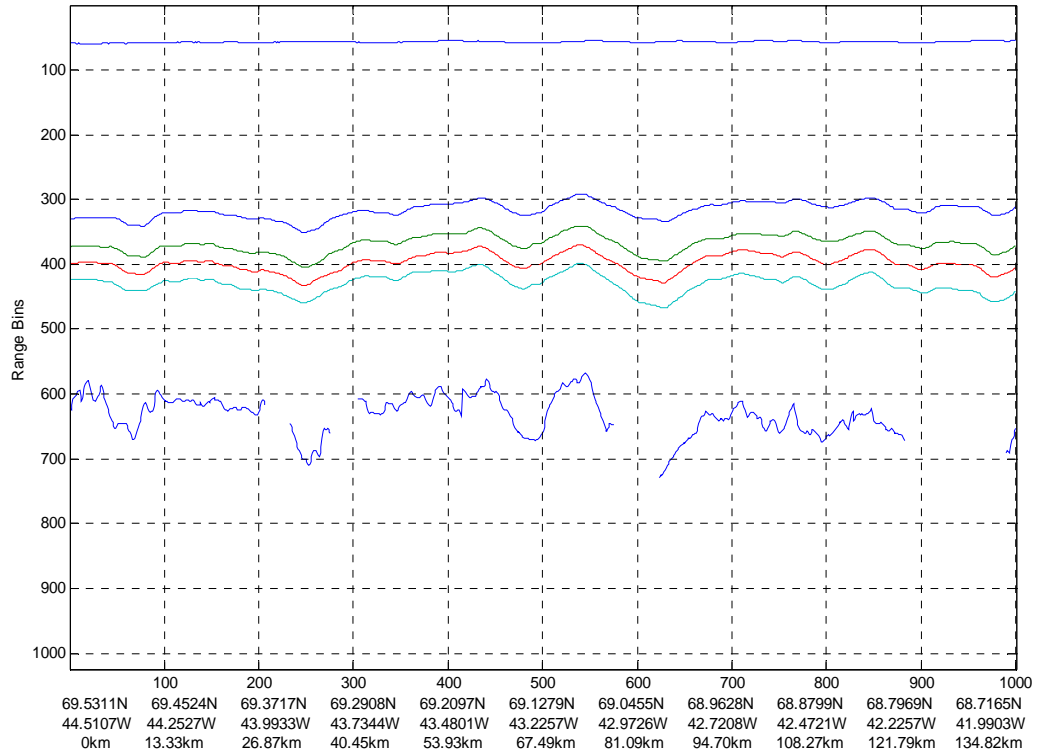


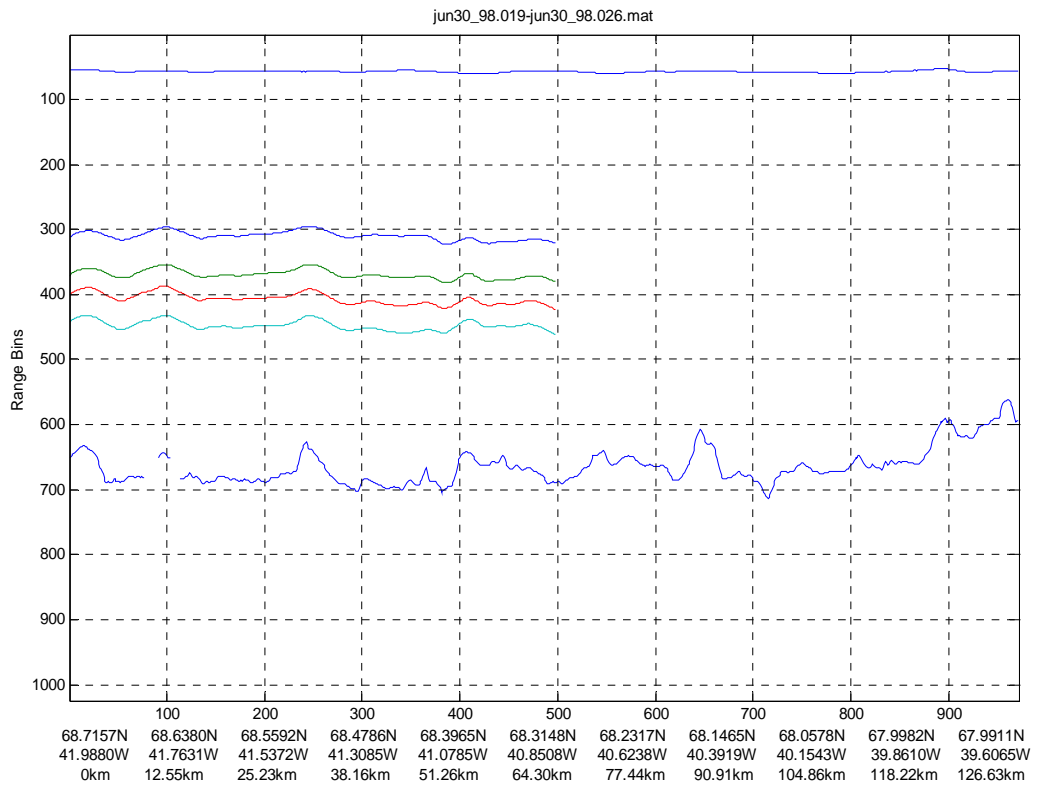
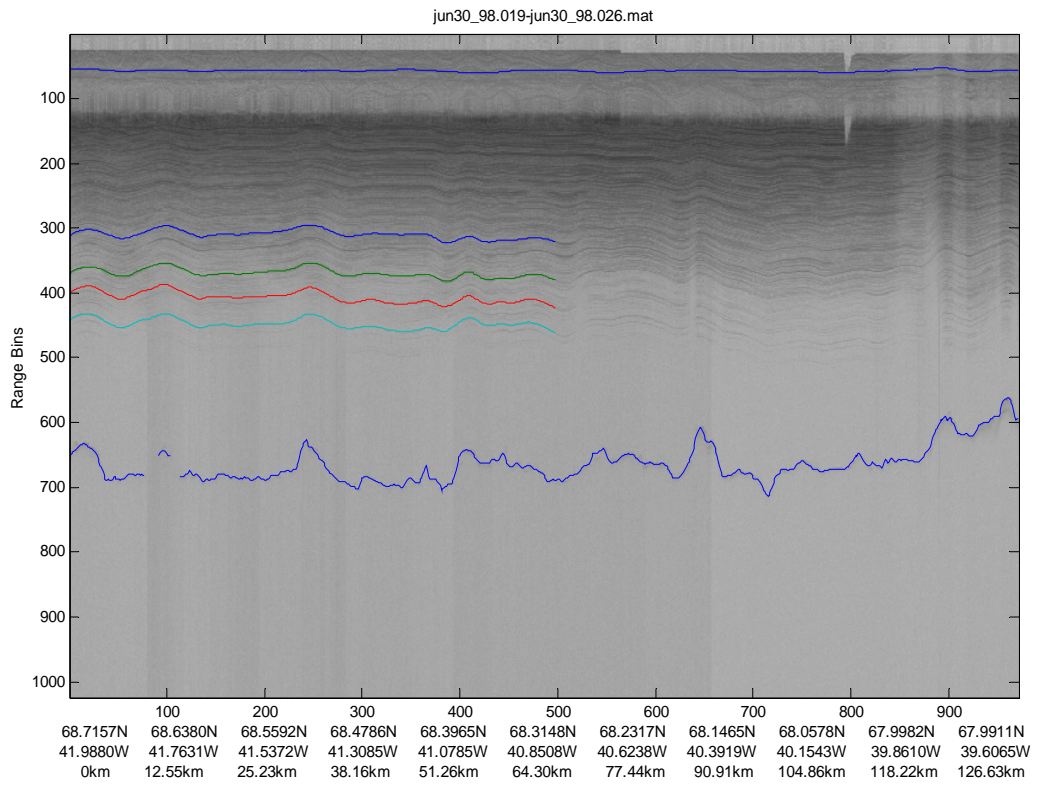


jun30_98.012-jun30_98.019.mat



jun30_98.012-jun30_98.019.mat





Appendix C Layer Tracing File Formats

C.1 Files with extension *.mat

Variable Name	Variable Short Description	Format
layer1	Pixel location of layer 1 for each column in radar echogram	Mathworks MATLAB
layer2	Pixel location of layer 2 for each column in radar echogram	Mathworks MATLAB
layer3	Pixel location of layer 3 for each column in radar echogram	Mathworks MATLAB
layer4	Pixel location of layer 4 for each column in radar echogram	Mathworks MATLAB
layer5	Pixel location of layer 5 for each column in radar echogram	Mathworks MATLAB
latitude	Latitude in degrees	Mathworks MATLAB
longitude	Longitude in degrees	Mathworks MATLAB

C.2 Files with extension *.pdf

Each *.pdf file contains two images per radar echogram file for quick perusal purposes. The first image has the ice surface, layer 1, layer 2, layer 3, layer 4, layer 5 and the bedrock location superimposed on the radar echogram. The second image has the ice surface, layer 1, layer 2, layer 3, layer 4, layer 5 and the bedrock location plotted.

C.3 Files with extension *.ht

Variable Name	Variable Short Description	Column	Format
LAT	Latitude in degrees	1	ASCII
LON	Longitude in degrees	2	ASCII
LAYER 1 THICK	Layer 1 thickness [m] for radar echogram column	3	ASCII
LAYER 2 THICK	Layer 2 thickness [m] for radar echogram column	4	ASCII
LAYER 3 THICK	Layer 3 thickness [m] for radar echogram column	5	ASCII
LAYER 4 THICK	Layer 4 thickness [m] for radar echogram column	6	ASCII
LAYER 5 THICK	Layer 5 thickness [m] for radar echogram column	7	ASCII

Note: NaN values correspond to locations where the variables were not determined.
Thickness values do not include the firm velocity correction as described in Ch. 4.